Chronology of gypsum dunes at Knolls, Utah: refining OSL techniques and timing of Holocene eolian processes

by

Victoria Teresa Fitzgerald

B.A., University of Texas at Austin, 2007

A THESIS

submitted in partial fulfillment of the requirements for the degree

MASTER OF SCIENCE

Department of Geology
College of Arts and Sciences

KANSAS STATE UNIVERSITY
Manhattan, Kansas

2019

Approved by:

Major Professor
Joel Q.G. Spencer

Copyright

Abstract

This study examines eolian samples from post-Lake Bonneville gypsum dunes in Knolls, UT, primarily to determine suitability of optically stimulated luminescence (OSL) dating protocols for gypsum geochronology. Sedimentologists often rely on proxies to understand geologic timescales, OSL may eliminate that need in environments with gypsum. Using OSL we aimed to identify the ages of punctuated climatic events that are linked to deposition of the gypsum rich dunes found in the study area. To accomplish this pursuit, systematic research of gypsum preparation protocols were required. Multiple experiments were undertaken to assess the effectiveness of mineral isolation and etching. Knowledge of gypsum behavior is of particular interest, as it is found in both lacustrine and marine environments and is typically less soluble than other evaporites found in both settings, such as sodium chloride. Gypsum has also been observed at several hundred meters water depth in the alkaline environment of the Arctic Ocean. Additionally, gypsum sand grains are accessible to researchers in geomorphic features like unconsolidated to semi-consolidated dunes, making them easier to sample for OSL analyses than gypsum or quartz found in an outcrop. Sampling strategy can be quickly determined for dunes that are exposed on all sides.

The focus of this study seeks to resolve discrepancies observed in the small body of literature on gypsum as an OSL chronometer. Relatively homogenous eolian gypsum sand grain samples with grain sizes ranging from <63 μm to >250 μm from two adjacent paleodunes (KNP-A and KNP-B) and one coppice dune (CD-5) were used to determine best preparation practices and identify if punctuated climatic events during the Holocene could be detected using gypsum. The sample site was selected for a case study on OSL dating techniques because previous work has constrained the maximum age of post-Lake Bonneville dune formation (~12 ka BP).

Preparation protocols, independently checked using various methods, were selected with minimal mineralogical impact and OSL sensitivity considerations in mind. Bulk composition and mineralogy of the sediment at various steps in sample preparation have been analyzed using X-Ray Diffraction, bulk elemental extraction, particle size analysis, Scanning Electron Microscopy and binocular microscopy. Etching experiments indicate that an air-dried, dry-sieved, and gypsum-rich fraction (90-125 μm) can be effectively isolated and etched in ~36 wt % HCl for 40 minutes. Of the various OSL measurement protocols attempted, we confirmed a modified single-aliquot regenerative-dose protocol produces detectable luminescence signals and equivalent doses (D_e) that are usable in age calculations. Age results are likely to be underestimated by approximately 0.5-0.8 ka, based on comparison to a single quartz OSL sample (KNP-A1) with an age of 2.2 ka and it's equivalent gypsum sample of 1.4 ka. This is the oldest age sampled from the stratigraphically lowest section of either KNP-A or KNP-B. Samples from KNP-B identify this smaller dune was deposited after KNP-A began developing. Age results from the stratigraphically lowest sample collected, KNP-B1, indicate deposition occurred at 0.88 ka. The active coppice dune (CD-5) gypsum OSL age is 0.09 ka. This study recommends further investigation into why the apparent discrepancy between gypsum and quartz OSL chronology exists.

Table of Contents

List of Figures

List of Tables

Chapter 1 - Introduction

Deposition of eolian sediments from dunes within closed hydrographic basins, known as endorheic basins, and around playas can serve as evidence of rapid climatic change, and are used as records of significant and punctuated climate events. It is well documented that depositional timing of eolian minerals such as quartz and feldspar can be measured using optically stimulated luminescence (OSL) for time periods of up to ~200 ka for quartz and up to ~600 ka for feldspar (Murray and Olley, 2002; Preusser et al., 2008; Rhodes, 2011). However, these minerals are not found in all depositional environments and further investigation into using alternative minerals, like gypsum, for OSL is required. Endorheic basins, such as the Tularosa basin gypsum dunes at White Sands, NM, often comprise a greater proportion of salts than quartz or feldspar minerals and would benefit from gypsum based OSL dating techniques. Choosing to investigate gypsum stems from its potential for expansion to wider depositional environments that may lack mineralogy used for direct age evaluation, including extraterrestrial applications on Mars (Szynkiewicz et al., 2008, 2010). Dunes such as those found at Knolls may also serve well as scalable, modern analogs of older eolian formations and reservoirs. By evaluating gypsum paleodunes that have not undergone diagenesis and are still unconsolidated, it is possible to evaluate preservation biases and processes in situ that researchers would otherwise have to interpolate in a rock formation. Gypsum can precipitate within minutes in arid conditions and develop salt crusts meters thick in playas over decadal to millennial time scales (Nichols, 2009). Gypsum is found in marine, lacustrine, and hydrothermal settings; isotope systems such as $\delta^{34}S$ and $\delta^{18}O$ from sediment comprised of gypsum can be examined for clues into the past. However, ages cannot be deciphered from these isotopic proxies and require use of depositional age proxies from detrital or surrounding organic rich material within siliciclastic lacustrine

sediments by other methods such as radiocarbon (^{14}C) dating (Oviatt, 2015). Use of ^{14}C dating may also come with drawbacks. In the case of Lake Bonneville, carbon reservoir effects from variable sources complicate the ^{14}C dating process (Reimer et al., 2013; Oviatt, 2015). This study aims to increase the small but growing body of knowledge of the geochronological capabilities of gypsum using samples from the gypsum dunes in Knolls, UT which lies in the Lake Bonneville basin.

1.1 This Thesis

For this thesis, Chapter 1 is the introduction to the project; Chapter 2 introduces dating method, mineralogical, and geological background; Chapter 3 is a manuscript that investigates OSL preparation and measurement techniques using modified single-aliquot regenerative-dose (SAR) protocols on gypsum minerals, and its use as a case study on dune samples from Knolls, Utah; lastly Chapter 4 is a summary of the research and main conclusions; individual chapters are followed by references and appendices.

The manuscript presented in Chapter 3 reviews the investigation and results of gypsum grain OSL preparation methods. The chemical and luminescence properties of gypsum require preparation and measurement protocols distinct from those developed for quartz and feldspar luminescence. Commonly used OSL preheat treatments (e.g. Preusser et al., 2008; Rhodes, 2011) were avoided. Mineralogical investigation of the response of the gypsum samples to a variety of preparation techniques preceded alternative OSL methods (Clark-Balzan, 2016; Mahan and Kay, 2012; Nagar, 2007; Thompson et al., 2010). A case study exploring the effectiveness of OSL protocols to constrain the depositional age of Holocene eolian-transported gypsum sands in the Lake Bonneville Basin considers whether the method is well suited for clastic gypsum grains that have been stratigraphically constrained.

1.2 Hypothesis and Objectives

The primary objective of this study is to determine whether eolian gypsum grains can produce accurate ages with the use of modified OSL dating methodologies. This includes experimentation with OSL methods to find appropriate procedures for studying luminescence signals in gypsum grains (Clark-Balzan, 2016; Mahan and Kay, 2012). The questions this research seeks to address are whether gypsum can serve as an effective luminescence chronometer with the use of modified OSL preparation methodologies and, if so, can it be used to provide a revised chronology of dunes at Knolls, Utah.

The problem presented is believed to be solvable given certain criteria, including effective preparation methodology to isolate the mineral, preserve the crystal lattice, and maintain luminescence charge traps. Gypsum OSL signals can be very weak (Mahan and Kay, 2012; Nagar, 2007), therefore, signals must also be measurable. Logically if gypsum luminescence centers can be identified and targeted successfully, natural and regenerative luminescence decay curves can be determined and used to quantitatively identify depositional ages of dunes and possible stabilization periods. Previous research suggests this is possible (Clark-Balzan, 2016; Mahan and Kay, 2012; Nagar, 2007). Nagar (2007) successfully identified a distinct OSL signal from gypsum that would require further exploration which Mahan and Kay (2012) and Clark-Balzan (2016) studied. Mahan and Kay (2012) attempted to date deposition of crystalline, in-situ gypsum, identifying nine ages from crystalline gypsum and seven ages from detrital quartz, noting a lower preheat was more favorable for gypsum OSL methods. Clark-Balzan (2016) furthered this with his modified ambient preheat OSL methodology. We aimed to model our modified OSL methods after Clark-Balzan (2016) and verify ages using an established OSL protocol on rare detrital quartz in our gypsum grain samples. We used a multifaceted

approach, outlined below, to develop the gypsum OSL methodology, and to guide interpretations of the depositional environment of dunes at Knolls, Utah:

1. Characterize sediment to confirm eolian transport and mineralogy
    a. X-Ray Diffraction (XRD) and Scanning Electron Microscopy (SEM) qualitative analyses of samples to determine bulk mineralogy and to define the effects of laboratory treatments
    b. Particle size analyses to provide quantitative evidence of mineral etching
2. Improve preparation techniques for OSL measurements using gypsum grains
    a. Analyze preparation steps systematically to determine best isolation and preservation treatments
    b. Determine the ideal laboratory conditions for preserving luminescence signal by conducting bleaching experiments under various laboratory lighting conditions
    c. Determine the effects of etching treatments
3. Apply OSL geochronological method to a case study on dunes from Knolls, UT; this step will examine the validity of this gypsum-based method
    a. Utilize modified SAR protocols based on Clark-Balzan (2016) to determine gypsum grain depositional chronology from samples in stratigraphic superposition
    b. Identify ages of dune formation, and periods of stabilization
    c. Use rare detrital quartz grains in gypsum samples as a comparison of stratigraphic age correlation and accuracy; quartz OSL methodology is well established and a reliable geochronometer of depositional ages

Chapter 2 - Background

"So, what you're telling me is, you shine a light on some rocks and they shine some light back at you." -Thomas Desmond Fitzgerald

This concept, which my husband summed up in one sentence after I tried to explain the idea of OSL over the course of at least half an hour, is indeed what happens. However, the physics behind the concept that helped establish this relatively new geochronological method—used to date geologically young sediment, archaeological findings, and to measure radio-dosimetry post exposure—is slightly more complicated.

2.1 Optically Stimulated Luminescence

OSL dating, as Thompson et al. (2010) describe, is based on the "photon-assisted" release of electrons from charge traps that naturally exist in a mineral crystal structure. Huntley et al. (1985) spearheaded this method verifying light-sensitive charge traps, and demonstrating that these charge traps can be used to quantify environmental radiation exposure since daylight resetting and post deposition, and consequently provide sediment burial ages. From this point, development of OSL began to flourish, resulting in the development of the SAR protocol for quartz (Murray and Wintle, 2000, 2003; Wintle and Murray, 2006). This protocol includes measurement of a natural OSL signal and the iterative regeneration of OSL from known radiation doses. Regenerative OSL data are used to construct a growth curve, similar to a calibration measurement. Interpolation of natural OSL with growth curve data enables estimation of the amount of radiation dose the natural signal is equivalent to, or equivalent dose (D_e). Normalization measurements correct for sensitivity changes enabling precise estimates of D_e from a single aliquot of quartz or feldspar grains. This protocol is the foundation of D_e assessment for gypsum OSL methodologies.

In the OSL method, inherent defects in a crystal lattice are exploited as charge traps. When sediment is buried, it is exposed to environmental radiation resulting in ionization of minerals. When ionization occurs, freed electrons can become trapped in lattice defects. Over time, trap populations increase; if mineral grains are "zeroed" at deposition, they have been exposed to sufficient natural sunlight to release electrons from most or all traps. Electrons can then recombine at a lower energy state resulting in the production of a photon. OSL laboratories use light emitting diodes to stimulate this energy release and recombination. Resulting photons are then detected using a photomultiplier tube (PMT) and translated into a decay curve. The total radiation dose or D_e a mineral receives is determined after calibrating the natural OSL signal against a regenerated OSL growth curve. Age calculations compare D_e with environmental dose-rate data. Measuring environmental dose rate on site using tools such as a gamma ray spectrometry scintillator or elemental analysis (ICPMS-OES/AES) after collection is common. These factors as well as numerous others (i.e. water content, cosmic parameters, altitude, etc.) are all parts of the calculations used to determine the age of last exposure.

Limitations were identified as research in quartz OSL became more sophisticated. Quartz is not located in all research sites and, arguably just as important, there are also sites where quartz may not have been adequately bleached, such as in glacial till (Lukas et al., 2007; Spencer and Owen, 2004) or in rapidly deposited fluvial and alluvial environments (Spencer et al., 2003; Spencer and Robinson, 2008; Ataee, 2019). Partially bleached sediment results in age overestimation (Duller, 2004) and the lack of quartz requires the use of proxies or other dating methods to fill the age data gap. In addition, mineral saturation of quartz limits OSL dating to samples with burial ages less than ~350 ka (Murray and Olley, 2002). With these limitations in mind, researchers turned their focus to feldspars. Given its widespread occurrence, higher

sensitivity to light, and saturation rates that surpass quartz, feldspars have luminescence signals that can be used to date older sediment (Hütt et al., 1988; Roberts, 2012; Thiel et al., 2011; Thomsen et al., 2008); however, not without its own limitations. Feldspar is prone to the loss of electrons from specific traps, known as anomalous fading, and much of the research in this field has been dedicated to correcting this (Wintle, 1973; Spooner, 1992, 1994). Thomsen et al. (2008) discovered a method to overcome fading using post-infrared high-temperature infrared stimulated luminescence (pIRIR) and research has continued to look forward (Roozeboom, 2015). It is with these constraints in mind, that we worked to expand suitability for OSL in different environments using gypsum grains.

2.2 Gypsum Mineralogy

Gypsum, or calcium sulfate dihydrate ($CaSO_4 \cdot 2H_2O$), is a hydrated monoclinic mineral with a hardness of ~2 and density of 2.34 g/cm^3. Gypsum dehydrates at approximately 100°C, resulting in mineral recycling between gypsum, its partially hydrated variations, and anhydrite (Adekola et al., 2018). This is relevant when considering the environmental conditions that samples may have been exposed to, as well as the laboratory conditions samples will be subjected to for OSL analyses. When considering what laboratory tests gypsum can withstand, it is significant to note HCl treatments at ~80°C for 1-5 hours result in the dissolution of gypsum with minor transformations of calcium sulfate dihydrate to anhydrite (Li and Demopoulos, 2005; Adekola et al., 2018). This information is relevant when considering temperature constraints and aliquot preparations of gypsum grain samples.

Cleavage exists on the 100 and 001 planes, while water molecules create a hydrophilic 010 plane (Feng et al., 2017). This is important when visually analyzing gypsum grains under the microscope. Assessments using SEM are especially significant as cleavage and elemental

mapping from the SEM can be compared to determine mineralogical correlations and effects of preparation methods.

2.3 Geological Setting

In order to know whether gypsum might yield accurate OSL results for Knolls, UT, knowledge of the area's geological background is necessary, and therefore a general understanding of post-Lake Bonneville history is required. The samples and study site lie within the footprint of Pleistocene megalake Bonneville depicted in Figure 2.1, which existed until around 12 ka. Its disappearance was caused by water loss as a result of dam failure at Red Rock Pass in Idaho and evaporation due to more arid climate conditions (Oviatt, 2015; Boden, 2016). Other quartz-based dune fields formed post-Bonneville are drawn on the map as an indicator of the relative area the overall gypsum dune fields associated with the Knolls field use. The gypsum fields are spatially more widespread and take up far greater areas than the quartz-grain-based fields that developed at similar times. Dean (1978) extensively mapped silica- and gypsum-based dunes of the Great Salt Lake Desert, estimating gypsum dunes at and around Knolls cover 389 km^2. The source of such abundant gypsum is believed to be from the desiccation of Lake Bonneville evidenced by the Salt Flats clays (Dean, 1978; Boden, 2016) and lake bottom clays of Great Salt Lake (Jones, 1953; Eardley and Stringham, 1952) which have selenite (gypsum) crystals growing with similar primary cleavage to that found in our samples. Both source and topography are likely reasons for these differences, however, this is not the focus of this study and is intended as a general reference of spatial scale.

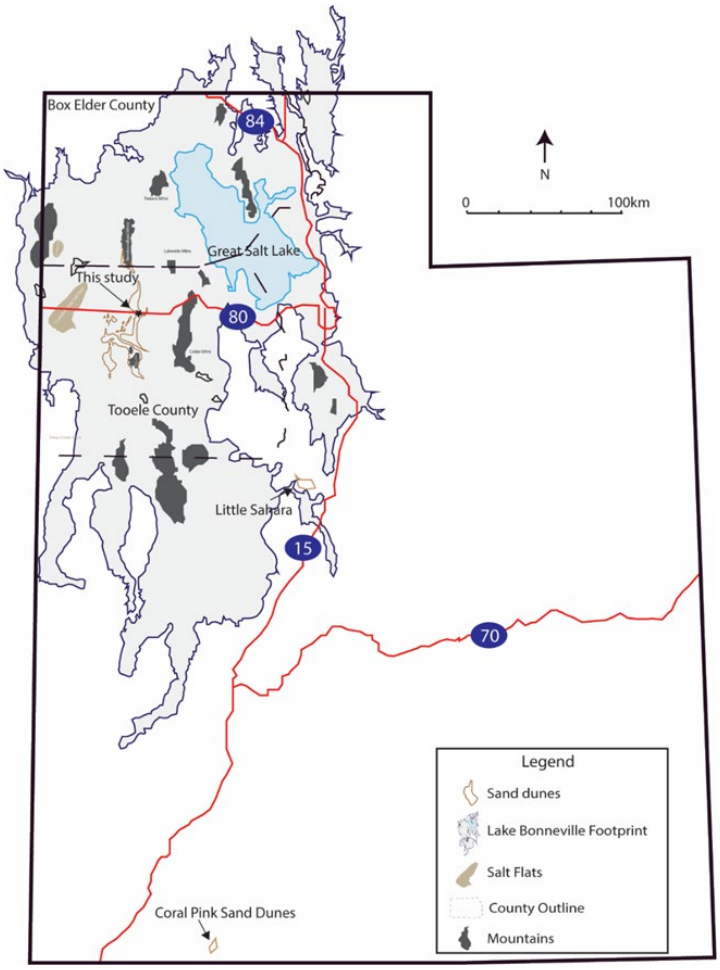

Figure 2.1 Extent of Pleistocene Bonneville shoreline compared to modern Utah state lines. Notable dune fields, mountainous areas, and modern Great Salt Lake are also shown. (Based on Nolan, 1927; Oviatt, 2015; Department of Commerce road maps; USGS county maps)

Lake Bonneville grew and shrank several times as depicted in the hydrograph of Figure 2.2. The chronology associated with the hydrograph includes the estimated age of the Knolls gypsum dunes in relation to the Bonneville basin. Prior to this study, there were no identified events between the Gilbert episode (~12-10 ka) to present of either significant climatic or geomorphologic change - such as the dune building event(s) that created the Knolls study site. The addition of the Knolls dune depositional ages increases our understanding of the paleoenvironment within the post-Lake Bonneville footprint.

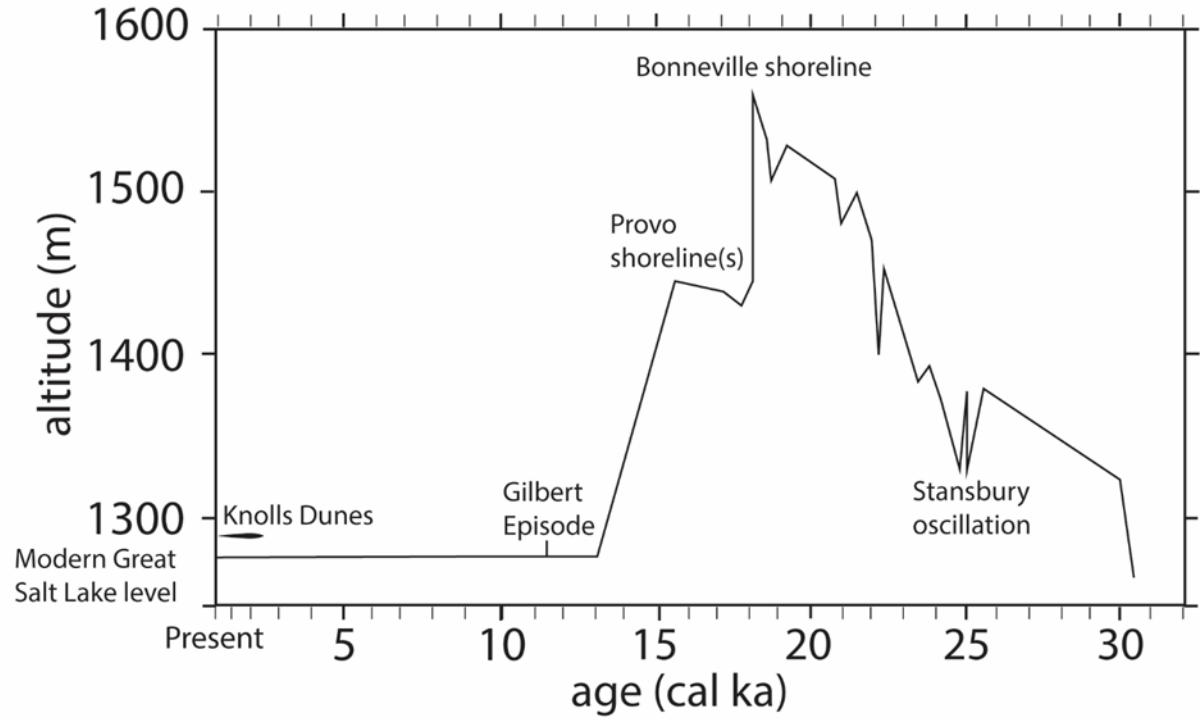

Figure 2.2 Hydrograph of Lake Bonneville cycles since 30 ka and shoreline ^{14}C ages with estimated Knolls dune OSL ages (black lens/line). Note the altitudes are adjusted for isostatic rebound except for altitudes below 1300 m as was standard in the original plot from Oviatt (2015). Redrawn from Oviatt (2015).

The Knolls dune field is named after Knolls, Utah (40.7230° N, 113.2897° W) located just east of our study site. The dunes where samples were collected from, are situated within the Great Salt Lake Desert and at the north entrance of the Bureau of Land Management Knolls Recreation Area. The sample site appears to be a small understudied field of gypsum dunes when observed from the ground (refer back to Fig. 2.1, black dot just to the south of Interstate Highway 80). However, when observed from above in map view (see Ch. 3, Fig. 3.1), the dunes sampled in this study are part of a larger series of dunes (Nolan,1927; Dean, 1978; Boden, 2016; Clark and Oviatt, 2019) outlined in brown (outline redrawn from Nolan, 1927), crossing Interstate Highway 80 and is known as the Knolls dune field hereafter.

The sampled dunes are isolated by man-made structures, and extend approximately 200 m by 600 m, bordered on all sides by either roads or rail line. The dunes abruptly end at the railroad to the south, leaving a slip face approximately 4 m in height often used by recreational vehicles visiting the BLM recreation area. Salt playas exist in the vicinity as extensions of the world renown active Salt Flats west of the study site and precipitate evaporites including gypsum extensively to the north. Commercial salt works operate north of the interstate. Gypsum dunes as documented by Boden (2016) extend far beyond our sample site and cover 11% of the Great Salt Lake Desert.

This study did not investigate the source of gypsum sand analyzed from the Knolls dunes, however it likely precipitated interstitially and grew secondarily in the mud of playas in the Great Salt Lake Desert as rising groundwater evaporated at the ground surface (Eardley, 1962; Dean, 1978; Boden, 2016; Oviatt and Clark, 2019). Wind would have then deflated these mudflats and playas, suspending silt- and clay-sized particles and saltating sand-sized particles, including gypsum crystal grains, into dunes (Boden, 2016; Oviatt and Clark, 2019). The mud in the Great Salt Lake Desert consists mainly of medium- to fine-grained sediment of Lake Bonneville (Boden, 2016). Primary evaporites exist mostly as NaCl salts in the Bonneville Salt Flats west of Knolls and are unrelated to the dune field.

Dune systems have complex histories and hold important environmental data in dry, desert regions that lack alternative proxies and archives. Repeated depositional and erosional processes often cause complications with structural interpretations and require a high-resolution sampling to mitigate enigmatic results (Leighton et al., 2013). The three-dimensional exposure at the Knolls site provides distinct and stratigraphically constrained semi-consolidated clastic gypsum with which to work. Internal primary sedimentary structures are clearly visible;

sampling intervals taken above and below bounding surfaces can provide researchers with new data and revised chronology.

Prior ^{14}C dating of Lake Bonneville samples including shells, tufa, and organic plant material used in conjunction with sedimentological evidence shows that the regional climate fluctuated following the last regression of Lake Bonneville, in what is known as the Gilbert episode, approximately 12 ka BP (Oviatt, 2015). This association with regional aridity provides a maximum age for the origination and construction event(s) of the Knolls dunes but does not provide sufficient resolution to determine whether multiple punctuated climatic events produced the localized geomorphic features over the last 12 ka. Lake Bonneville Basin has been well studied, and as a result various proxies are available that can provide reliable and independent geochronologic constraints (Gilbert, 1890; Oviatt and Shroder, 2016). We use these time constraints to test the outcome of our gypsum grain OSL ages.

Chapter 3 - Manuscript

INVESTIGATING THE POTENTIAL OF OSL PROTOCOLS ON EOLIAN GYPSUM SAMPLES FROM KNOLLS, UTAH

Fitzgerald, Victoria T.*, Spencer, Joel Q.G., Oviatt, Charles G., Rader, Mikaela

Department of Geology - Kansas State University, Manhattan, KS 66502, USA

**Corresponding author: vtf@ksu.edu*

Keywords: luminescence dating, preparation methods, gypsum OSL

3.1 Abstract

Eolian processes and resulting dunes are direct geomorphic expressions of punctuated climatic events and overall paleoclimate. Spatial and temporal changes can be well defined and resulting ages act as archives of sedimentary environments of deposition. Gypsum is both an evaporite and sulfate and is abundant around the world, but has yet to become an established mineral of choice for geochronologists when considering OSL dating techniques. If refined, the addition of gypsum grain dosimetry to sedimentary environments dominated by this mineralogy may improve the resolution of paleoclimate history and our understanding of sedimentary processes involving evaporites and sulfates. Effective preparation of mineral grains for optically stimulated luminescence (OSL) dating is a key factor for determining accurate ages. Gypsum grain preparation for OSL dating and adapted single aliquot regenerative-dose (SAR) experimental procedures were used to characterize clastic, eolian gypsum grain samples and determine the depositional ages of dunes at Knolls, Utah. Given the thermal transformation of gypsum, all preparation and measurement steps were modified to temperatures below the

transformation threshold of 90°C. Water was avoided during sieving to reduce the chance of flocculation and mitigate grain dissolution. The eolian gypsum samples from Knolls, Utah, were air-dried and dry-sieved then treated with ~36 wt% HCl at 60°C for 40 min, all under low-intensity red-light conditions. Samples were then air-dried again, mounted on discs, and subjected to a modified SAR protocol that included a long ambient-temperature preheat for 10,000 s and OSL measurement at 30°C. Heavy liquid separations were determined to be unsuitable for mineral isolation. Samples typically displayed small natural luminescence signals within the detectable range using this method. Age results using gypsum determined the most basal sample of all dunes sampled, Knolls Paleodune A (KNP-A) was deposited 1.45 ± 0.08 ka; the stratigraphically highest sample, coppice dune 5 (CD-5) was deposited 0.09 ka. The single quartz sample dated by OSL determined the same most basal sample of KNP-A was deposited 2.26 ± 0.22 ka. Interpretations of this discrepancy include several hypotheses which might be tested in future studies. The relative ease with which gypsum may be thermally transformed may cause loss of trapped electrons creating a consistently smaller D_e. Grain size and density differences between quartz and gypsum might also give rise to age discrepancy; smaller grain size and lighter density of gypsum clasts may suggest relatively longer periods of saltation and reworking prior to final deposition than larger, more dense grains of quartz. This study has clearly shown that the dunes at Knolls are in fact much younger than previous research, which suggested the gypsum dunes were developed closer to the end of the Gilbert episode approximately 12.5 ka BP.

3.2 Introduction

Dating eolian dunes using OSL dating methods can be robust (Ashley et al., 2011, 2017; Johnson et al., 2019) but is limited by choice of mineral, with the vast majority of studies relying

on the use of quartz or feldspar grains. However, there are many locations - like Great White Sands, New Mexico; Salt Basin Dunes, Guadalupe Mountains, Texas; and the Atacama Desert, Chile - that are of geologic interest and almost entirely consist of gypsum. Continuous wave optically stimulated luminescence (CW-OSL), hereafter referred to as OSL, has the potential to be used as the source of luminescence dating techniques in areas comprised mainly of gypsum.

Previous studies have used OSL to determine the depositional age of dune samples using only gypsum grains. However, all but two of the studies (O'Connor et al., 2011; Clark-Balzan, 2016) relied on a secondary method of dating such as U-series or electron spin resonance to determine gypsum formation and depositional age. Another study used only in situ crystalline gypsum rather than eolian transported sediment to determine the age of formation (Mahan & Kay, 2012). Gypsum signal stability has been the focus of much of the research in this field and variability of results may in part be due to how the gypsum grains have been prepared, although the effect of temperature and dehydration have also been addressed (O'Conner et al., 2011; Clark-Balzan, 2016). In particular, ambient temperature preheats during single-aliquot regenerative-dose (SAR) protocols have been used (Detschel and Lepper, 2009; Thompson et al., 2010; O'Connor et al., 2011) , however, the use of long pauses with ambient preheats have only been addressed by Clark-Balzan (2016). Previous attempts to use gypsum as an OSL chronometer successfully utilized blue light stimulation (470 ± 30nm) at ambient temperature with detection of luminescence in a UV band (O'Connor et al., 2011; Clark-Balzan, 2016). O'Conner et al. (2011) presented data indicating sensitivity corrections for gypsum range from 1-14% with short pauses. Clark-Balzan (2016) successfully used long ambient temperature preheats for 10,000 s to replace short high temperature preheats during SAR protocols resulting in recycling ratios within two sigma of unity. The long ambient pauses overcame sensitivity

changes, but still resulted in age underestimation. Variable OSL age results exist across these studies, likely due to the variability across samples and sample preparation; therefore this study focused on determining preparation protocols which minimized the effects on mineralogy and most likely preserved the luminescence signal of gypsum.

Protocols optimizing OSL preparation and producing accurate and precise ages of gypsum are vital to improving our understanding of the physical and temporal processes involved in resulting sedimentary rock stratigraphy. The typical quartz and feldspar OSL protocols are not directly interchangeable for use with gypsum, a soluble mineral with an easily thermally-transformed crystallographic structure. Gypsum is a hydrated evaporite, chemically precipitated at or near the surfaces of arid environments (Schreiber and Tabakh, 2000). As such, mineral precipitation occurs due to evaporation of solution from within underlying rocks, by supersaturated brine pools, or by groundwater interaction. Resulting gypsum ($CaSO_4 \cdot 2H_2O$) crystals are soluble and may be dehydrated gradually to form hemihydrite ($CaSO_4 \cdot ½ H_2O$) at a temperature of 356 K or 82.85 °C and eventually anhydrite ($CaSO_4$) at higher temperatures (100-250°C) (Prasad et al., 2001; Ramachandran et al., 2002). Crystallographic changes from monoclinic to orthorhombic structures that accompany dehydration are likely to significantly alter the luminescence characteristics of gypsum (Clark-Balzan, 2016), and thus must be minimized to ensure accurate and consistent dosimetric behavior. We hypothesize that this transformation alters luminescence characteristics necessary to calculate accurate depositional ages, resulting in age underestimation as demonstrated in previous studies testing OSL of gypsum under various preheat conditions (Clark-Balzan, 2016; Mahan and Kay, 2012). For this reason, in the work described here temperature criteria were established as part of this study based on Clark-Balzan (2016). This paper proposes important mineralogical considerations when

using gypsum for OSL dating and discusses experiments to test if depositional age rather than formation age was acquired for our gypsum samples.

3.3 Study Area

All samples used for this study were collected from dunes at Knolls, Utah (Fig. 3.1 and 3.2 for reference). Dunes KNP-A and KNP-B are adjacent to each other and 30 m apart. The coppice dune lies 60 m SE of KNP-B and is stabilized by vegetation (Fig. 3.1 and 3.2).

KNP-A is the larger of the dunes standing approximately 7 m in height and consists of partially cemented and semi-consolidated gypsum sands with large scale cross stratification from the most basal section of the dune above the surface to approximately 6 m high. At this point a visible bounding surface is observed where planar laminations overly truncated crossbeds. These laminae continue for approximately 1 m. The dune would be described as a barchan dune if it were not for the indurated features. It can be reasonably interpreted that this dune is actually two dunes superimposed on each other or possibly a dune with interdune overlying it. Duricrusts protect most of the dune from further erosion and extend to a depth of no more than 2-3 cm. Laminations above and below the bounding surface display inverse grading.

KNP-B is smaller and capped by a bush/tree trunk. This dune is also semi-consolidated and has more bioturbation than KNP-B. Burrows for bugs to small mammals are visible and every attempt to sample away from plants and bioturbated sediment was made. KNP-B is separated from KNP-A by 30 m of interdune, although the interdune's cemented surface has cross-stratified laminae that extend from the base of KNP-A to KNP-B, where the apparent dip and actual dip meet. This is the basal section that was sampled for OSL ages and is overlain by a bounding surface that is less clear due to draped duricrusts. Figure 3.3 displays two bounding surfaces, but only because it was not immediately clear where the surface started. The lower

bounding surface identified at KNP-B is a true bounding surface and is characterized by planar to hummocky bedding that overlies truncated cross-strata (Fig. 3.4).

The Knolls dunes are believed to have formed after the last Late Pleistocene regressive phase of Lake Bonneville, which was a time of closed basin hydrography and a rapidly warming climate that reduced the lake to mudflats and playas (Gilbert, 1890). Ground water evaporation in these playas and mudflats contributed to gypsum growth in interstitial spaces (Gilbert, 1890). Deflation from the renowned Salt Flats west of our site and consistent winds blowing down the mountains to the east have kept the dune field active, with significant movement (Fig. 3.5) from 1953 to 1972.

Sediment at Knolls dunes appears homogenous visually; microscope analysis reveals a composition mainly comprised of a single or bimodal mineralogy, gypsum and calcite, of various fraction sizes (Fig. 3.6) with noted frosting of gypsum crystals. Frosting and subangular to rounded grains were observed in gypsum and serve as an indicator of eolian transport. Calcite present was observed as pill shaped and is assumed to be the remnants of shrimp pellets previously observed by the Utah Geological and Mineralogical Survey and others (Eardley, 1962; Oviatt, 2015; Boden, 2016). Trace quartz and feldspars associated with Tertiary deposits in the Great Salt Lake Desert exist in samples as well (Jones, 1953).

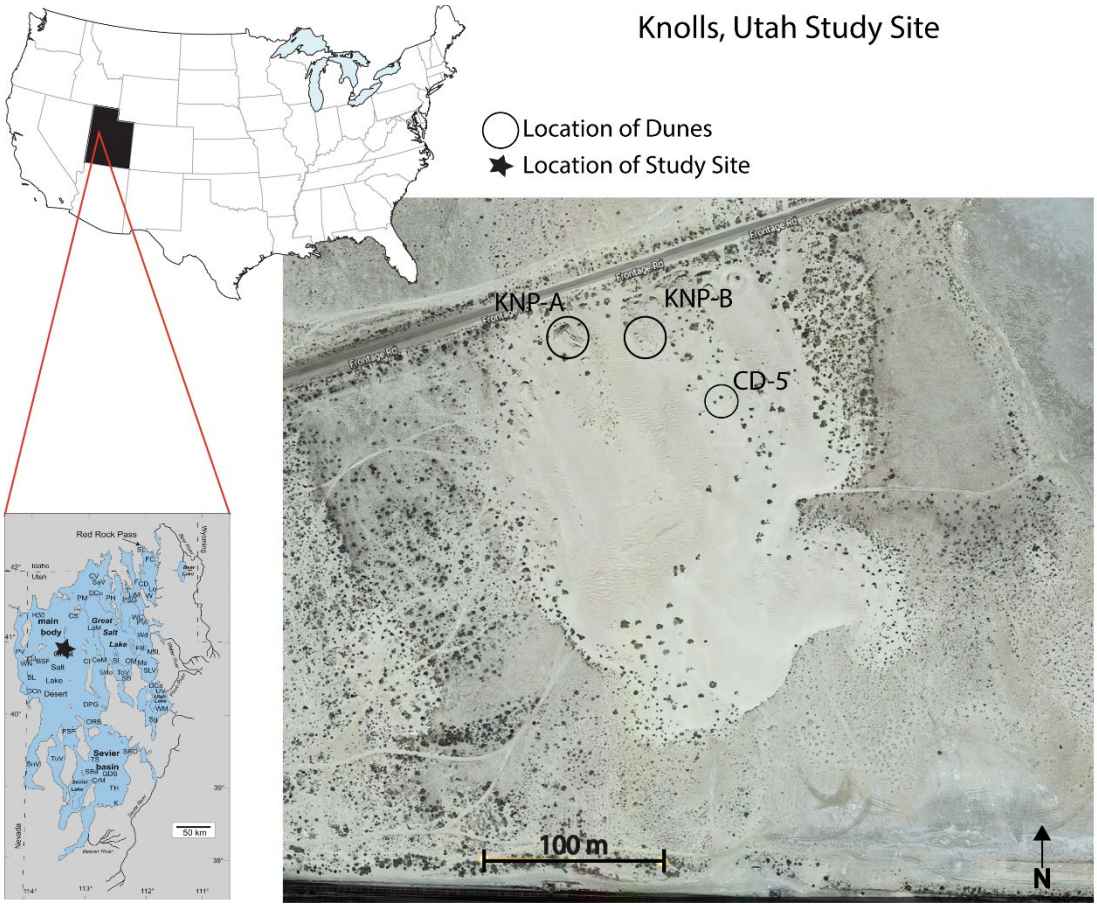

Figure 3.1 Knolls, Utah overview map; Lake Bonneville footprint at largest extent of lake (lower left image); approximate location of sampled Knolls dunes, the Bureau of Land Management (BLM) recreation area is directly south of this image and not pictured; (Oviatt, 2015; Google Earth, 2015)

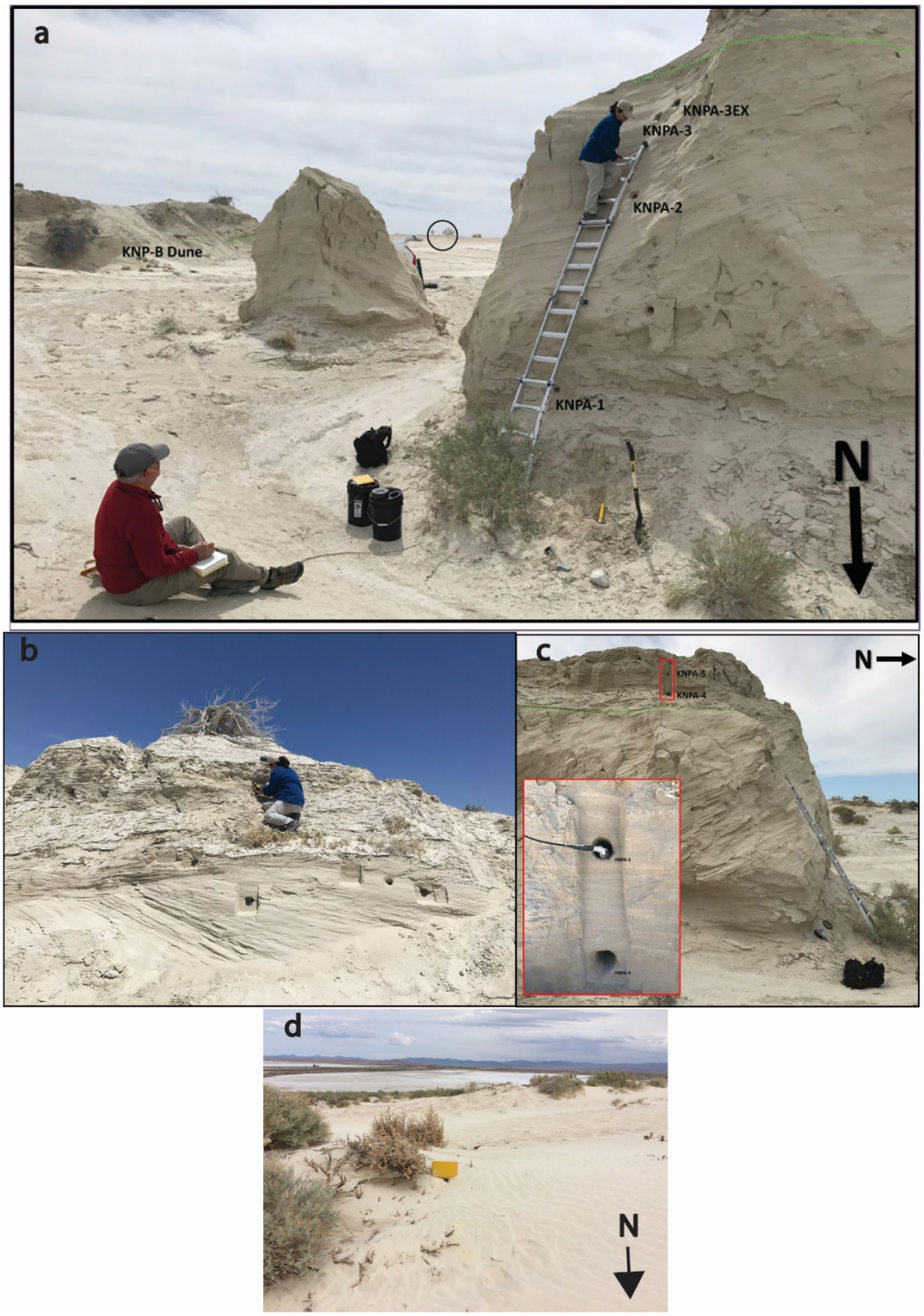

Figure 3.2 Study Site overview of all dunes sampled. a) location of KNP-A (far right); KNP-B (far left); CD-5 (small black circle in center of image); b) image of KNP-B while sample KNP-B4 is being collected; c) image of KNP-A (green dotted line is interpreted bounding surface) with inset of sample locations of KNP-A4 and A5; d) image of modern, active, coppice dune (CD-5) sampled approximately 7cm from surface.

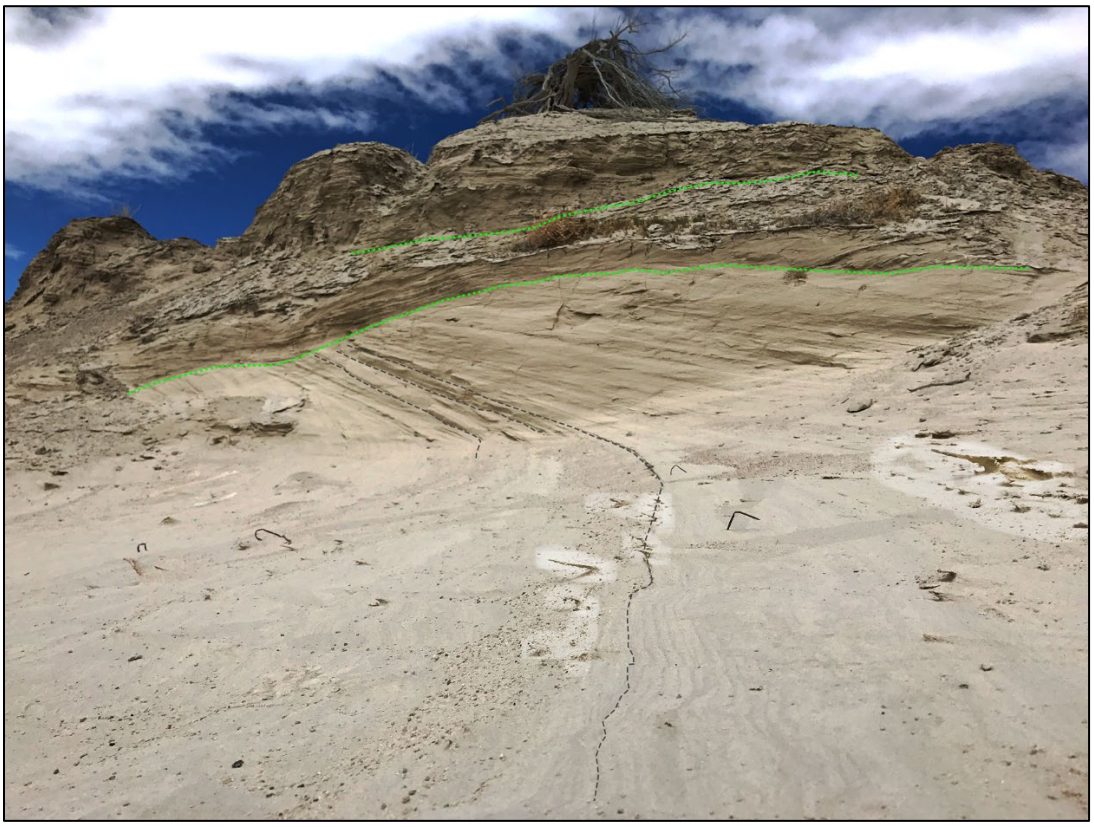

Figure 3.3 Knolls paleodune B (KNPB) with visible cross strata (gray dotted line) and bounding surface (lower green dotted line). Note the cemented, pavement-like interdune leading into the semi-consolidated dune sediment.

Knolls, Utah lies between the Bonneville Salt Flats and the Great Salt Lake. The dunes formed here are significant to our understanding of Holocene paleoclimate in western Utah and possibly the region. As archives of punctuated climatic events, researchers can tease proxies out of dunes to better understand temperatures and atmospheric compositional changes. However, without a geochronology to accompany this data, studies are left with general correlations and cannot provide the precision and predictive analyses associated with timed cycles. The dunes studied in this paper may provide the geochronology necessary for researchers to update and correlate paleoclimate proxies, improving our comprehension of climate change in the last 10,000 years.

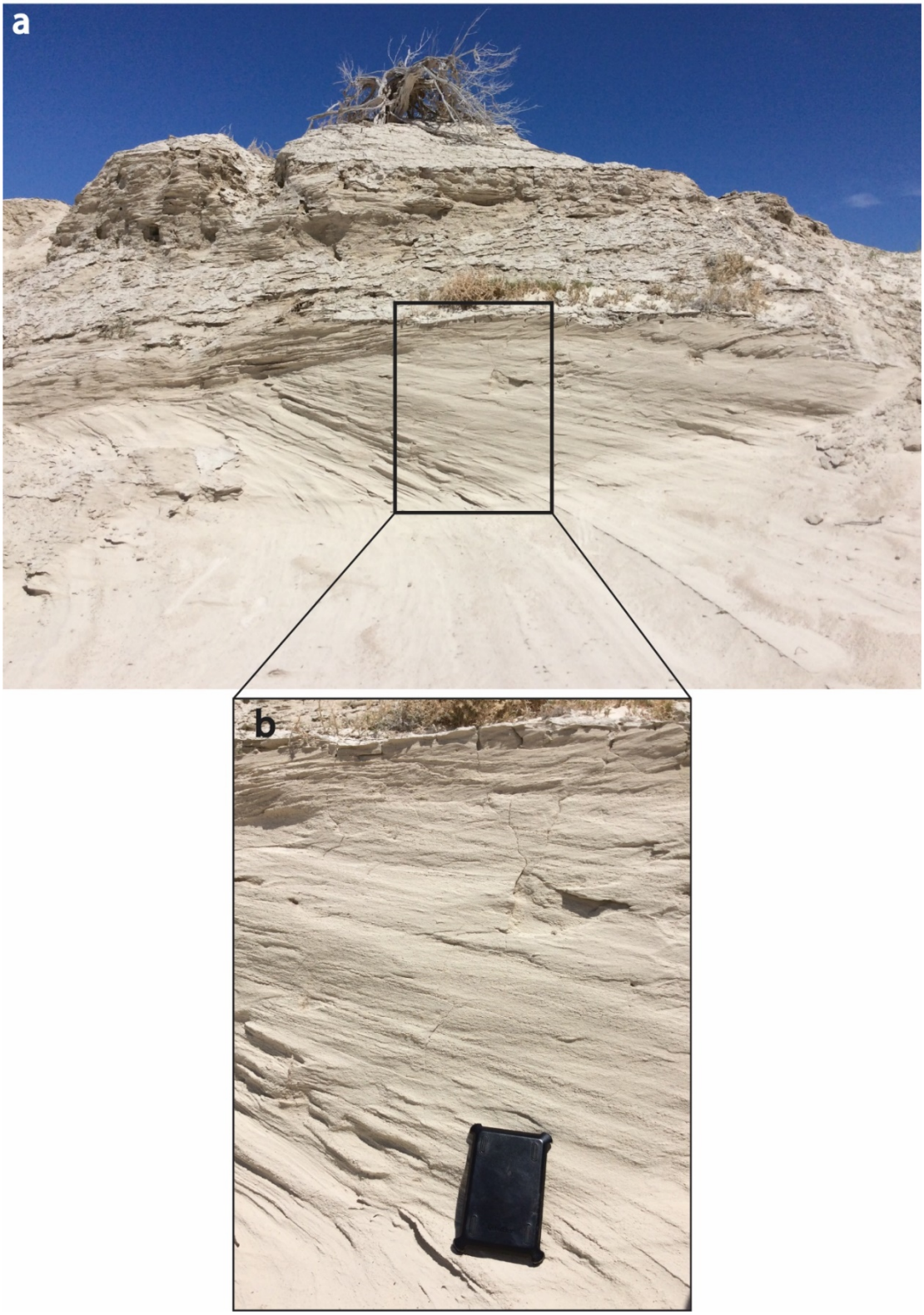

Figure 3.4 Image of KNP-B sedimentology. a) overview of dune, note the anchored dead bush/tree on top and small grasses overlying (several cm above) interpreted bounding surface; b) inset with close up of cross strata truncation at hummocky to planar laminae.

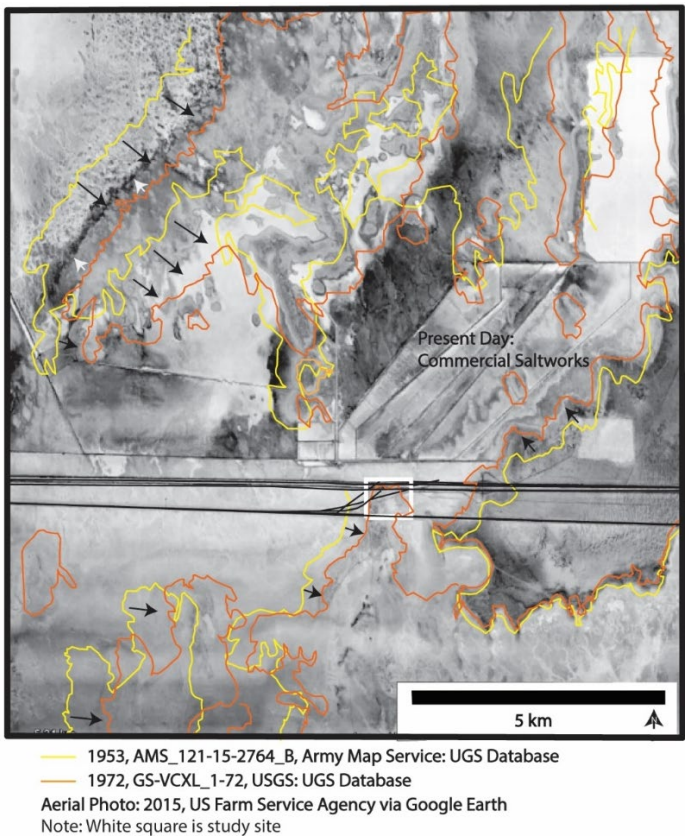

Figure 3.5 Knolls Dune Study Site overview; historical migration (>6 decades) patterns seen in yellow and orange with most recent dune placement in background aerial photo.

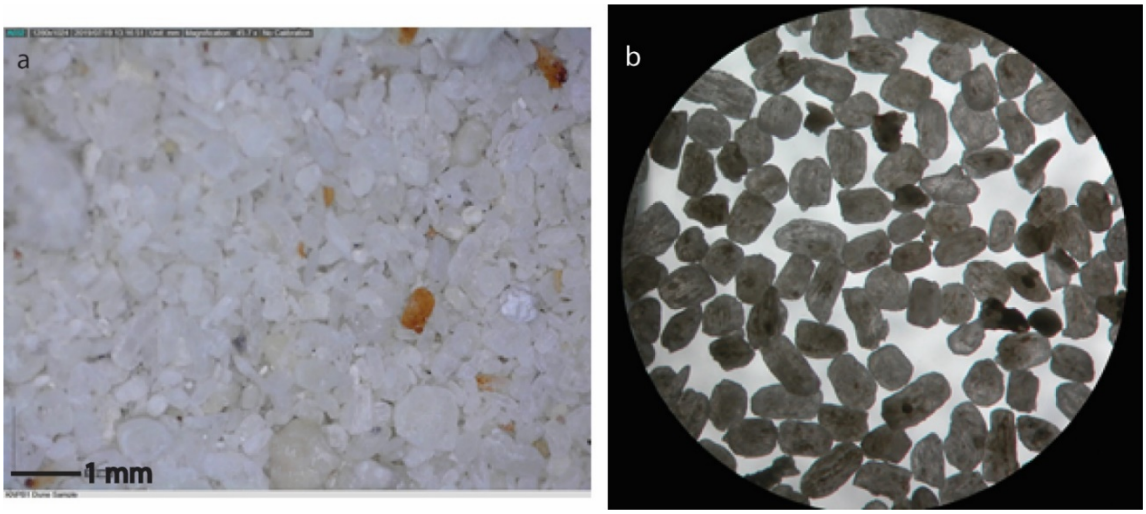

Figure 3.6 Sediment from Knolls Dune B (sample KNP-B1); a) non-sieved sample image of Knolls Dune B sand grains using a Dino-Lite™ microscope, b) 212-250 µm sieved fraction under transmitted light microscope.

3.4 Methods

3.4.1 Sampling and Instrumentation Details

Samples used in this study were collected from sections of two adjacent eroded and indurated paleodunes, KNP-A (40°43'28"N, 113°16'50"W), KNP-B (40°43'29"N, 113°16'49"W), from altitudes between 1284 m to 1296 m above sea level (Figs. 3.1 and 3.2); in addition, a sample located SE of KNP-B was collected from a surficial Coppice dune (CD-5, 40°43'28"N, 113°16'46"W) considered to be active and a suitable modern analog. Paleodune samples were collected from steep exposed faces with traceable laminations on three sides (refer back to Fig. 3.1). Three representative samples were taken from below the bounding plane identified by truncation of cross stratified sands. The overlying planar laminations were sampled at two intervals chosen as representative samples of the overall section. All samples were composed of fine to coarse sand grains and mineralogy included approximately 95% gypsum grains, 1-4% quartz grains and 1-4% oolites or broken carbonates. The assumed oldest section and base of the semi-consolidated dune KNP-A was not sampled due to difficulty identifying primary sedimentary structures through duricrusts draped around the base. Samples were collected by hammering sections of galvanized steel conduit pipe, ~4 cm-in diameter and ~15 cm-in-length, into exposures that had been cleaned back to remove weathered surface sediment. Sampling strategy ensured samples were taken from recognized beds with primary sedimentary structures with no observable post-depositional disturbance (e.g. bioturbation caused by burrowing, roots, insect activity, etc.). The ends of the tubes were sealed with black duct tape to prevent movement of sediment grains during transit.

Luminescence measurements were conducted using a Risø TL/OSL DA-20 reader (Bøtter-Jensen et al., 2003), equipped with a $^{90}Sr/^{90}Y$ β source delivering ~0.131 Gy/s to each

aliquot. Continuous wave (CW) OSL SAR protocols using standard blue LED 470±30 nm emission, but with modified low-temperature measurement of 30°C and ambient-10000 s preheat (Clark-Balzan, 2016), were completed using 3 and 5 mm diameter gypsum aliquots mounted on 10 mm stainless steel discs with Silkospray™ and spray masks. Established quartz methodology was followed for quartz aliquots. Initial measurements of quartz grains were completed by mounting 1 mm aliquots onto 10 mm diameter stainless steel discs with Silkospray™. However, after several failed preheat and dose recovery measurements, aliquots of 3mm size were used to complete analyses. Standard detection optics comprising an EMI 9635QA photomultiplier tube and 7.5 mm Hoya U340 UV filter were used.

3.4.2 Preparation Methods

A variety of preparation steps were investigated as indicated in Table 3.1. Thermal transformation was mitigated by air-drying samples between each preparation step. Experimental products were initially assessed using X-Ray Diffraction (XRD) for qualitative mineral identification; mineral isolation was confirmed using Scanning Electron Microscopy (SEM) for select sample preparations chosen to be used for OSL analyses. After passing mineral identification through either XRD or SEM, dose recovery tests were conducted to determine which samples produced recoverable luminescence signals.

Sieving	10 wt % HCl	30 wt % H_2O_2	2.37 g/cm^3 Lithium metatungstate	2.70 g/cm^3 Lithium metatungstate	48 wt % HF
Wet					
Dry	30 min				
Dry	30 min	3-5 days			
Dry	30 min	3-5 days	60 min		
Dry	30 min	3-5 days	60 min	60 min	
Dry	30 min	3-5 days	60 min	60 min	40 min

Table 3.1 Preparation methods pursued to determine effective gypsum OSL protocols. All samples were air-dried before proceeding with sieve treatments and in between each preparation step. H_2O_2 treatment times varied and were dependent on cessation of

conspicuous effervescence. Lithium metatungstate (LMT) is the heavy liquid used to separate gypsum (2.37 g/cm^3) and quartz (2.70 g/cm^3). Final HCl treatment post HF treatment was not pursued due to conspicuous change in gypsum crystallinity indicated in SEM analyses.

Wet and dry sieving processes were analyzed for efficacy of grain size isolation. Wet sieving was attempted, although data from Feng et al. (2017) suggest gypsum etch pits occur <1 min after contact with water and Peruffo et al. (2013) document etch pit coalescence at times >15min. Dry sieving was conducted using a Retsch model AS200 sieve shaker for 45 min at 80 amplitude after sediment was air-dried at room temperature over the course of several days to 2 weeks.

The drying of samples is also an important consideration when preparing gypsum for OSL techniques. Established silicate protocols outlined in papers such as Spencer and Owen (2004), use oven drying at 50°C for several hours. Oven drying procedures were removed from consideration due to the possibility of mineral transformation and loss of luminescence signal. Air-drying was a technique established early in the preparation process to reduce exposure time to elevated temperatures; likewise, wet sieving was eliminated to prevent dissolution of soluble gypsum grains. Gypsum is known to be a natural flocculant (Peruffo et al., 2013; Boden, 2016), therefore wet sieving also inhibits accurate grain size fraction distributions. All drying between treatments was completed at ambient temperatures for approximately 1-2 weeks. This was the average time a sample required before a final dry mass was determined via two unchanged measurements of mass at least 12 hours apart. After an effective drying process was established, further treatments were used on air-dried and sieved samples. A 10 wt % HCl treatment, which is a standard carbonate removal procedure, followed by H_2O_2 treatments to remove organics were completed. Lithium metatungstate was used to separate gypsum from quartz and quartz from any

feldspar grains that might exist and separation success was determined using SEM and associated elemental mapping.

Magnetic separation using a S.G. Frantz LB-1 Magnetic Barrier Laboratory Separator was briefly pursued as an alternative to density separation. The side slope was set to -3 and the forward slope was set to 3.5 (S.G. Frantz engineer, personal communication, 2017). Approximately 3 g of gypsum were used for separation tests under standard laboratory fluorescent white lighting. Repeated magnetic separations (0.1, 0.3, 0.5, 0.7, 0.9 amps) were conducted on the same subsample of gypsum. Any separates from the main sample were kept and examined using standard binocular microscopy.

3.4.3 Etching Determinations

Standard quartz and feldspar protocols determine the amount of rind etched from a grain using standard equations to derive the volume of a sphere. It is known that gypsum dissolution occurs preferentially along its cleavage plane. This study assumed etching measurements worked similarly to standard quartz protocols following the same equations (eq. 1-5 below). Etching experiments by way of mass loss tests were used to determine the extent of rind removal from grains exposed to varying wt % HCl and treatment times. One experiment tested 30-60 min treatments of 10 wt % HCl washes at room temperature to examine whether time was a significant variable to consider when attempting to etch a gypsum grain using HCl. A second experiment tested whether a higher concentration of HCl (~36 wt %) at 60°C (e.g. Mahan and Kay, 2012; Nagar, 2007) would etch grains without interfering with OSL measurements.

The calculations used to determine the amount of etching includes the following variables: m= mass, v= volume, r= radius. It is assumed that all samples have the same density and that all grains are spherical.

Equation 1-5 Calculations used to determine amount of rind removed from sand-sized grains after etching treatment.

Given: where *m*= mass and *v*=volume (1)

$$\frac{m_1}{v_1} = \frac{m_2}{v_2} \rightarrow \frac{m_1}{m_2} = \frac{v_1}{v_2}$$

Where the volume of a sphere is: (2)

$$V = \frac{4}{3}\pi r^3$$

Therefore: (3)

$$\frac{m_1}{m_2} = \frac{r_1^3}{r_2^3} \rightarrow r_2^3 = \frac{r_1^3}{\frac{m_1}{m_2}}$$

and

$$r_2 = \sqrt[3]{(54^3/\frac{m_1}{m_2})} \quad (4)$$

Given radius of pre-etched grains, r_1, determined to be 54 µm by estimating the mean diameter of 90-125 µm grains. Mean diameter = 108 µm.

Post treatment: (5)

thickness of rind removed = 54 µm – grain radius post treatment, r_2 (from eq. 4)

Subsamples of grains treated with HF were analyzed using SEM to confirm results from previous research (Mahan and Kay, 2012; Clark-Balzan, 2016) which showed that gypsum grains are impervious to etching with HF.

3.4.3 Bleaching Efficiency Experiments

Three bleaching experiments were undertaken to determine the effects of light on gypsum luminescence under varying conditions. Aliquots, 3 mm in size, of four unique preparation methods using either 63-90 µm or 212-250 µm grains underwent bleach efficiency experiments

under standard laboratory white lighting, sun light, low intensity red lighting, low intensity amber lighting, and a control that was left in complete darkness. The first two experiments measured luminescence signal change over six hours using aliquots of 63-90 μm and 212-250 μm grain sizes. These different size fractions were intentionally chosen for these experiments to test the dependence of luminescence bleaching with grain size variation. Previous studies on quartz have shown that a difference in grain size can influence rates of bleaching and D_e. Therefore, by testing a fine sand and a coarse sand fraction, this study could identify if the bleaching of gypsum luminescence was dependent on grain size.

The third experiment was intended to simulate environmental conditions representative of eolian transport over a one- and two-hour period. All three experiments were used to confirm best laboratory lighting set up for gypsum luminescence measurements. The six-hour period used in the first two experiments estimated the worst-case scenario for maximum exposure to laboratory lighting during preparation. To clarify, sometimes, even the amount of time grains are exposed to laboratory safe-lighting during OSL preparation can decrease a signal; therefore it was important to test the six hour "worst-case exposure" period to ensure laboratory treatment times were not a major variable affecting study results

3.4.4 OSL Protocol and Dosimetry

The SAR protocol used for gypsum preparation experiments was derived from the small body of gypsum OSL publications (Detschel and Lepper, 2009; Thompson et al., 2010; O'Connor et al., 2011; Mahan and Kay, 2012; Clark-Balzan, 2016). Modified protocol based on Clark-Balzan (2016) was chosen for use with all samples and included low temperature (30°C) long duration (10,000 s) preheats prior to OSL measurements (Table 3.2).

Step	SAR Protocol	This Study
1	Apply Regeneration Dose	0 Gy (natural signal), thereafter 3.275, 6.55, 9.825, 0, 3.275 Gy regeneration doses
2	Preheat	Pause 10,000 s at ambient temperature
3	Measure OSL	Blue Stimulate Luminescence (BSL), 30° C, 100 s, 90% power
4	Apply Constant Test Dose	6.55 Gy test dose
5	Preheat	Pause 10,000 s at ambient temperature
6	Measure OSL	BSL, 30° C, 100 s, 90% power
7	Return to step 1	
	Signal Integrals	Early Background: Initial 1.5 s Late Background: Initial 1.5s
	Background Integrals	Early Background: 1.5- 5 s (~2.5 times > initial e.g. Cunningham and Wallinga, 2010) Late Background: 70-100 s

Table 3.2 Gypsum SAR protocol and integrals used for OSL analyses

A comparison was made of equivalent dose data calculated using subtraction of late background integrals (Murray and Wintle, 2000) with early background integrals (Cunningham and Wallinga, 2010), and a linear fit for growth curves. Typical acceptance thresholds of 10% for recycling and 5% for recuperation ratios (Murray and Wintle, 2003) were used. We note that very low natural OSL responses in quartz sometimes require that the recuperation criteria to be adjusted. Dose rate analysis followed methods described in Spencer and Owen (2004, and references therein).

Elemental concentration data was obtained for dose-rate calculations. Approximately 20 mL of dried bulk sediment for each sample was pulverized using a tungsten carbide ring and puck mill within a shatter box for two minutes. Fifteen of these prepared samples were sent to Activation Laboratories (ActLabs) in Ancaster, Ontario, Canada for Fusion inductively coupled

plasma mass spectrometry (FUS-ICP-MS) and optical emission spectrometry (FUS-ICP-OES) to determine the elemental concentrations of U, Th, K and Rb.

Calculations used to determine β and λ dose rate components were derived using the conversion factors of Adamiec and Aitken (1998) and calculations based on Spencer and Owen (2004). Cosmic dose rate calculations were based on Prescott and Hutton (1994).

3.5 Results and Discussion

3.5.1 Preparation Methods

As discussed above, dry sieving was determined to have the best results for separating gypsum grains. Wet sieving was unsuccessful and resulted in multi-sized spheres (2 mm to 2.5 cm diameter) of gypsum. Previous studies have found that the semi-soluble nature of gypsum in water is responsible for the flocculating behavior; therefore, wet sieving is not recommended for gypsiferous soil analysis or gypsum sand preparation (Porta, 1998; Boden, 2016). Additionally, recently published research observed the dissolution of gypsum in water upon contact, increasing the size of etch pits at various points along the crystal structure and ultimately reducing the overall size of the grain (Feng et al., 2017). All particle size and distribution analyses were derived from mechanical dry sieving, as it resulted in assumed less change to grain morphology and mineralogy based on literature (Peruffo et al., 2013; Boden, 2016) and visual observations of flocculation during wet sieving attempts. Dry-sieved particle size distribution is depicted in Figures 3.7 and 3.8. Distribution of grain size in KNP-A suggests semi-consolidated "parasequence" of dune cross-beds is coarsening upwards before reaching a bounding surface characterized by truncation and overlying planar laminations. As displayed in Figure 3.7 these laminations fine upwards for almost 2.5 m before another cycle of coarsening in grain size

distribution is observed. KNP-B also starts with a semi-consolidated parasequence of cross-bedding that coarsens upward before reaching a truncated bounding surface (Fig. 3.8). However, this dune fines upward in planar laminae and displays partially cemented draping crusts near the surface. Lower energy eolian transport likely occurs for KNP-B due to size and position. KNP-A is larger and stands at an angle to KNP-B that benefits KNP-A ability to accumulate sediment; as the prevailing winds blow from the NNW and deposit grains on it before they can reach KNP-B. Another likely explanation for differences between these two dunes is dune migration, where planar bedding is representative of interdune features.

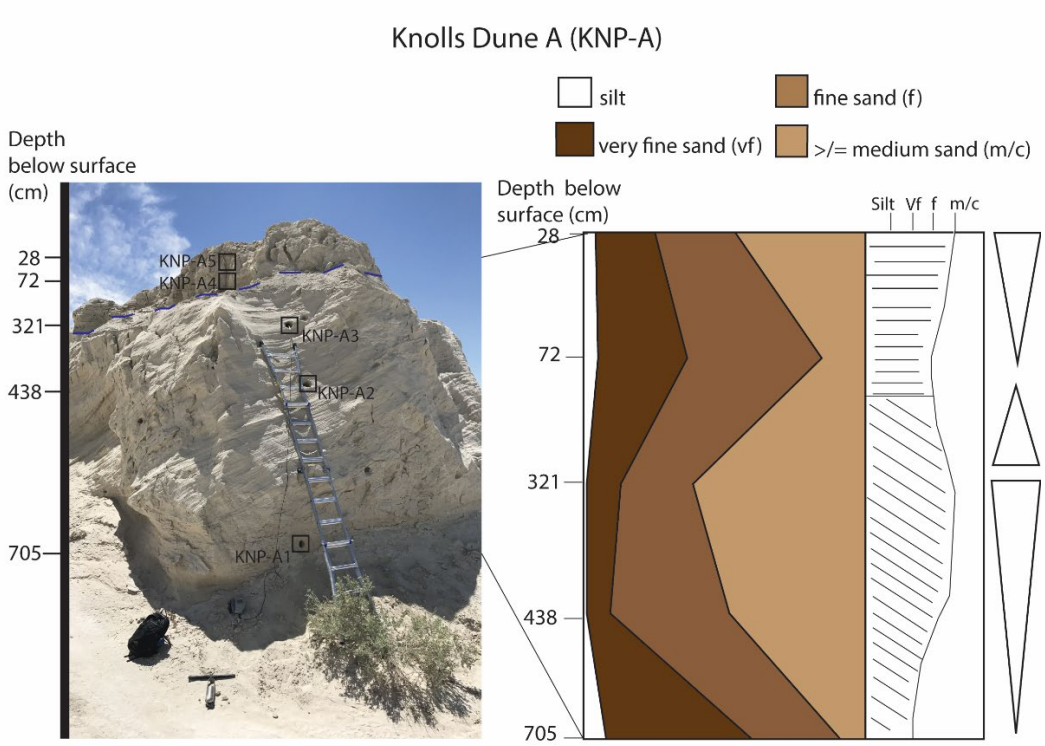

Figure 3.7 Knolls Dune A sample site and modal grain size distribution lithostratigraphy; bounding surface (blue dotted line) delineates cross-bedding from overlying planar laminations; USGS grain size standards: >/= 250µm = medium-coarse sand; 125-250 µm = fine sand; 64-125 µm = (63-125 µm) very fine sand; < 64 µm = (< 63 µm) silt

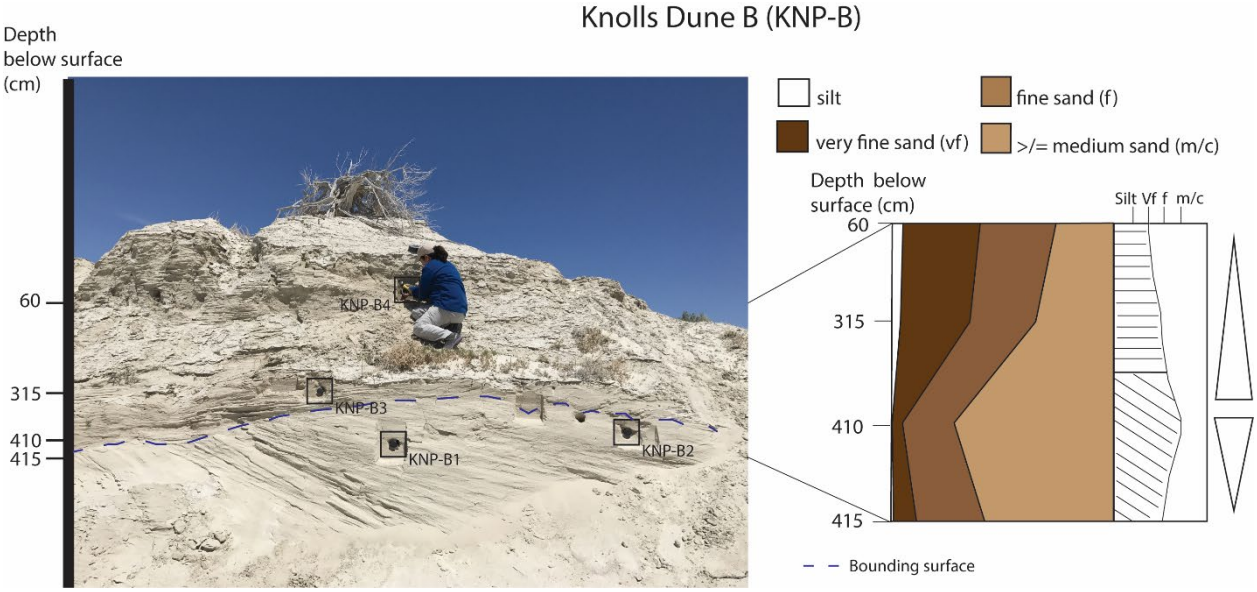

Figure 3.8 Knolls Dune B sample site and modal grain size distribution lithostratigraphy; bounding surface (blue dotted line) delineates cross-bedding from overlying planar laminations; USGS grain size standards: >/= 250µm = medium-coarse sand; 125-250 µm = fine sand; 64-125 µm = (63-125 µm) very fine sand; < 64 µm = (< 63 µm) silt

Figure 3.9 depicts XRD analyses of several preparation methods which provide evidence that samples without heavy liquid separation did not have any discernable quartz grains or inclusions leaving the success of using lithium metatungstate as an unknown. However, more definitive SEM results indicate that use of lithium metatungstate to separate gypsum grains from quartz or other minerals induce a chemical reaction and the precipitation of CaW. Precipitation was visible in lithium metatungstate recovered by density separation experiments and appeared as clouds shaped like loose threads or strings. Scanning electron microscopy of dried recycling filters (Fig. 3.10) confirmed that Ca^{+} reacted with the tungsten (W) resulting in calcium tungstate precipitation. All ρ= 2.37 g/cm^{-3} lithium metatungstate with a density (ρ) of 2.37 g/cm^{-3} was isolated from other heavy liquids and used only for gypsum separations before disposal. This particular density was used to float gypsum and sink any “heavy minerals” such as quartz or

feldspars. Use of LMT is not recommended for use in future experiments due to the heavy liquid's inability to reconstitute after exposure to gypsum.

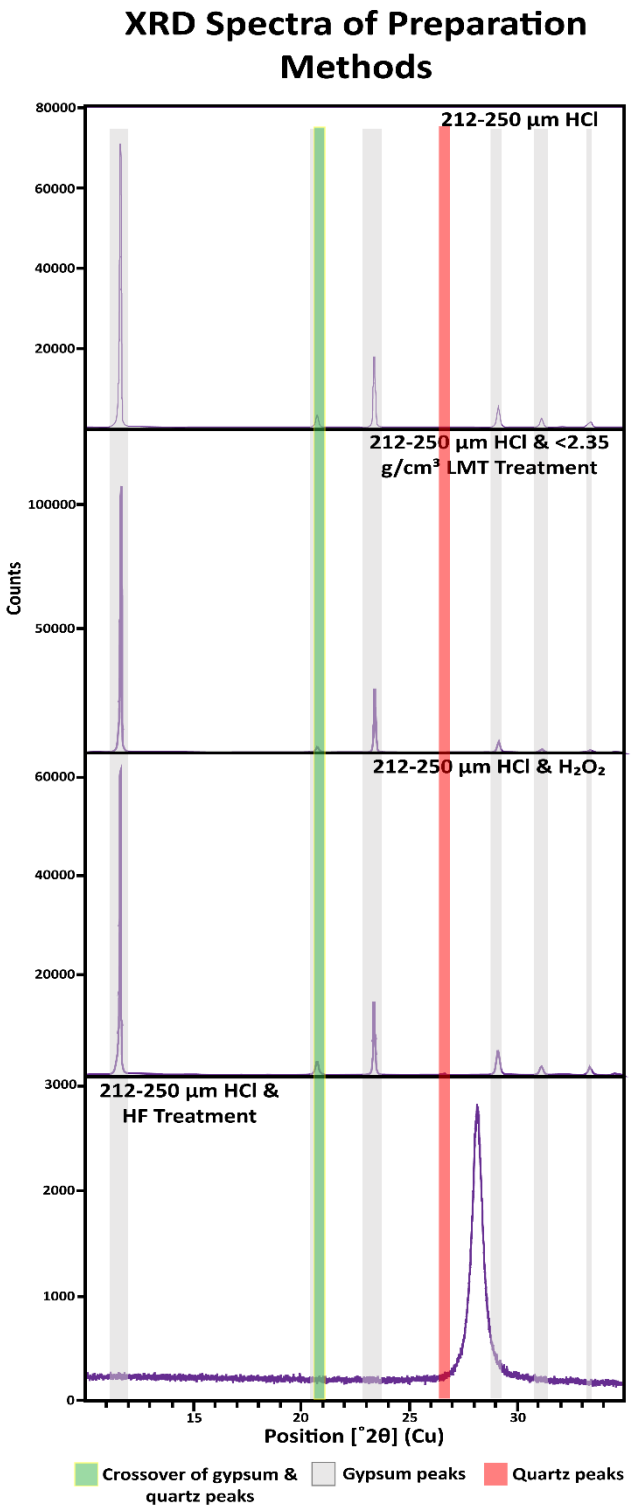

Figure 3.9 XRD analyses of multiple treatment methods. Crossover of one quartz peak (green) with gypsum and the lack of correlating peaks (red) suggests quartz does not exist in sample.

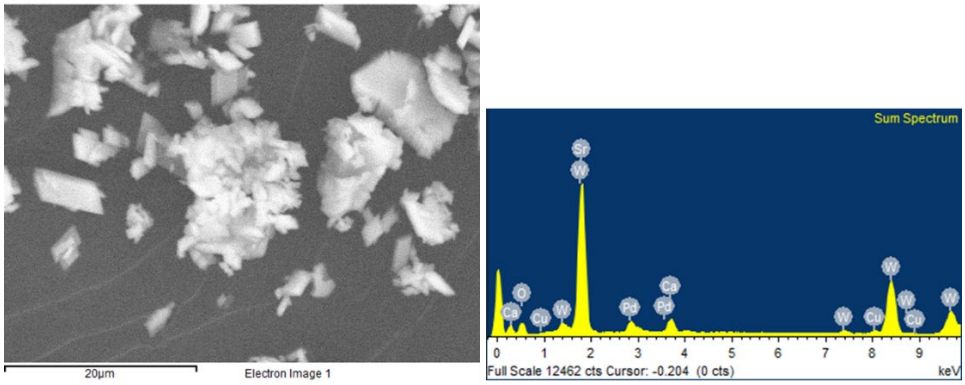

Figure 3.10 Precipitate resulting from lithium metatungstate and gypsum reaction (left image). Associated spectral analysis on right. Palladium (Pd) signals are from Pd sputter-coat sample received prior to being analyzed in SEM.

The gypsum grains in the samples taken from Knolls, UT, display sharp XRD peaks indicative of minerals with highly crystalline structures (refer back to Fig. 3.9). When observed under a binocular microscope, grains appear sub-angular to rounded with distinct micaceous cleavage and appeared to be detrital or clastic gypsum grains, many of which are frosted further supporting eolian origins (refer back to Fig. 3.6).

Visual observation from Frantz magnetic separation analyses indicated successful isolation of inclusion riddled gypsum grains (darker, with some gray grains) from purer gypsum (light tan to white). However, due to time constraints, this experiment was abandoned prematurely with only qualitative microscopic observations to report. Experiments merit follow up outside the scope of this research paper.

3.5.2 Bleaching Experiments

Bleaching data is derived from a comparison of successive recycling measurements interleaved with different bleaching experiments. Aliquots were subjected to various lighting conditions between each recycling measurement and results (Fig. 3.11) suggest gypsum samples should be treated under low intensity red lighting for the best preservation of luminescence.

Control samples, i.e. those aliquots left in complete darkness during experiments, consistently had greater variance in post experiment measurements than those subjected to six hours of laboratory red lights. This may be an effect of unstable α-radiation since routine etching was avoided as a result of complete substitution reactions with F^- in the HF etchant. Previous electron spin resonance research (Nagar, 2010) suggests unstable, shallow luminescence centers in gypsum which might be indirectly correlative to this study. If this is the case, exposure to subdued-red lighting seems to anneal most of the instability associated with luminescence. Reasons for this are unknown and merit future research. Amber light exposure was detrimental to the OSL luminescence signal suggesting the wavebands emitted by this lighting set up may excite and free electrons from respective luminescence traps we target while conducting age recovery procedures. White fluorescent laboratory lighting consistently and effectively bleaches aliquots within the 6-hour time frame. This was expected and provides more evidence of gypsum's eolian origins and OSL ages being depositional in nature.

Results of the second experiment conducted over 1- to 2-hour times with exposure to sunlight, subdued-amber light, subdued-red light, and a control kept in total darkness for the duration of the experiment, were less straight-forward (Fig. 3.12). It appears that 1-hour exposure times to either amber-, red-light or complete darkness have little deleterious effects on luminescence, but do change in any direction by about 0.10 Lx/Tx. However, at the 2-hour mark, both the control and the red-light exposed aliquot's luminescence measurement changed. In one set up, the two aliquots were measured very closely together, while in another set up, the two measurements diverged. It is likely that preparation exposure times may instigate the activation of OSL instability in gypsum. Within 1-hour the sunlight aliquots luminescence had been reset.

Overall, grain size and preparation method showed no significant trends that might be avoided or considered when handling gypsum for OSL purposes. Preliminary interpretations from these two experiments suggest wavelength ranges from laboratory lighting are the main factors behind changes in luminescence, and 1-hour of sun light exposure is enough time to sufficiently bleach an aliquot. Based on these findings, gypsum can be sufficiently bleached within 1-hour of exposure to sunlight and laboratory fluorescent white-lighting. These results support the hypothesis that OSL ages are in fact recording the burial age of gypsum rather than the time at which gypsum crystals formed.

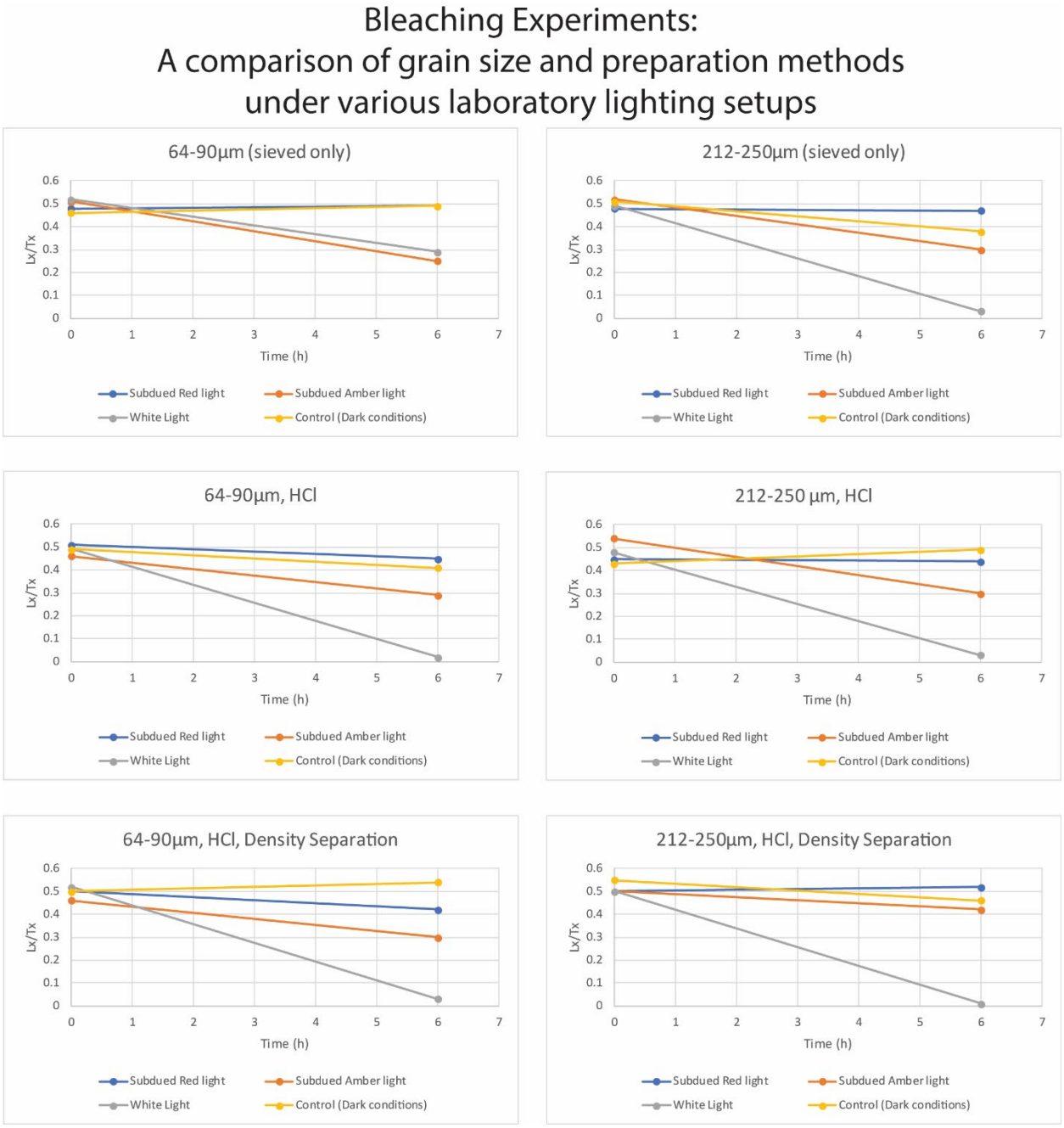

Figure 3.11 Results of 6-hour bleaching experiment on 63-90 and 212-250 micron gypsum grains from sample KNP-A3EX

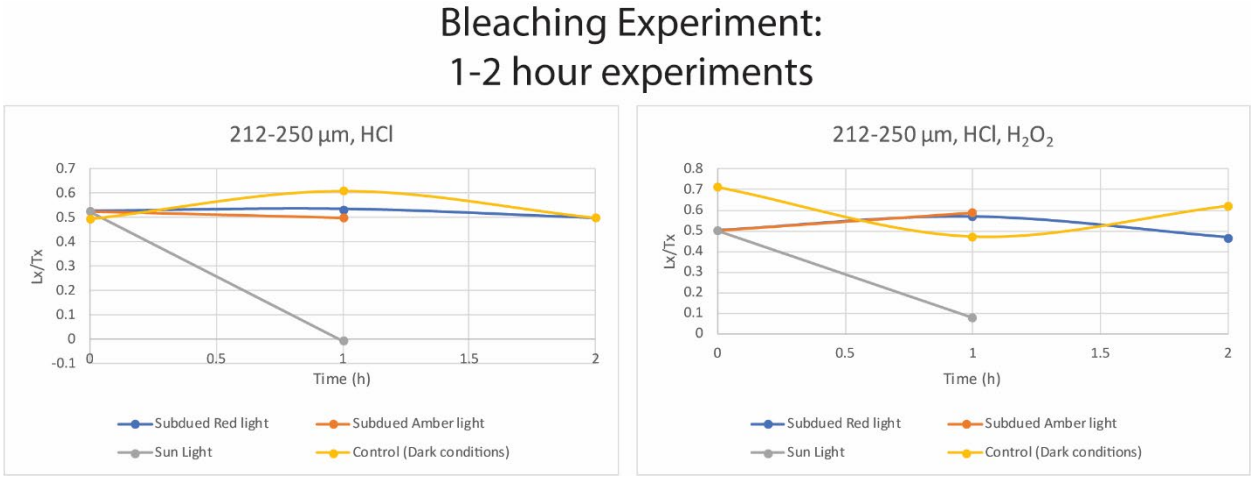

Figure 3.12 Results of 1- and 2-hour bleaching experiments on 212-250 µm gypsum grains from sample KNP-A3EX.

3.5.3 Etching Determinations

Routine quartz OSL preparation involves etching minerals using HF. This treatment was used during several experiments to determine effects on gypsum and gypsum luminescence. Reduced and erratic luminescence signals resulted. Grains post etching were fragile and powdery, making it difficult to move all remaining grains for aliquot mounting and OSL measurement. Scanning electron microscopy confirmed that gypsum chemically reacts with HF through a complete substitution reaction resulting in a mineral grain of CaF_2 (Fig. 3.13).

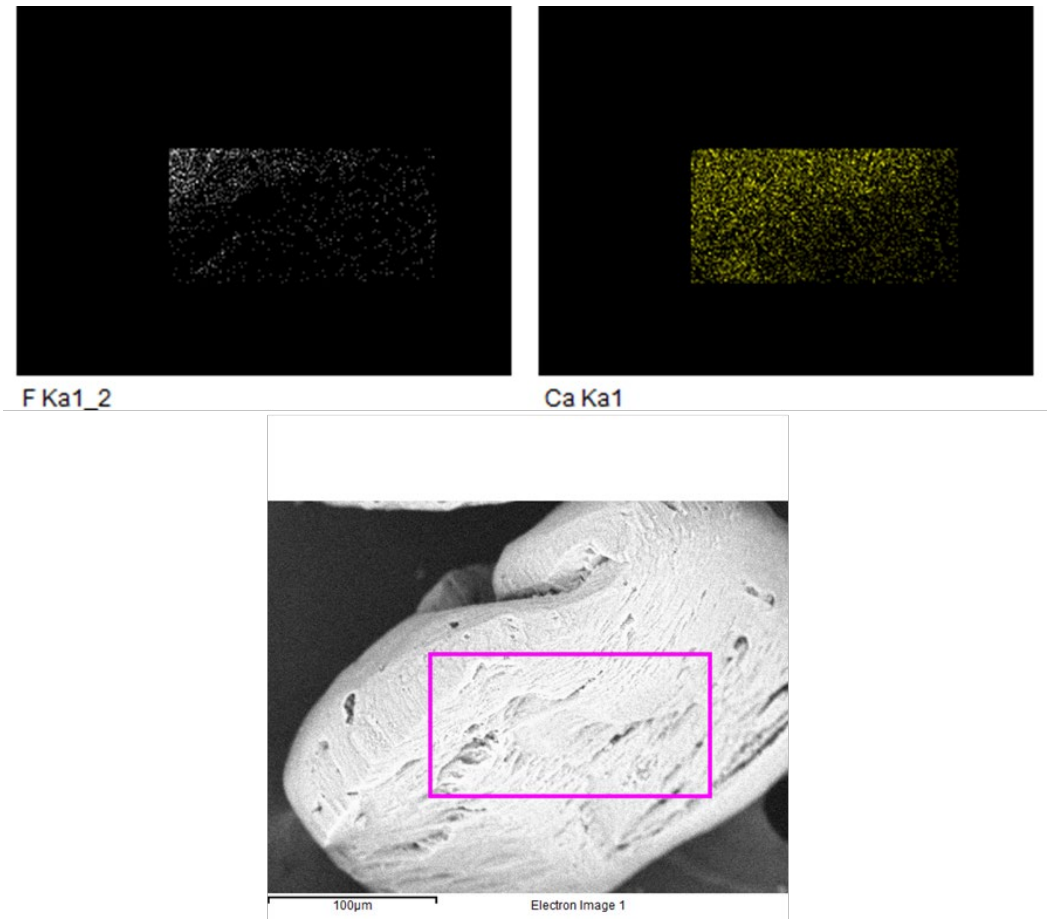

Figure 3.13 SEM results of HF treatments on a gypsum grain from Knolls, UT. Lower image was a gypsum grain which underwent HF etching; purple square outlines where elemental mapping of grain was recorded post treatment. Upper two images display only 2 elements present, Ca and F; the grain has been subjected to a chemical reaction completely replacing SO_4 complex with F.

As a result of SEM findings that concluded gypsum had been converted to CaF (Fig. 3.13), two experiments exploring the potential of HCl as an etchant were undertaken. HCl was proposed for use due to known dissolution in ambient and elevated temperatures (Li and Demopoulos, 2005; Adekola et al., 2018). During these experiments both acid concentration and temperature were manipulated to test the efficacy of HCl as an etchant. The amount of etching was quantified using equations based on volume of a sphere, where the sphere is the grain (See

eq. 1-5). Results of the calculations are listed in Tables 3.3 and 3.4 as total and average rind removed in microns.

Etching experiment 1 used 10 wt % HCl suggest gypsum samples lost between 1% - 5% mass, which is equal to ~1 µm of rind removal during 30, 40, and 50 minute experiments.

Etching Experiment 1: Gypsum 90-125µm--> 10wt% HCl @ Room Temperature										
Mass (g)	Bulk Sediment (g)	10% HCl for 30 min	Mass Difference (g)	10% HCl for 10 min	Mass Difference (g)	10% HCl for 10 min	Mass Difference (g)	Assume mean of 108µm diameter grain	grain radius (µm) post treatment	radius in µm removed from grain using treatment
Sample 1	10.3710	10.2310	**0.1400**	-	-	-	-	30 min	53.7559	0.2441
Sample 2	10.4526	9.9537	**0.4989**	9.9026	**0.0511**	-	-	40 min	53.0358	0.9642
Sample 3	10.9368	-	-	10.7793	**0.1575**	10.3948	**0.3846**	50 min	53.0928	0.9072
								AVG Rind removal (µm)		0.7052

Table 3.3 Etching experiment 1 used 10 wt % HCl over 30, 40, and 50 min treatments. Mass loss converted to average micron reduction of grain or rind.

Etching Experiment 2: Gypsum 90-125µm --> ~36wt% HCl @ 60°C for 40min					
Sample ID	Pre-Treatment Mass (g)	Total Post-Treatment Mass (g)	Rind Removal in microns Equation	grain radius (µm) post treatment	radius in µm removed from grain using treatment
KNP-A1	29.30	7.50	[redacted]	34.29	19.71
KNP-A4	18.50	4.80		34.44	19.56
KNP-A5	12.50	3.20		34.29	19.71
KNP-B1	7.20	1.50		32.01	21.99
KNP-B3	18.00	4.40		33.76	20.24
KNP-B4	23.00	5.10		32.68	21.32
CD-5	18.30	4.70		34.32	19.68
			AVG Rind removal (µm)		20.29

Table 3.4 Etching experiment 2 used ~36 wt % HCl at 60°C for 40 min treatment. Mass loss converted to average micron reduction of grain rind radius.

Etching experiment 2 used ~36 wt % HCl over 60 min at 60°C resulting in an average loss of ~20 microns of grain size. For the purposes of etching we consider this the amount of

rind removed that has accumulated luminescence due to alpha particle exposure external to the grain. Although elevated temperatures were avoided in all previous preparation methods, the lack of rind removal noted in experiment 1 and the inability to use HF led us to experiment with warm HCl dissolution methods (Li and Demopoulos, 2005). Qualitative SEM observations display clear dissolution of gypsum grains along the 010 cleavage plane (Fig. 3.14).

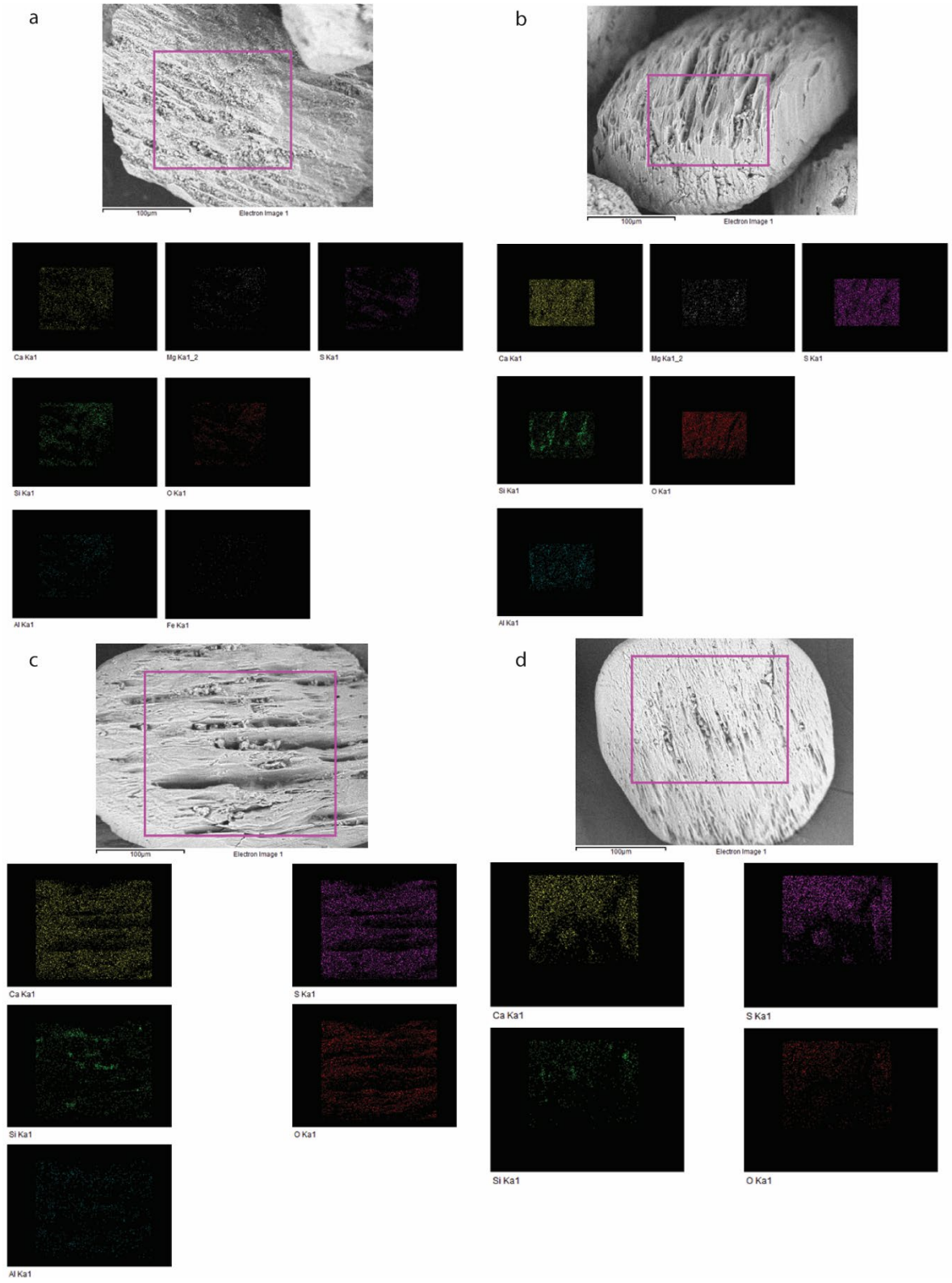

Figure 3.14 SEM images and associated elemental maps of 212-250 µm gypsum fraction post OSL preparation treatments. Abraded surfaces observed in images is assumed to be a result of HCl etching; a) no treatment, only sieved; abrasions are present but not deep b)

30 minute HCl treatment; surface abrasions are deeper and follow 010 cleavage c) 40 minute HCl treatment; deep abrasions present d) 30 minute HCl treatment and H_2O_2 treatment; abrasions present, but not as deep. Elemental maps show presence of elements, only Pd has been removed. All samples have Pd sputter-coat before entering SEM analyses.

3.5.4 OSL Analysis

For any one sample, a test dose of 50 s β (~6.5 Gy) was given and the equivalent dose values measured were reasonably consistent (within 5% error). Equivalent doses were reasonable as they logically decreased moving upward stratigraphically following the law of superposition. This was only possible because SAR data were successful using early background integrals suggested by Cunningham and Wallinga (2010) for young quartz deposits. Success here is defined as more accepted aliquots during OSL analyses. The signal integral taken included the first 1.5s (channels 1-3), while the background signal used accounted for 1.5-5.0s (channels 3-10), virtually eliminating noise from relatively weak OSL signals (>80% aliquot acceptance). Test dose error and recuperation did not have a significant influence on luminescence acceptance rates, remaining below 10% and 5% respectively. Late Background integrals (signal channels: 1-3, and background channels: 140-200) generally could not pass criteria as often, leaving all but four samples without a D_e. However, unlike gypsum, the single quartz sample benefited from using the Late Background integral (Fig. 3.15) for aliquot acceptance. Integration times had little effect on the resulting D_e. Because the D_e changed so little, both quartz and gypsum were analyzed using early background integrals. This made comparison of ages less complicated with fewer variables to consider.

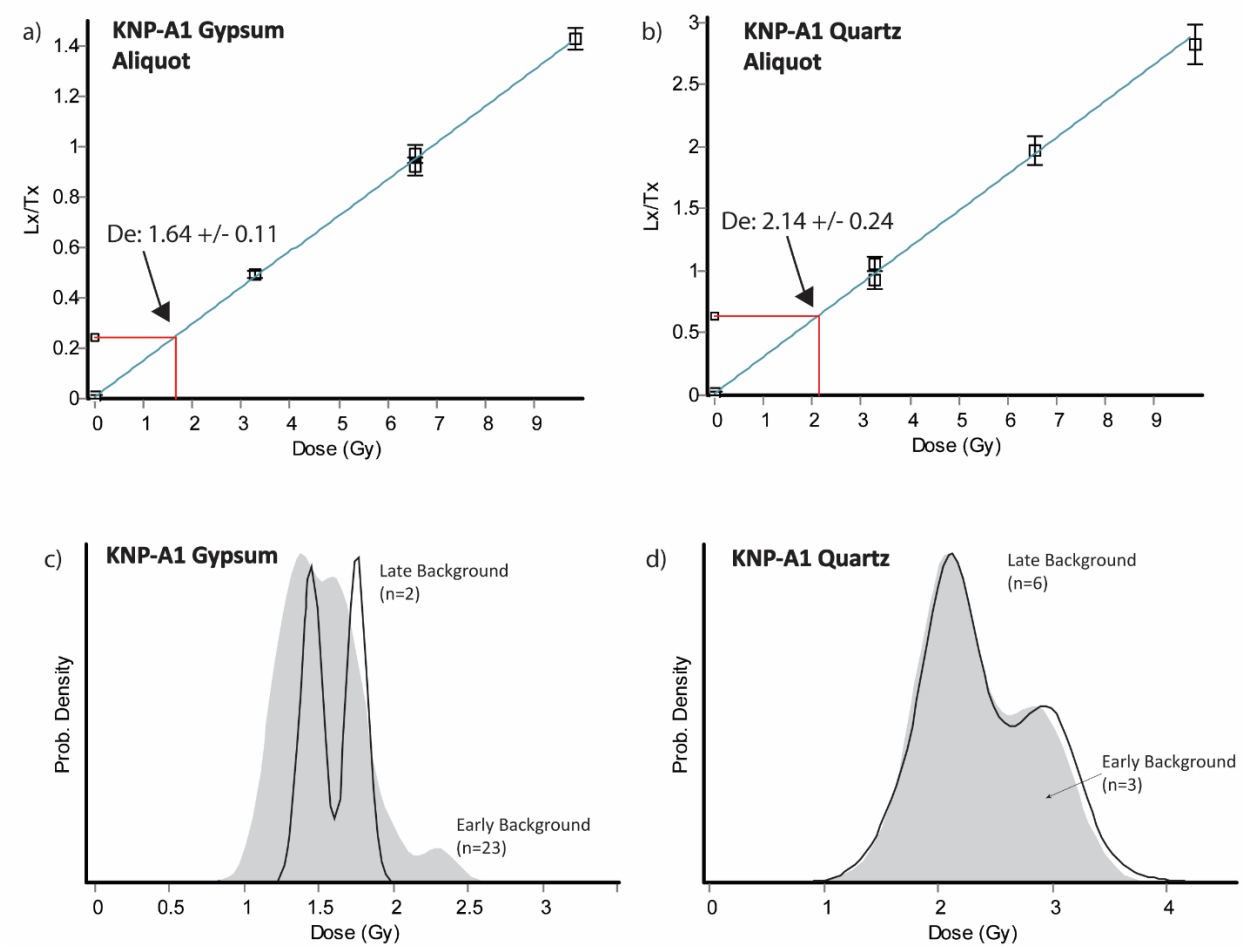

Figure 3.15 Example of typical gypsum growth curve and equivalent dose (D_e) using early background (0-1.5 s; 1.5-5 s), for sample KNP-A1. b) Example of quartz growth curve and D_e from same sample using early background. c) Probability density functions (PDFs) of D_e comparing both early and late background (0-0.5 s; 80-100 s) for gypsum from sample KNP-A1. Similarly d) shows the PDFs for quartz from the same sample.

Depth Below Surface (cm)	Sample	Grain Size (μm)	Water Content[0] (%)	U[1] (ppm)	Th[1] (ppm)	K[1] (%)	Rb[1] (ppm)	Cosmic dose rate[2] (Gy/ka)	Total dose rate (Gy/ka)
705	KNP-A1	90-125	2.5	2.1 ±0.21	3.5 ±0.35	0.2905 ±0.01	25 ±2.50	0.11062 ±0.011	1.1053 ±0.061
705	KNP-A1*	125-175	2.5	2.1 ±0.21	3.5 ±0.35	0.2905 ±0.01	25 ±2.50	0.11067 ±0.011	1.1053 ±0.061
438	KNP-A2	90-125	2.5	1.1 ±0.11	1.2 ±0.12	0.0996 ±0.00	8 ±0.80	0.15124 ±0.015	0.5838 ±0.031
321	KNP-A3	90-125	2.2	1.1 ±0.11	1.3 ±0.13	0.1079 ±0.01	8 ±0.80	0.17515 ±0.018	0.9849 ±0.038
72	KNP-A4	90-125	5.1	2.2 ±0.22	3.1 ±0.31	0.2573 ±0.01	17 ±1.70	0.24352 ±0.024	1.5329 ±0.064
28	KNP-A5	90-125	3.1	1.6 ±0.16	2.2 ±0.22	0.1826 ±0.01	12 ±1.20	0.25878 ±0.026	1.3059 ±0.053
415	KNP-B1	90-125	2.0	1.1 ±0.11	0.9 ±0.09	0.0747 ±0.00	4 ±0.4	0.15880 ±0.016	0.9072 ±0.035
405	KNP-B2	90-125	1.8	1.5 ±0.15	1.0 ±0.10	0.0830 ±0.00	6 ±0.6	0.15775 ±0.016	1.0155 ±0.042
315	KNP-B3	90-125	4.2	1.8 ±0.18	2.7 ±0.27	0.2241 ±0.01	23 ±2.30	0.17666 ±0.018	1.3332 ±0.054
60	KNP-B4	90-125	3.4	2.0 ±0.20	2.9 ±0.29	0.2407 ±0.01	21 ±2.10	0.24779 ±0.025	1.4843 ±0.062
7	CD-5	90-125	2.1	1.3 ±0.13	1.5 ±0.15	0.1245 ±0.01	12 ±1.20	0.26669 ±0.027	1.1518 ±0.046

* Quartz OSL sample for comparison with gypsum sample
[0] Water content uncertainty is assumed to be 5%.
[1] Elemental concentrations from ICP -OES/-MS data, Act Laboratories Ontario, CA.
[2] Cosmic dose rate calculations according to Prescott and Hutton (1994).

Table 3.5 Radionuclide data and dose rate of samples from Knolls study site. Water content = moisture mass/ dry sample mass, expressed as a percentage. Water content for sample KNP-A1 is an estimate using value for KNP-A2 (closest sample elevation and depth) because data unavailable.

Depth Below Surface (cm)	Sample	Time intervals	Recycling ratios	Recuperation (%)	No. accepted/ total aliquots	Common Age De (Gy)	Central Age De (Gy)	Overdispersion % (Gy)
705	KNP-A1	Late BG	1.04 ±0.04	7.86 ±1.11	20/24	1.6 ±0.0	1.5 ±0.1	14.1 ±0.6 (0.2 ± 0.0)
		Early BG	1.02 ±0.05	1.96 ±1.28	23/24	1.5 ±0.1	1.5 ±0.1	15.3 ±0.6 (0.2 ± 0.0)
705	KNP-A1*	Late BG	1.11 ±0.13	7.46 ±3.83	6/15	2.5 ±0.1	2.4 ±0.2	13.1 ±0.3 (0.3 ± 0.1)
		Early BG	1.06 ±0.13	2.88 ±3.15	3/15	2.5 ±0.2	2.4 ±0.2	11.1 ±0.8 (0.3 ± 0.1)
438	KNP-A2	Late BG	-	-	0/6	-	-	-
		Early BG	1.02 ±0.04	3.76 ±3.41	6/6	0.7 ±0.0	0.7 ±0.0	12.3 ±2.3 (0.1 ± 0.1)
321	KNP-A3	Late BG	1.06 ±0.04	8.71 ±1.05	1/6	-	1.07 ±0.09	-
		Early BG	1.04 ±0.05	3.82 ±0.75	6/6	0.9 ±0.0	0.8 ±0.1	19.1±2.9 (0.2 ± 0.0)
72	KNP-A4	Late BG	1.03 ±0.03	9.54 ±1.01	1/6	-	0.94 ±0.06	-
		Early BG	1.03 ±0.05	4.30 ±3.16	6/6	0.8 ±0.0	0.7 ±0.1	21.1 ±3.1 (0.1 ± 0.0)
28	KNP-A5	Late BG	-	-	0/24	-	-	-
		Early BG	1.03 ±0.05	4.38 ±4.06	22/24	0.5 ±0.0	0.5 ±0.0	0.0 ±0.0 (0.0 ± 0.0)
415	KNP-B1	Late BG	-	-	0/6	-	-	-
		Early BG	1.04 ±0.05	1.12 ±2.71	6/6	0.7 ±0.0	0.7 ±0.0	0.0 ±0.0 (0.0 ± 0.0)
405	KNP-B2	Late BG	-	-	0/6	-	-	-
		Early BG	1.04 ±0.05	10.53 ±6.30	6/6	0.5 ±0.0	0.5 ±0.0	20.4 ±3.7 (0.1 ± 0.0)
315	KNP-B3	Late BG	-	-	0/6	-	-	-
		Early BG	1.03 ±0.05	4.56 ±2.30	6/6	0.6 ±0.0	0.6 ±0.1	21.6 ±3.4 (0.1 ± 0.0)
60	KNP-B4	Late BG	-	-	0/24	-	-	-
		Early BG	1.03 ±0.04	3.09 ±3.13	23/24	0.5 ±0.0	0.5 ±0.0	13.2 ±0.8 (0.1 ± 0.0)
7	CD-5	Late BG	-	-	0/24	-	-	-
		Early BG	1.02 ±0.05	147.82 ±461.62	14/24	0.1 ±0.0	0.1 ±0.0	0.0 ±0.0 (0.0 ± 0.0)

* Quartz OSL sample for comparison with gypsum sample

Table 3.6 OSL analyses comparing use of early and late background time integrations. Use of early background time intervals yields higher accepted gypsum aliquots per sample.

Similar to Mahan and Kay (2012), we observed very low concentrations of K, U, and Th in the gypsum grains using ICP-OES/MS to determine dosimetry (Table 3.5). Early and late background integral comparison displaying aliquot acceptance rate and reasonable D_e are displayed in Table 3.6.

Age calculations of ten gypsum aliquots and one quartz aliquot indicate dune development occurred within the last 2,500 years. Age data suggests high precision of the eolian gypsum OSL method, however poor accuracy potentially exists based on the one independent quartz result of sample KNP-A1. High age precision is supported by noted morphology, particularly, frosting and sub-rounded gypsum grains; the complete bleaching of grains within 1-hour experiments using both fluorescent lighting and natural sun light; consistency in

stratigraphic D_e,and relatively similar dose rates above and below the identified bounding surfaces of KNP-A and KNP-B. The assumed consistent underestimation of gypsum depositional ages may be due to the hydrated nature of the mineral which may cause fading of luminescence. Although literature does not provide evidence of this, it is logical to expect episodic aridity and seasonal humidity or moisture to influence at least the upper deposits of eolian-transported grains. If gypsum formation ages were recorded instead of depositional age, we would expect results to be older than quartz ages not younger. Further research is required to resolve this issue and to investigate if it is possible to have clastic gypsum record minor mineralogical transformations as formation ages. The result of only one quartz OSL sample age for comparison should also be considered when attempting to resolve the issue of gypsum underestimation. There may be a mathematical correction that can be applied to the age calculation if more quartz ages prove statistically significant differences.

Figure 3.16 is a combination table and figure listing age data both spatially and temporally. The list is first written in two columns separating the two adjacent dunes sampled for this study. Intervals sampled are listed by depth below the surface and depicted temporally in the center of the figure. Visually understanding the order of deposition can help understand general trends of dune development and sedimentation rates. Based on dune position, it was expected that dune KNP-B development would begin later as observed prevailing wind patterns suggested eolian transport currently moves grains over or around the larger dune, KNP-A, first. Reverse grading and a general coarsening upward trend was observed found throughout the site. Both observations of wind direction and resulting expectations that KNP-B is currently sheltered and has been since the original dune building event prove to be valid given the calculated ages of

assumed deposition. Gypsum ages (and the one quartz age) are in agreement with stratigraphic correlations (Fig. 3.16).

Modern coppice dune sample CD-5, is estimated to be 0.09 ka in age which strengthens experimental data indicating gypsum grains were well bleached when transported before burial. This age also provides a starting point for distribution of ages in the two paleodunes. It was expected that the larger dune was likely older than the smaller dune and the ages provided by gypsum, although underestimated, confirm an older depositional age at the basal section of KNP-A. Approximately 1.4 ka ago, or 2.26 ka using the single quartz age, the dune was deposited. KNP-A1, A2, and A3 all lie below the bounding surface of this dune and ages agree with this observation and stratigraphy. After the sediment at KNP-A3 was deposited, KNP-B began a dune building event. This is particularly interesting because although samples were not intended to capture the bounding surfaces of either dune, KNP-B2 and KNP-A4 may have captured the roughly estimated age of bounding surface deposition. Samples KNP-B3, and B4 lie above this surface and interleave KNP-A5. These results confirm a punctuated climatic event occurred within the last 2 ka. Resolving the age underestimation using a quartz sample will give more credence to this discovery and can then be linked to known climate outliers, such as the Medieval warm period which occurred approximately 1,000 years ago.

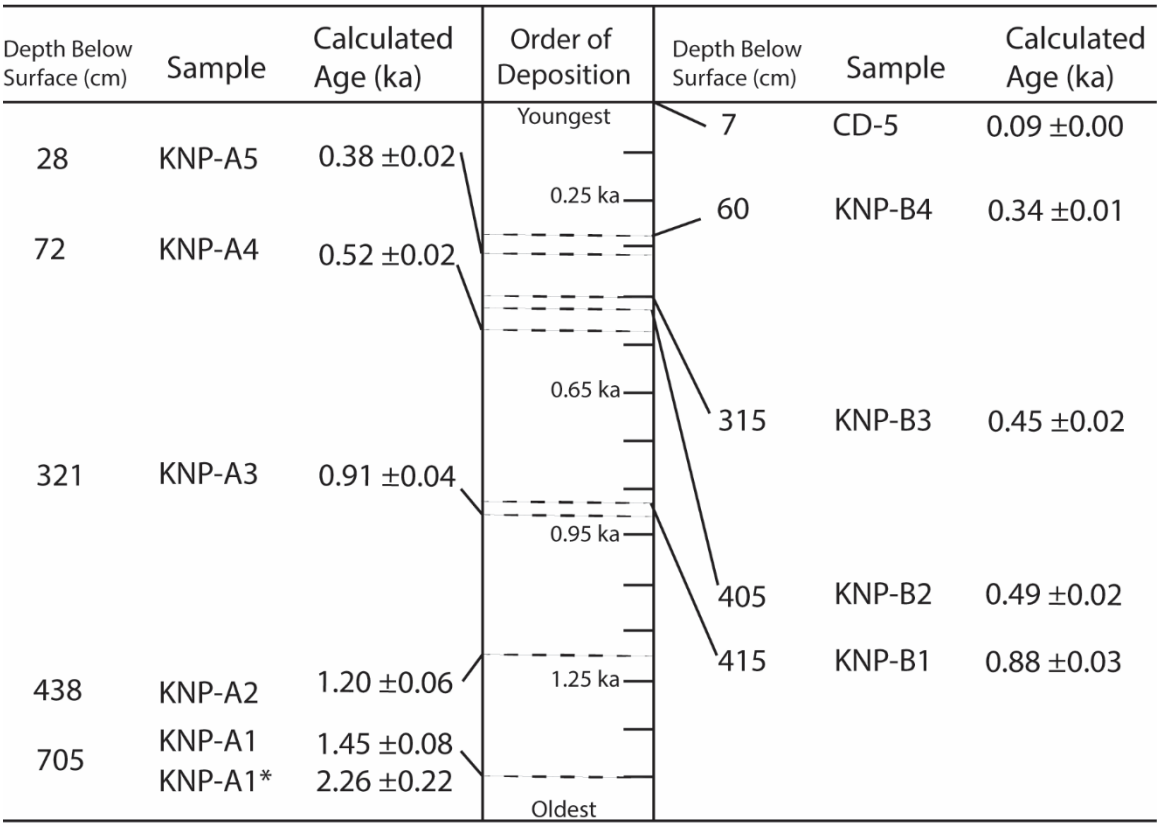

Figure 3.16 Calculated ages of nine gypsum samples from Knolls, UT study site. Visual context depicting temporal deposition of two adjacent sand dunes.

3.6 Conclusions

Results from this research indicate that gypsum can be prepared effectively for use in OSL geochronology. However, in order to do so, the following aspects of the experimental protocols should be implemented:

- Gypsum samples used for OSL should be prepared in subdued red lighting or risk loss of luminescence
- Preparations should be dry-sieved, without H_2O_2 treatment, followed by a warm (~60°C) ~36wt% HCl treatment of 40 minutes which results in approximate 20µm rind removal

- Grain size can change upon contact with water, and is a natural flocculant for clay minerals, so be wary of grain size fraction statistics if the decision to use wet sieving or laser based grain size analysis (with water based measurements) are used
- Refrain from using lithium metatungstate or any heavy liquid tungstate with calcium bearing minerals as it precipitates CaW and destroys integrity of heavy liquid reconstitution
- Magnetic separation may be wise if gypsum is contaminated with diamagnetic minerals; paramagnetism can be teased out, possibly leading to gypsum, quartz separations
- Further experiments followed by SEM may be beneficial for confirming specific Frantz suitability for this technique.

Furthermore, modified OSL dating techniques of gypsum produced promising results, and indicate gypsum ages are in agreement with stratigraphic correlations, but may be providing underestimated ages. Discrepancy in calculated ages may exist due to gypsum overgrowth of quartz (Clark-Balzan, 2016), however, more data is required to determine the cause of age underestimation, beginning with more quartz aliquots for comparison.

Chapter 4 - Summary and Conclusions

Luminescence dating techniques can be expanded to "exotic" minerals like gypsum, given adequate research and consideration into mineralogical transformations that can occur at each step of preparation protocols and during luminescence measurement. This study provided results of each preparation method and suggests an abbreviated preparation protocol that mitigates structural changes and signal loss. It is acknowledged that not all gypsum samples will be created equally, although basic truths do exist. Gypsum dissolution occurs upon contact with water and naturally flocculates so wet sieving for grain size fraction should be avoided. Use of HF chemically reacts with gypsum in a complete substitution of SO_4 replacement with F^+, rendering a sample's luminescence signal destroyed. Additionally, and in an effort to conserve laboratory budgets and supplies, serious consideration should be taken when using heavy liquid separations including tungsten. The reaction that occurs limits the reusable liquid's ability to reconstitute. Further evidence is required, but logically you may also be losing some gypsum luminescence to the reaction and CaW precipitate.

Equivalent dose estimates were consistently reasonable and stratigraphically correlated well. Early background time integrals were successful at both accepting aliquots and evaluating the equivalent dose. Dose rate was relatively similar across dunes when associated samples were compared (those taken from below the bounding surface in KNP-A compared to those from below in KNP-B), which further links a punctuated climate event to the deposition of the bounding surface. KNP-B began development much later than KNP-A, likely due to location, position and the direction of prevailing winds. KNP-B2 likely captured the approximate age of bounding surface deposition and indirectly a punctuated climate event. Although this study could not refine the accuracy of gypsum OSL as intended, it did find a way to produce precise ages.

Future research should focus on finding a correction so that the event associated with the bounding surfaces of the paleodunes can be teased out of paleoclimate history. Underestimated depositional ages of the dunes at Knolls, Utah were acquired using gypsum with ages ranging from 0.09 ka to 1.45 ka. The single quartz aliquot comparison at KNP A-1 interval resulted in a depositional age of 2.26 ka. Further research is necessary to understand the difference in age results.

Further considerations and future work on dunes at Knolls, Utah may benefit from the use of ground penetrating radar across the vertical core sample site (samples were not used in this study) so that the true dune base can be documented and bounding surfaces can be more definitively observed. Additional quartz dates for comparison to the gypsum age results would likely lead to quantitative adjustments of the age equation for gypsum and more accurate depositional ages. Undertaking these tasks would greatly benefit the luminescence community and further sedimentological understanding of the role of gypsum in eolian basin analysis. However, this would require a substantial amount of work to investigate and is beyond the scope of this study.

References

Adamiec, G., Aitken, M., 1998, Dose-rate conversion factors: update: Ancient TL. v. 16, p. 37–50.

Adekola, F.A., Olosho, A.I., Baba, A.A., Adebayo, S.A., 2018, Dissolution kinetics studies of Nigerian gypsum ore in hydrochloric acid: Journal of chemical technology and metallurgy. v. 53(5), p. 845-855

Ashley, G.M., Ndiema, E., Spencer, J.Q.G., Harris, J.W.K., Kiura, P.W., 2011, Paleoenvironmental context of archaeological sites, implications of subsistence strategies under Holocene climate change, northern Kenya: Geoarchaeology. v. 26, p. 809-837.

Ashley, G.M., Ndiema, E., Spencer, J.Q.G., Du, A., Lordan, P.T., Kiura, P.W., Dibble, L., Harris, J.W.K., 2017, Paleoenvironmental Reconstruction of Dongodien, Lake Turkana, Kenya and OSL Dating of Site Occupation during Late Holocene Climate Change: African Archaeological Review. v. 34, p. 345-362.

Ataee, N., 2019, Development of luminescence dating methods in tectonically active settings: dating seismically related fanglomerates in alluvial fans located in Coachella Valley, southern California (Master's Thesis, Kansas State University, Manhattan, Kansas). Retrieved from: https://krex.k-state.edu/dspace/bitstream/handle/2097/39677/NinaAtaee2019.pdf?sequence=1

Boden, T.H., 2016, Gypsiferous Sand Dune Deposits on SITLA Lands in the Great Salt Lake Desert Project Area, Tooele County, Utah: Resources and Geology of Utah's West Desert. Utah Geological Association Publication. v. 45, p. 105-130.

Bøtter Jensen, L., Anderson, C. E., Duller, G. A. T. and Murray, A. S., 2003, Developments in radiation, stimulation and observation facilities in luminescence measurements: Radiation Measurement. v. 37, p. 535−541.

Clark, D.L., and Oviatt, C.G., 2019. Interim geologic map of the Bonneville Salt Flats and east part of the Wendover 30' x 60' quadrangles, Tooele County, Utah, East Part—Year 2. Utah Geological Survey Open-File Report 702, 24 p., 2 pl., scale 1:62,500. https://doi.org/10.34191/OFR-702

Clark-Balzan, L., 2016, Source and characteristics of blue, infrared (IR), and post-IR IR stimulated signals from gypsum-rich samples: Ancient TL. v. 34(1), p. 6-13.

Cunningham, A.C. and Wallinga, J., 2010, Selection of integration time intervals for quartz OSL decay curves: Quaternary Geochronology. v. 5(6), p. 657-666.

Detschel, M. and Lepper, L., 2009, OSL dating properties of Martian sediment analogue materials exposed to a simulated Martian solar spectral environment: Journal of Luminescence. v. 129(4), p. 393-400.

Dean, L.E., 1978, Eolian Sand Dunes of the Great Salt Lake Basin: Utah Geology. v. 5(2), p. 103-111.

Duller, G.A.T., 2004, Luminescence dating of Quaternary sediments: recent advances: Journal of Quaternary Science. v. 19, p. 183-192.

Eardley, A.J., 1962, Gypsum Dunes and Evaporite History of the Great Salt Lake Desert: Utah Geological and Mineralogical Survey Special Studies. v. 2, p. 7-17.

Eardley, A.J., and Stringham, B., 1952, Selenite crystals in the clays of the Great Salt Lake: Journal of Sedimentary Petrology. v. 22, p. 234-238.

Feng, P., Brand, A., Chen, L., Bullard, J., 2017, In Situ Nanoscale Observations of Gypsum Dissolution by Digital Holographic Microscopy: Chemical Geology. v. 460, p. 25-36.

Gilbert, G.K., 1890. Lake Bonneville. In: U.S. Geological Survey. Monograph 1..

Huntley, D.J., Godfrey-Smith, D.I., and Thewalt, M.L.W., 1985, Optical dating of sediments: Nature. v. 313, p. 105-107.

Hütt, G., Jaek, I., and Tchonka, J., 1988, Optical dating: K-feldspars optical response stimulation Spectra: Quaternary Science Reviews. v. 7, p. 381-385.

Jones, D.J., 1953, Gypsum-Oölite Dunes, Great Salt Lake Desert, Utah: Bulletin of the American Association of Petroleum Geologist. v. 37(11), p. 2530-2538.

Johnson W.C., Halfen, A.F., Spencer, J.Q.G., Hanson, P.R., Mason, J.A., Young., A.R., 2019. Late MIS 3 stabilization of dunes in the eastern Central Great Plains, USA: Aeolian Research. v. 36, p. 68-81

Leighton, C.L., Bailey, R.M., and Thomas, D.S.G., 2013, The utility of desert sand dunes as Quaternary chronostratigraphic archives: evidence from the northeast Rub' al Khali: Quaternary Science Reviews. v. 78, p. 303-316.

Li and Demopoulos, 2005, Solubility of $CaSO_4$ Phases in Aqueous HCl + $CaCl_2$ Solutions from 283 K to 353 K: Journal of Chemical Engineering Data. v. 50, p. 1971-1982.

Lukas, S., Spencer, J.Q.G., Robinson, R.A.J., Benn, D.I., 2007. Problems associated with luminescence dating of Late Quaternary glacial sediments in the NW Scottish Highlands. Quaternary Geochronology 2, 243-248.

Mahan, S. and Kay, J., 2012, Building on previous OSL dating techniques for gypsum: A case study from Salt Basin playa, New Mexico & Texas: Quaternary Geochronology. v. 10, p. 345-352.

Murray, A.S., Olley, J.M., 2002, Precision and accuracy in the optically stimulated luminescence dating of sedimentary quartz: a status review: Geochronometria. v. 21, p. 1-16.

Murray, A.S., Wintle, A.G., 2000, Luminescence dating of quartz using an improved single aliquot regenerative-dose protocol: Radiation Measurements. v. 32, p. 57–73.

Murray, A.S., Wintle, A.G., 2003, The single aliquot regenerative dose protocol: potential for improvements in reliability: Radiation Measurements. v. 37, p. 57-73.

Nagar, Y.C., 2007, Methodological aspects of radiation dosimetry of natural radiation environment using luminescence techniques: new minerals and applications. Physical Research Laboratory, Ahmedabad, India, unpublished PhD thesis.

Nagar, Y.C., Sastry, M., Bhushan, B., Ashok, S., Mishra, K., Shastri, A., Deo, M., Kocurek, G., Magee, J., Wadhawan, S., Juval, N., and Pandian, M.S., 2010, Chronometry and formation pathways of gypsum using Electron Spin Resonance and Fourier Transform Infrared Spectroscopy: Quaternary Geochronology. v. 5, p. 691-704.

Nichols, G., 2009, Chapter 10- Lakes In: *Sedimentology and Stratigraphy*. Wiley-Blackwell Publishing. 2nd Edition. p. 151-161.

Nolan, T.B., 1927, Potash brines in the Great Salt Lake Desert, Utah: U.S. Geological Survey Bulletin 795. p. 25-44.

O'Connor, V.A., Lepper, K., Morken, T. O., Thorstad, D. J., Podoll, A., and Giles, M. J., 2011, A survey of the signal stability and radiation dose response of sulfates in the context of adapting optical dating for Mars: Journal of Luminescence. v. 131, p. 2762-2768.

Oviatt, C.G., 2015, Chronology of Lake Bonneville, 30,000 to 10,000 yr. BP: Quaternary Science Reviews. v. 110, p. 166-171.

Oviatt, C.G. and Shroder, J.F., Jr., Eds., 2016. *Lake Bonneville: A Scientific Update*. Developments in Earth Surface Processes 20. Elsevier. p. 659.

Peruffo, M., Mbogoro, M.M., Edwards, M.A., and Unwin, P.R., 2013, Holistic approach to dissolution kinetics: linking direction-specific microscopic fluxes, local mass transport effects and global macroscopic rates from gypsum etch pit analysis: Physical Chemistry, v. 15, p. 1956–1965.

Porta, J., 1998, Methodologies for the analysis and characterization of gypsum in soils: A review: Geoderma. v. 87, p. 31-46.

Prasad, P.S.R., Pradhan, A., and Gowd, T.N., 2001, In situ micro-Raman investigation of dehydration mechanism in natural gypsum: Current Science, v. 80, p. 1203-1207.

Prescott, J.R., Hutton, J.T., 1994, Cosmic ray contributions to dose rates for luminescence and ESR dating: large depths and long-term time variations: Radiation Measurements. v. 23, p. 497–500.

Preusser, F., Degering, D., Fuchs, M., Hilgers, A., Kadereit, A., Klasen, N., Krbetschek, M., Richter, D. and Spencer, J.Q.G., 2008, Luminescence dating: basics, methods and application: Eiszeitalter & Gegenwart/ Quaternary Science Journal. v. 57, p. 95-149.

Ramachandran, V.S., Paroli, R.M., Beaudoin, J.J. and Delgado, A.H., 2002, Chapter 11- Gypsum and Gypsum Products In: *Handbook of Thermal Analysis of Construction Materials*. William Andrew Publishing/Noyes. Electronic ISBN: 978-0-8155-1775-7. p. 449-489.

Reimer, P.J., Bard, E., Bayliss, A., Beck, J.W., Blackwell, P.G., Ramsey, C.B., Buck, C.E., Cheng, H., Edwards, R.L., Friedrich, M., Grootes, P.M., Guilderson, T.P., Haflidason, H., Hajdas, I., Hatté, C., Heaton, T.J., Hoffmann, D.L., Hogg, A.G., Hughen, K.A., Kaiser, K.F., Kromer, B., Manning, S.W., Niu, M., Reimer, R.W., Richards, D.A., Scott, E.M., Southon, J.R., Staff, R.A., Turney, C.S.M., van der Plicht, J., 2013, IntCal13 and

Marine13 Radiocarbon Age Calibration Curves 0-50,000 Years Cal BP: Radiocarbon. v. 55 (4). p. 1869–1887

Rhodes, E.J., 2011, Optically Stimulated Luminescence Dating of Sediments over the past 200,000 years: Annual Review. Earth Planet, Science. v. 39, p. 461-488.

Roberts, H.M., 2012, Testing Post-IR IRSL protocols for minimizing fading in feldspars, using Alaskan loess with independent chronological control: Radiation Measurements. v. 47, p. 716-724.

Roozeboom, J.E., 2015. Exploration and application of post-infrared high-temperature infrared stimulated luminescence dating techniques: investigation of marine terrace deposits along the northern San Andreas Fault (Master's thesis, Kansas State University, Manhattan, Kansas). Retrieved from https://krex.k-state.edu/dspace/bitstream/handle/2097/19050/JenniferRoozeboom2015.pdf?sequence=1&isAllowed=y

Schreiber, C. and El Tabakh, M., 2000, Deposition and early alteration of evaporites: Sedimentology. v. 47, p. 215-238.

Spencer, J.Q., Owen, L.A., 2004, Optically stimulated luminescence dating of Late Quaternary glaciogenic sediments in the upper Hunza valley: validating the timing of glaciation and assessing dating methods: Quaternary Science Reviews. v. 23, p. 175-191.

Spencer, J.Q.G., Robinson, R.A.J., 2008. Dating intramontane alluvial deposits from NW Argentina using luminescence techniques: problems and potential. Geomorphology 93, 144-156.

Spencer, J.Q., Sanderson, D.C.W., Deckers, K., Sommerville, A.A., 2003. Assessing mixed dose distributions in young sediments identified using small aliquots and a simple two-step SAR procedure: the F-statistic as a diagnostic tool. Radiation Measurements 37, 425-431.

Spooner, N.A., 1992, Optical dating: Preliminary results on the anomalous fading of luminescence from feldspars: Quaternary Science Reviews. v. 11, p. 139-145.

Spooner, N.A., 1994, The anomalous fading of infrared-stimulated luminescence from feldspars: Radiation Measurements. v. 23, p. 625-632.

Szynkiewicz, A., Pratt, L., Glamoclija, M., Moore, C., Singer, E., and Bustos, D., 2008, White Sands gypsum dunes: A Terrestrial Analog to North Polar Dunes on Mars?: Planetary Dunes Workshop: A Record of Climate Change, p. 7011.

Szynkiewicz, A., Ewing, R., Moore, C., Glamoclija, M., Bustos, D., and Pratt, L., 2010, Origin of terrestrial gypsum dunes-Implications for Martian gypsum-rich dunes of Olympia Undae: Geomorphology, v. 121, p. 69-83.

Thiel, C., Buylaert, J.P., Murray, A.S., Terhorst, B., Hofer, I., Tsukamoto, S., and Frechen, M., 2011, Luminescence dating of the Stratzing loess profile (Austria) – Testing the potential of an elevated temperature post-IR IRSL protocol: Quaternary International. v. 234, p. 23-31.

Thompson, J.W., Burdette, K.E., Inrig, E.L., Dewitt, R., Mistry, R., Rink, W.J., and Boreham, D.R., 2010, Optically Stimulated Luminescence Dosimetry with Gypsum Wallboard (Drywall): Radiation Protection Dosimetry. v. 14(1), p. 1-9.

Thomsen, K.J., Murray, A.S., Jain, M., and Bøtter-Jensen, L., 2008, Laboratory fading rates of various luminescence signals from feldspar-rich sediment extracts: Radiation Measurements. v. 43, p. 1474-1486.

Wintle, A.G., 1973, Anomalous fading of thermoluminescence in mineral samples: Nature. v. 243, p. 143-144.

Wintle, A.G., Murray, A.S., 2006, A review of quartz optically stimulated luminescence characteristics and their relevance in single-aliquot regeneration dating protocols: Radiation Measurements. v. 41, p. 369-391.

Appendix A - Moisture Content

This is the raw data of calculated field moisture content for all samples. All samples were air-dried at room temperature in complete darkness to prevent mineral transformation and mitigate luminescence signal degradation. Water content % was determined by the equation: (water content = moisture mass/ dry sediment mass) * 100%

Sample	Initial Net Mass (g)	Final Net Mass (g)	Mass of Moisture (g)	**Water Content (%)**
KNP-A2	217.3	211.9	5.4	**2.49**
KNP-A2 Exp Ends	39.1	38.2	0.9	**2.30**
KNP-A3	220.4	215.6	4.8	**2.18**
KNP-A3 Exp Ends	37.0	36.2	0.8	**2.16**
KNP-A4	206.9	196.2	10.7	**5.17**
KNP-A4 Exp Ends	29.4	28.1	1.3	**4.42**
KNP-A5	175.6	170.2	5.4	**3.08**
KNP-A5 Exp Ends	57.1	55.2	1.9	**3.33**
KNP-B1	208.5	204.4	4.1	**1.97**
KNP-B1 Exp Ends	43.7	42.9	0.8	**1.83**
KNP-B2	157.8	155.0	2.8	**1.77**
KNP-B2 Exp Ends	80.0	78.7	1.3	**1.63**
KNP-B3	195.9	187.7	8.2	**4.19**
KNP-B3 Exp Ends	53.4	51.2	2.2	**4.12**
KNP-B4	187.7	181.4	6.3	**3.36**
KNP-B4 Exp Ends	56.9	55.0	1.9	**3.34**
CD-5	177.6	173.8	3.8	**2.14**
CD-5 Exp Ends	51.2	50.3	0.9	**1.76**
K7-1	222.3	214.5	7.8	**3.51**
K7-1 Exp Ends	57.3	55.4	1.9	**3.32**

Appendix B - X-Ray Diffraction (XRD) Data

B.1 Bulk Mineral Comparison

Example of XRD peaks across dune pre and post treatments. Vertical gray bars indicate expected peak for mineral gypsum. Bottom graph displays anomalous peak; it was later determined that this peak coincides with CaF_2 (fluorite or fluorite precipitate).

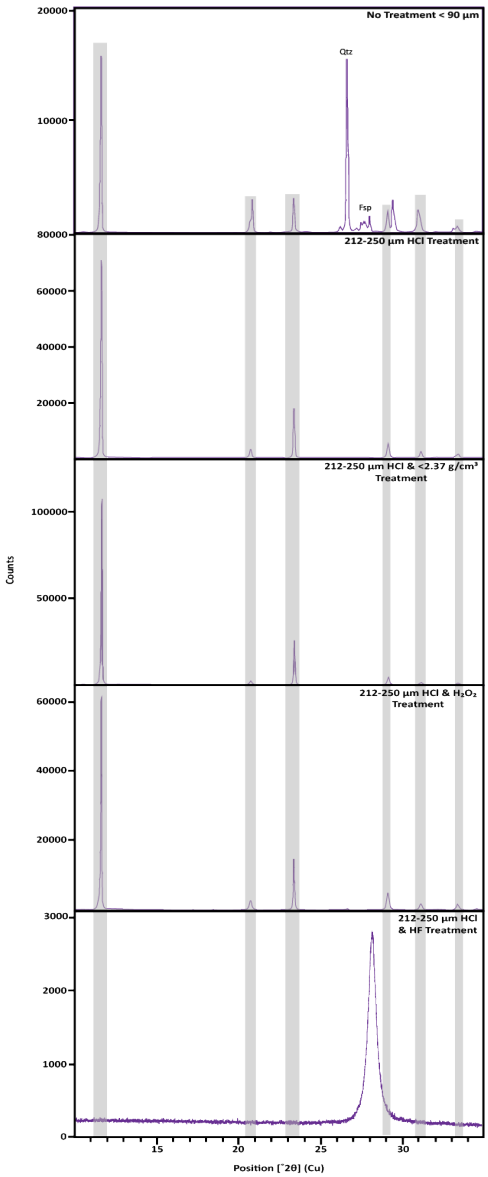

Appendix C - Particle Size Analysis

This appendix outlines experimental data attained through three experiments: mass loss, sieve fraction analysis, and a particle size analysis using a Malvern Mastersizer 3000 laser diffraction particle size analyzer with a Hydro EV wet dispersion accessory. It is important to note that ultimately the Malvern particle size analysis was excluded from my research due to quality control criteria in the software used for the machine and recently published research (Fang et al., 2017) observing gypsum dissolution begin as soon as flowing water contacts gypsum crystals.

C.1 Mass Loss Experiment

The objective of this experiment was to determine if there were indications of gypsum etching in subsequent 10 wt % HCl treatments after carbonate dissolution in standard 30 minute 10 wt % HCl treatment. Data sourced from surface sand of modern coppice dunes forming behind brushy vegetation. Dashed lines indicate sample did not receive treatment specified. See Appendix E for supporting scanning electron microscopy.

Surface sand (Grab Bag) Mass Loss Data							
Mass (g)	Bulk Sediment (g)	10 wt% HCl 30 min (g)	Mass Difference (g)	10 wt % HCl 10 min (g)	Mass Difference (g)	10 wt % HCl 10 min (g)	Mass Difference (g)
Sample 1	10.3710	10.2310	**0.1400**	-	-	-	-
Sample 2	10.4526	9.9537	**0.4989**	9.9026	**0.0511**	-	-
Sample 3	10.9368	-	-	10.7793	**0.1575**	10.3948	**0.3846**

C.2 Sieve Fraction Data

Sieve Fraction data was analyzed using seven sieve fraction sizes, followed by a recalculation using the USGS standard sand grain sizes seen below.

	Bottom -->Top				
Sieve Fraction (µm)	KNP-A1 Mass (%)	KNP-A2 Mass (%)	KNP-A3 Mass (%)	KNP-A4 Mass (%)	KNP-A5 Mass (%)
>250	8.9	47.7	60.7	15.2	45.9
125-250	30.7	41.5	25.3	46.7	28.2
64-125	50.7	8.2	11.8	30.7	20.9
< 64	7.9	1.4	1.4	5.3	4.4
Total (%):	98.2	98.8	99.2	97.8	99.4
% Lost:	1.8	1.2	0.8	2.2	0.6

	Bottom--> Top			
Sieve Fraction (µm)	KNP-B1 Mass (%)	KNP-B2 Mass (%)	KNP-B3 Mass (%)	KNP-B4 Mass (%)
>250	58.0	71.3	34.5	25.7
125-250	30.5	23.1	30.5	33.9
64-125	10.4	4.6	29.1	34.5
< 64	1.0	0.4	4.0	5.2
Total (%):	99.8	99.4	98.2	99.3
% Lost:	0.2	0.6	1.8	0.7

	Surface/Modern		Massive QTZ	2013 Paleodune A Samples			
Sieve Fraction (µm)	CD-4 Mass (%)	CD-5 Mass (%)	K7-1 Mass (%)	KN-01 Mass (%)	KN-02 Mass (%)	KN-03 Mass (%)	KN-04 Mass (%)
>250		19.7	0.4		36.7	37.8	37.3
125-250		51.4	63.1		37.3	35.2	24.8
64-125		26.5	34.1		19.0	14.4	27.9
< 64		1.4	1.4		6.0	2.8	8.8
Total (%):		99.0	99.0		99.0	90.2	98.8
% Lost:		1.0	1.0		1.0	9.8	1.2

C.3 Particle Size Data

Note that "Run" number is associated with the number of 10 wt % HCl treatments a sample of gypsum sediment underwent. Samples were initially pretreated with hydrogen peroxide to remove organics per particle size analyzer protocol. Hydrogen peroxide treatment times varied per sample and were rinsed in deionized water after reaction had stopped before proceeding with first HCl treatments. Dried samples were scooped, to ensure representative sampling, into the wet dispersion accessory of the particle analyzer while the propeller was set for 1500rpm. Particle size data are reported as % by volume (% Volume In).

Knolls Paleodune A1 (KNPA1)				Coppice Dune 4 (CD4)			
Size (μm)	% Volume In			Size (μm)	% Volume In		
	Run 1	Run 2	Run 3		Run 1	Run 2	Run 3
0.01	0	0	0	0.01	0	0	0
0.0114	0	0	0	0.0114	0	0	0
0.0129	0	0	0	0.0129	0	0	0
0.0147	0	0	0	0.0147	0	0	0
0.0167	0	0	0	0.0167	0	0	0
0.0189	0	0	0	0.0189	0	0	0
0.0215	0	0	0	0.0215	0	0	0
0.0244	0	0	0	0.0244	0	0	0
0.0278	0	0	0	0.0278	0	0	0
0.0315	0	0	0	0.0315	0	0	0
0.0358	0	0	0	0.0358	0	0	0
0.0407	0	0	0	0.0407	0	0	0
0.0463	0	0	0	0.0463	0	0	0
Knolls Paleodune A1 (KNPA1)				Coppice Dune 4 (CD4)			
Size (μm)	% Volume In			Size (μm)	% Volume In		
	Run 1	Run 2	Run 3		Run 1	Run 2	Run 3
0.0526	0	0	0	0.0526	0	0	0
0.0597	0	0	0	0.0597	0	0	0
0.0679	0	0	0	0.0679	0	0	0
0.0771	0	0	0	0.0771	0	0	0

0.0876	0	0	0	0.0876	0	0	0
0.0995	0	0	0	0.0995	0	0	0
0.113	0	0	0	0.113	0	0	0
0.128	0	0	0	0.128	0	0	0
0.146	0	0	0	0.146	0	0	0
0.166	0	0	0	0.166	0	0	0
0.188	0	0	0	0.188	0	0	0
0.214	0	0	0	0.214	0	0	0
0.243	0	0	0	0.243	0	0	0
0.276	0	0	0	0.276	0	0	0
0.314	0	0	0	0.314	0	0	0
0.357	0	0	0	0.357	0	0	0
0.405	0	0	0	0.405	0	0	0
0.46	0	0	0	0.46	0	0.08	0.1
0.523	0	0	0	0.523	0.13	0.22	0.25
0.594	0	0	0	0.594	0.23	0.36	0.4
0.675	0.06	0	0.07	0.675	0.29	0.47	0.51
0.767	0.07	0.08	0.09	0.767	0.32	0.51	0.54
0.872	0.08	0.08	0.09	0.872	0.31	0.49	0.51
0.991	0.07	0.08	0.09	0.991	0.28	0.44	0.45
1.13	0.07	0.07	0.09	1.13	0.25	0.39	0.4
1.28	0.06	0.07	0.08	1.28	0.25	0.38	0.39
1.45	0.07	0.07	0.08	1.45	0.26	0.41	0.42
1.65	0.07	0.08	0.09	1.65	0.29	0.45	0.46
1.88	0.08	0.09	0.1	1.88	0.32	0.49	0.51
2.13	0.09	0.1	0.12	2.13	0.33	0.53	0.54
2.42	0.1	0.11	0.13	2.42	0.34	0.54	0.55
2.75	0.11	0.13	0.15	2.75	0.33	0.54	0.55
3.12	0.12	0.14	0.16	3.12	0.32	0.53	0.53
3.55	0.13	0.15	0.18	3.55	0.3	0.51	0.5
4.03	0.14	0.16	0.19	4.03	0.28	0.48	0.46
4.58	0.14	0.16	0.19	4.58	0.26	0.46	0.43
5.21	0.14	0.16	0.19	5.21	0.24	0.42	0.39
5.92	0.14	0.15	0.18	5.92	0.22	0.39	0.35
Knolls Paleodune A1 (KNPA1)				Coppice Dune 4 (CD4)			
Size (μm)	% Volume In			Size (μm)	% Volume In		
	Run 1	Run 2	Run 3		Run 1	Run 2	Run 3
6.72	0.15	0.15	0.18	6.72	0.2	0.35	0.32
7.64	0.16	0.17	0.2	7.64	0.18	0.33	0.3
8.68	0.2	0.2	0.23	8.68	0.17	0.31	0.29
9.86	0.25	0.26	0.3	9.86	0.18	0.31	0.3

11.2	0.33	0.35	0.4	11.2	0.19	0.32	0.32
12.7	0.43	0.47	0.53	12.7	0.21	0.35	0.35
14.5	0.54	0.59	0.66	14.5	0.24	0.38	0.38
16.4	0.64	0.69	0.77	16.4	0.26	0.4	0.39
18.7	0.7	0.75	0.82	18.7	0.28	0.41	0.38
21.2	0.72	0.74	0.79	21.2	0.27	0.39	0.33
24.1	0.68	0.65	0.68	24.1	0.24	0.34	0.25
27.4	0.61	0.51	0.5	27.4	0.19	0.26	0.15
31.1	0.54	0.37	0.33	31.1	0.12	0.16	0.06
35.3	0.55	0.33	0.26	35.3	0	0.07	0
40.1	0.72	0.5	0.43	40.1	0	0	0
45.6	1.14	0.98	0.96	45.6	0	0	0
51.8	1.87	1.86	1.92	51.8	0	0	0.01
58.9	2.92	3.14	3.33	58.9	0	0.19	0.44
66.9	4.24	4.73	5.07	66.9	0.3	0.8	1.41
76	5.71	6.47	6.95	76	1.1	1.95	2.99
86.4	7.15	8.12	8.69	86.4	2.49	3.62	5.04
98.1	8.38	9.43	10.03	98.1	4.4	5.65	7.31
111	9.23	10.2	10.72	111	6.61	7.78	9.44
127	9.59	10.3	10.64	127	8.83	9.67	11.03
144	9.41	9.72	9.8	144	10.68	10.98	11.77
163	8.71	8.55	8.32	163	11.82	11.44	11.46
186	7.56	6.97	6.44	186	12.01	10.92	10.11
211	6.1	5.18	4.43	211	11.15	9.44	7.92
240	4.47	3.43	2.59	240	9.35	7.23	5.3
272	2.88	1.91	0.76	272	6.93	4.7	2.67
310	1.51	0.41	0	310	4.33	2.16	0.06
352	0.15	0	0	352	1.73	0.01	0
400	0	0	0	400	0.01	0	0
454	0	0	0	454	0	0	0
516	0	0	0	516	0	0	0
586	0	0	0	586	0	0	0
666	0	0	0	666	0	0	0
756	0	0	0	756	0	0	0
Knolls Paleodune A1 (KNPA1)				**Coppice Dune 4 (CD4)**			
Size (μm)	% Volume In			Size (μm)	% Volume In		
	Run 1	Run 2	Run 3		Run 1	Run 2	Run 3
859	0	0	0	859	0	0	0
976	0	0	0	976	0	0	0
1110	0	0	0	1110	0	0	0
1260	0	0	0	1260	0	0	0

1430	0	0	0		1430	0	0	0
1630	0	0	0		1630	0	0	0
1850	0	0	0		1850	0	0	0
2100	0	0	0		2100	0	0	0
2390	0	0	0		2390	0	0	0
2710	0	0	0		2710	0	0	0
3080	0	0	0		3080	0	0	0
3500					3500			

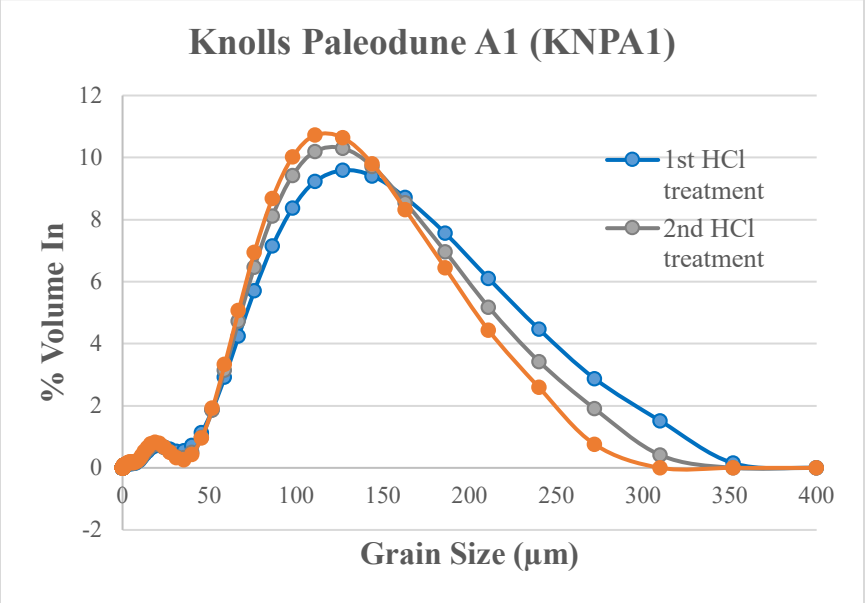

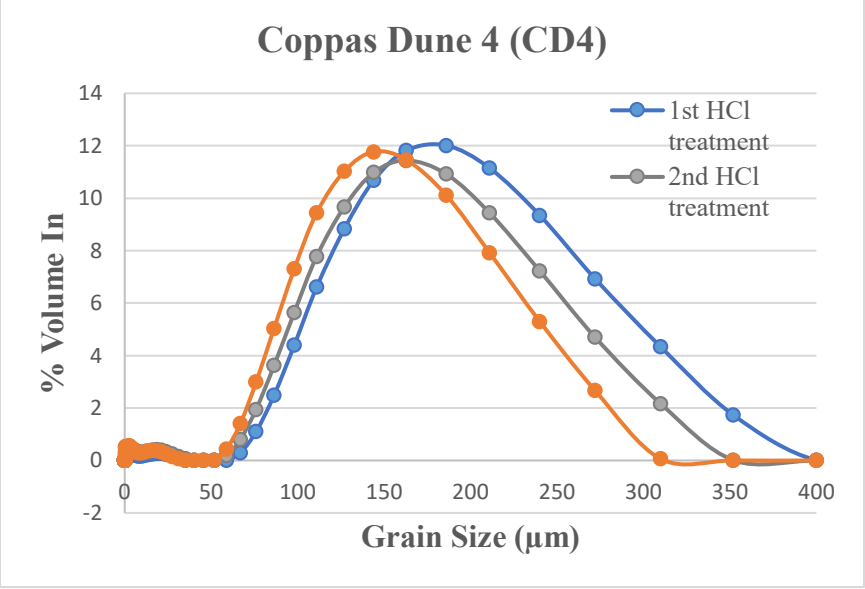

Appendix D - SEM & EDS Data

This appendix outlines results from scanning electron microscopy (SEM) conducted at the Kansas State University NICKS laboratory using a Hitachi S-3500N and Oxford Link Pentafet Model 7021 Energy Dispersive X-Ray Spectrometer (EDS). Several experimental samples used for gypsum and quartz dating as well as samples used to evaluate best preparation methods of gypsum were analyzed.

D.1 212-250 μm Coppice Dune 4 (CD4) Sediment

Coppice Dune 4 was visually observed to be primarily comprised of eolian-transported gypsum; This sample was dry-sieved and the 212-250 μm fraction extracted for further analysis. XRD analysis in Appendix B confirmed mineralogy. SEM and EDS data provided here support this analysis and provide detailed mapping and quantitative elemental composition.

Peak possibly omitted : 2.848 keV (palladium sputter coating)

Processing option : All elements analyzed

Number of iterations = 3

Standard :

O SiO2 1-Jun-1999 12:00 AM

Mg MgO 1-Jun-1999 12:00 AM

Al Al2O3 1-Jun-1999 12:00 AM

Si SiO2 1-Jun-1999 12:00 AM

S FeS2 1-Jun-1999 12:00 AM

Ca Wollastonite 1-Jun-1999 12:00 AM

Fe Fe 1-Jun-1999 12:00 AM

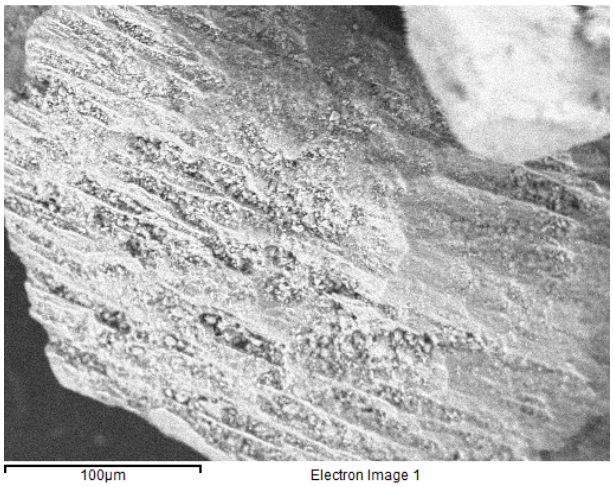

Element	Weight%	Atomic%
O K	5.86	66.75
Mg K	0.34	2.57
Al K	0.31	2.11
Si K	1.26	8.14
S K	1.14	6.46
Ca K	2.79	12.68
Fe K	0.39	1.29
Totals	12.09	

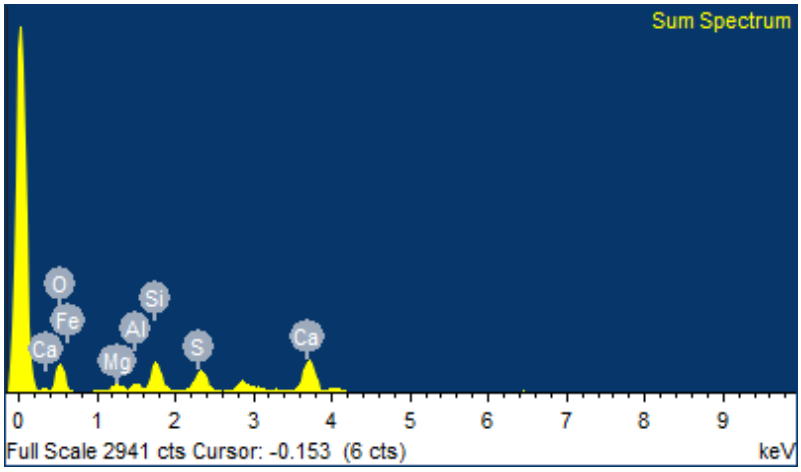

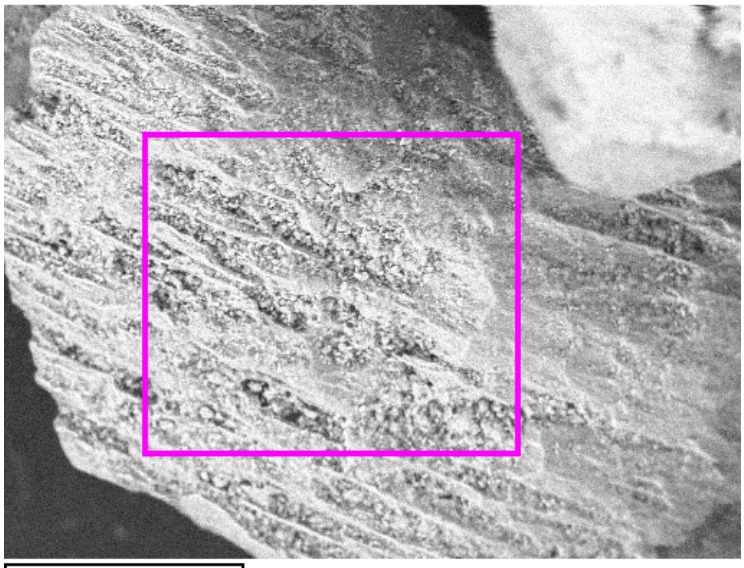

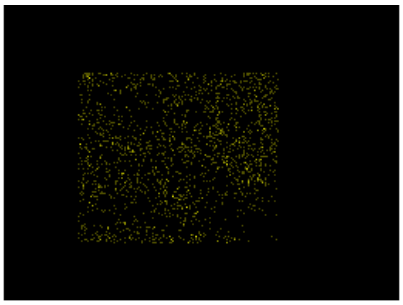
Ca Ka1


Mg Ka1_2

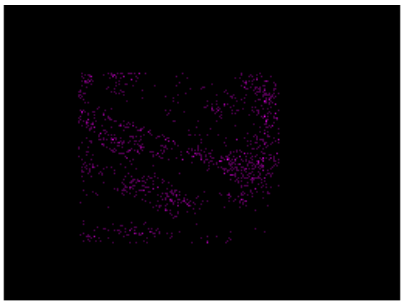
S Ka1

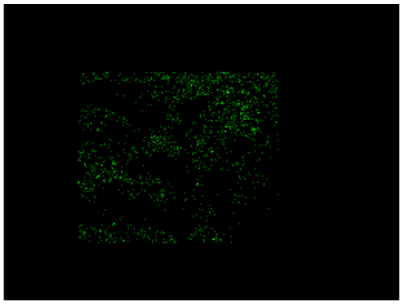
Si Ka1

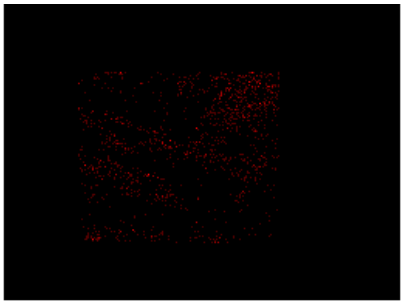
O Ka1

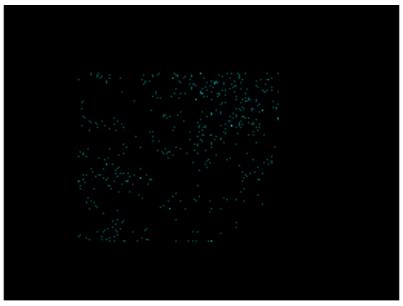
Al Ka1

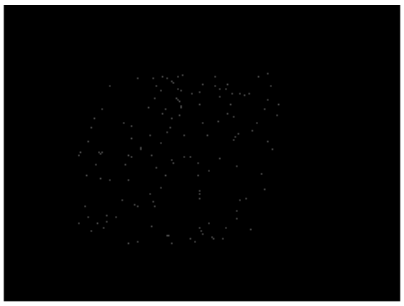
Fe Ka1

D.2 212-250 μm + 30 min HCl Coppice Dune 4 (CD4) Sediment

Sediment was dry-sieved, the 212-250 μm fraction extracted and treated with a 30 minute 10 wt % hydrochloric acid wash. SEM and EDS data provided here support this analysis and provide detailed map and quantitative elemental composition.

Peak possibly omitted : 2.842 keV (palladium sputter coating)

Processing option : All elements analyzed

Number of iterations = 4

Standard :

O SiO2 1-Jun-1999 12:00 AM

Mg MgO 1-Jun-1999 12:00 AM

Al Al2O3 1-Jun-1999 12:00 AM

Si SiO2 1-Jun-1999 12:00 AM

S FeS2 1-Jun-1999 12:00 AM

Ca Wollastonite 1-Jun-1999 12:00 AM

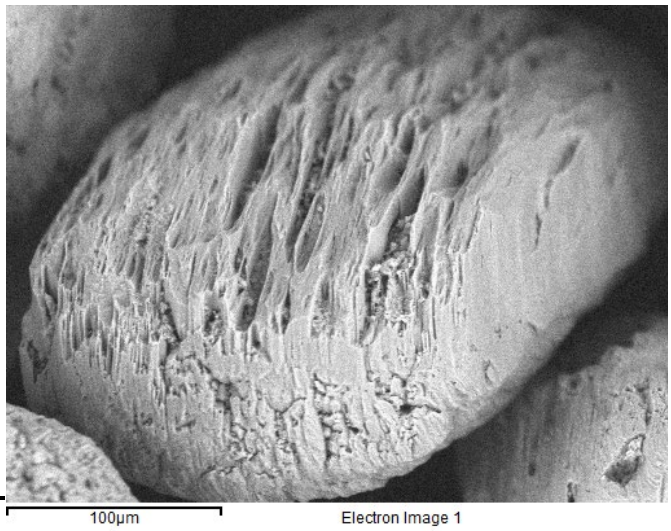

Element	Weight%	Atomic%
O K	14.95	75.76
Mg K	0.14	0.46
Al K	0.20	0.61
Si K	0.70	2.02
S K	4.43	11.19
Ca K	4.92	9.95
Totals	25.33	

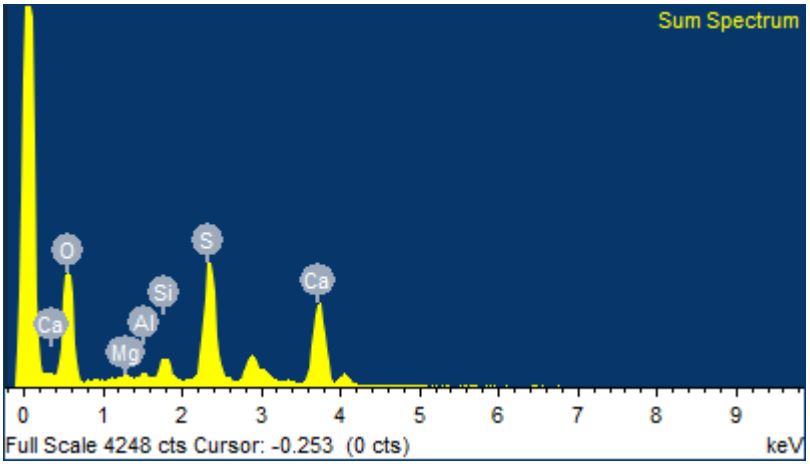

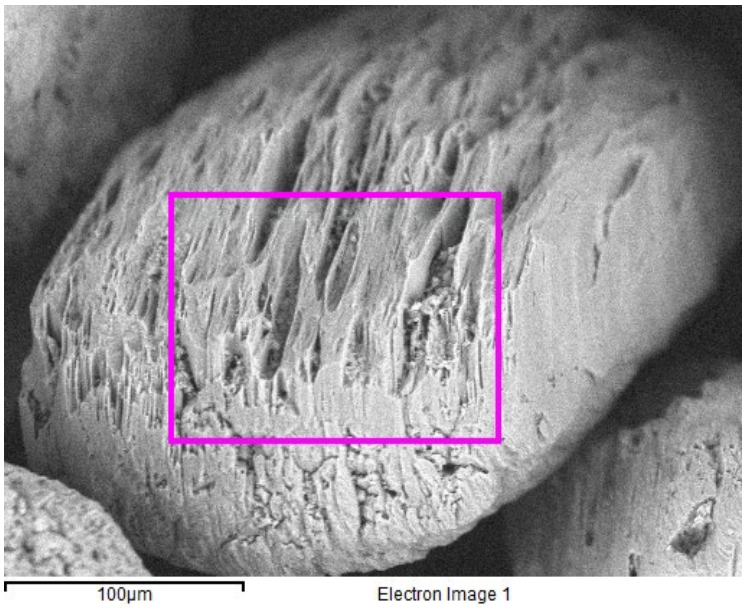

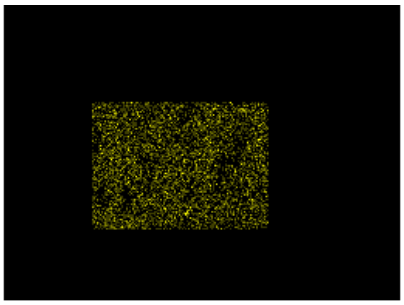
Ca Ka1


Mg Ka1_2

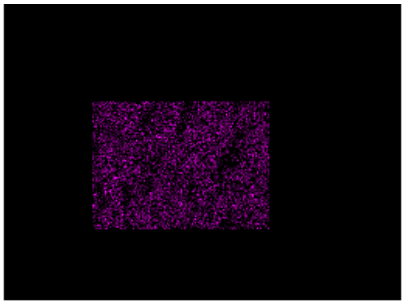
S Ka1

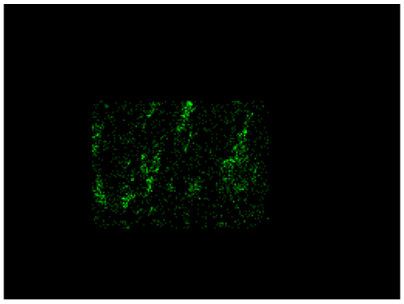
Si Ka1

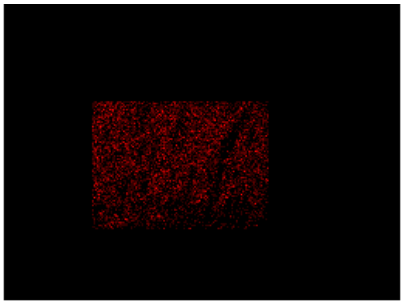
O Ka1

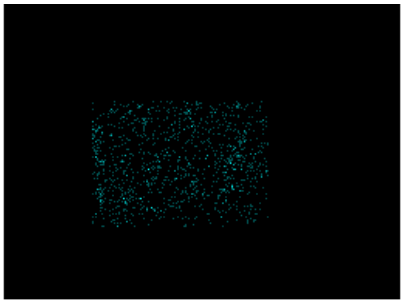
Al Ka1

D.3 212-250 μm + 40 min HCl Coppice Dune 4 (CD4) Sediment

Sediment was dry-sieved, the 212-250 μm fraction extracted, treated with a 30 minute 10 wt % hydrochloric acid wash, followed by an additional 10 minute 10 wt % hydrochloric acid wash to determine if mass loss continued beyond traditional 30 minute treatments. SEM and EDS data provided here support mass loss findings (see Appendix C), etching assumptions, and provide detailed map and quantitative elemental composition.

Peaks possibly omitted : 2.842, 8.789 keV

Processing option : All elements analyzed

Number of iterations = 4

Standard :

O SiO2 1-Jun-1999 12:00 AM

Al Al2O3 1-Jun-1999 12:00 AM

Si SiO2 1-Jun-1999 12:00 AM

S FeS2 1-Jun-1999 12:00 AM

Ca Wollastonite 1-Jun-1999 12:00 AM

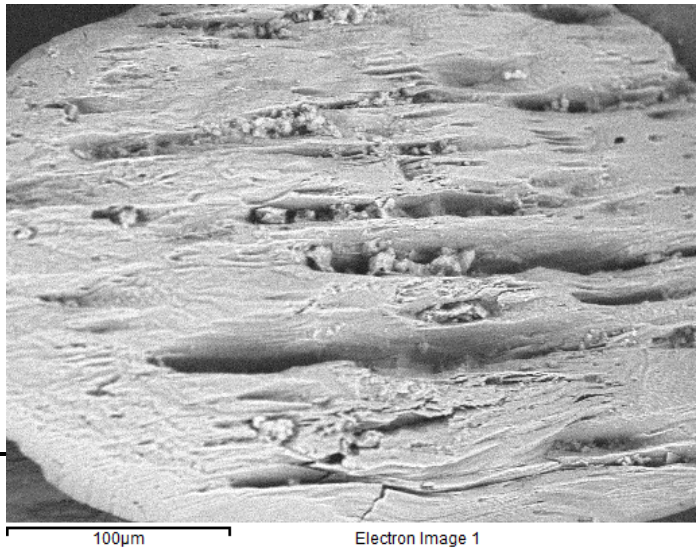

Element	Weight%	Atomic%
O K	9.51	72.88
Al K	0.09	0.39
Si K	0.39	1.71
S K	3.25	12.43
Ca K	4.12	12.59
Totals	17.36	

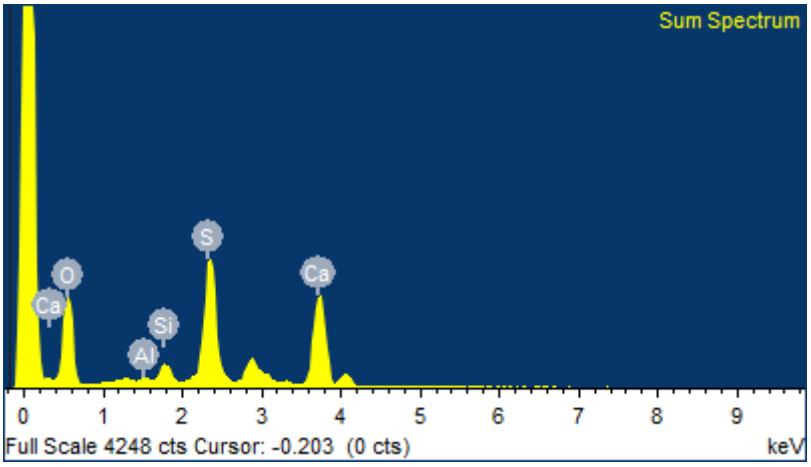

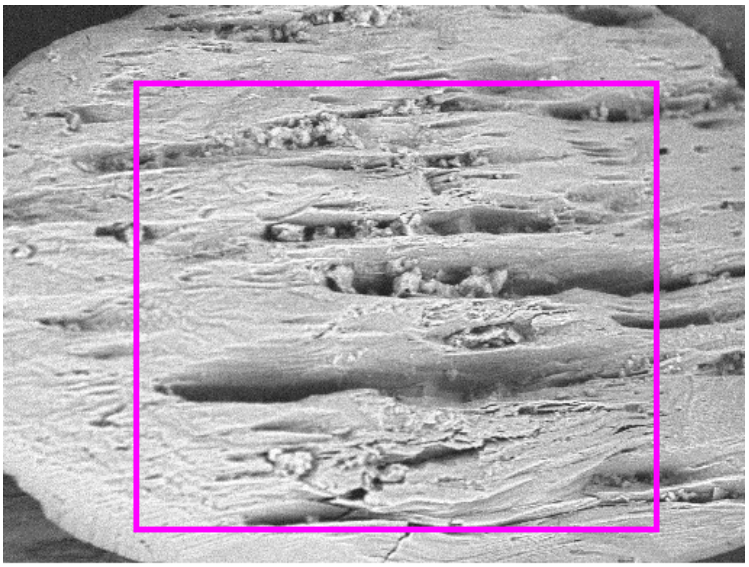

Electron Image 1

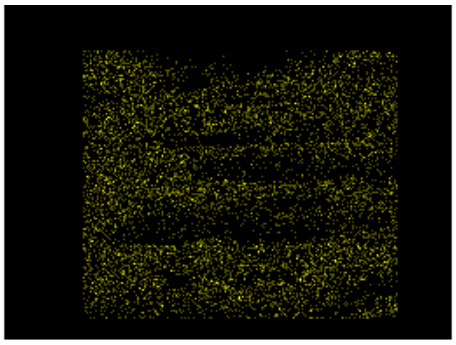

Ca Ka1

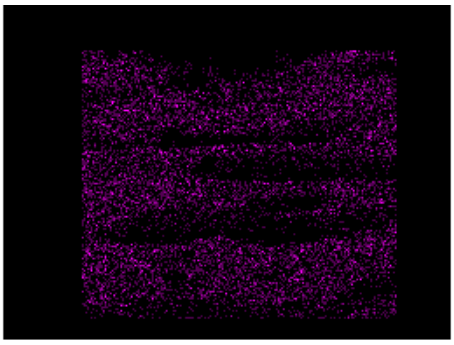

S Ka1

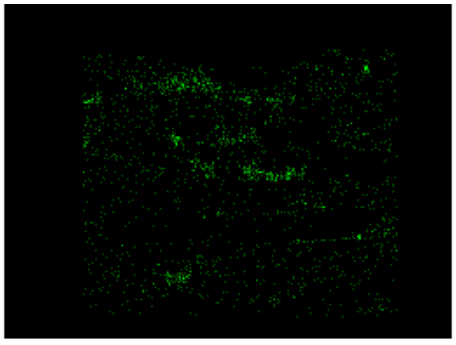

Si Ka1

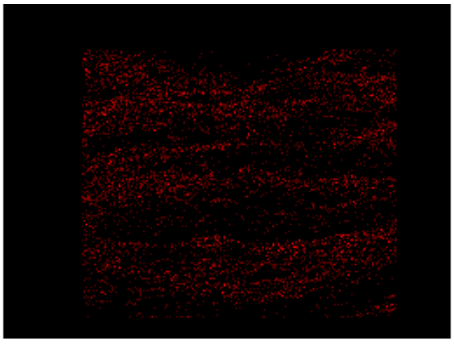

O Ka1

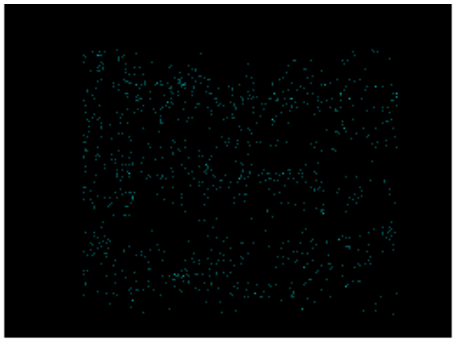

Al Ka1

D.4 212-250 μm + 30 min HCl + H2O2 Knolls Paleodune A3ex (KNP-A3ex)

Sediment was dry-sieved, the 212-250 μm fraction extracted, treated with a 30 minute 10 wt % hydrochloric acid wash, followed by a 35% hydrogen peroxide wash until reaction completed, typically around 2-3 days. SEM and EDS data provided here investigate effects the hydrogen peroxide has on primarily gypsum samples being prepared for OSL dating.

Peak possibly omitted : 2.838 keV

Processing option : All elements analyzed

Number of iterations = 3

Standard :

O SiO2 1-Jun-1999 12:00 AM

Si SiO2 1-Jun-1999 12:00 AM

S FeS2 1-Jun-1999 12:00 AM

Ca Wollastonite 1-Jun-1999 12:00 AM

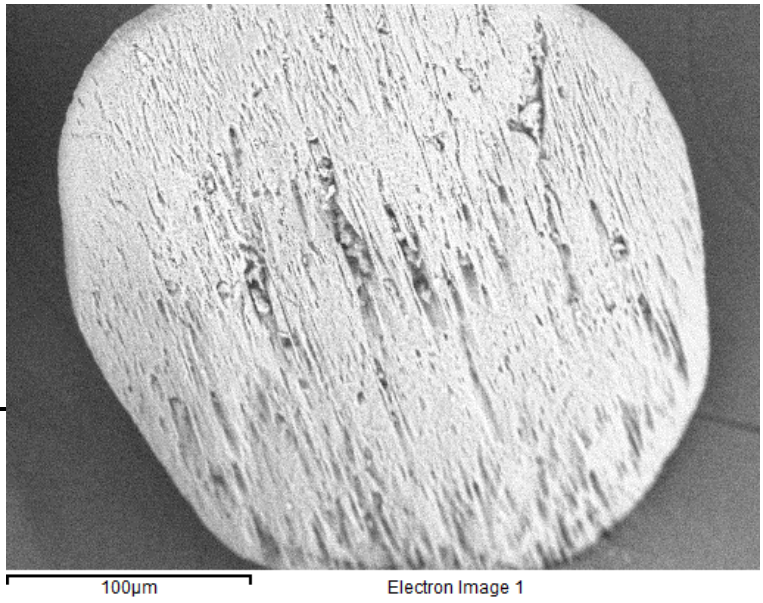

Element	Weight%	Atomic%
O K	3.96	63.48
Si K	0.18	1.60
S K	2.13	17.08
Ca K	2.79	17.84
Totals	9.06	

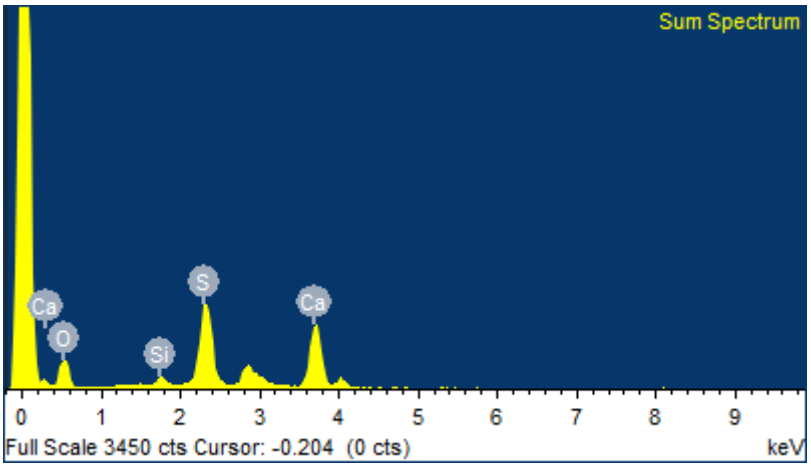

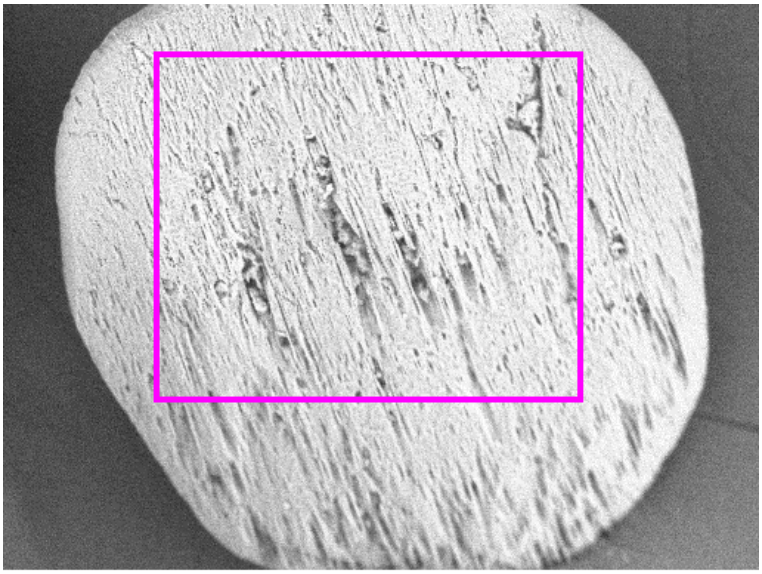

Electron Image 1

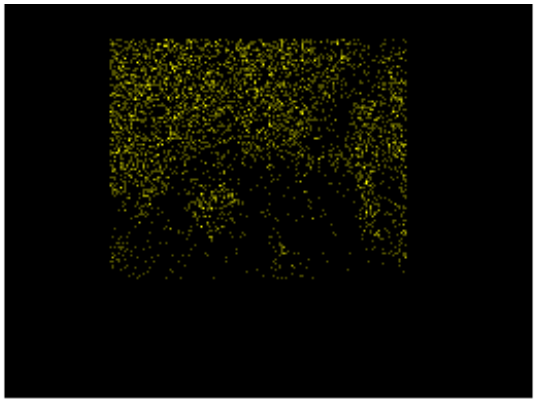

Ca Ka1

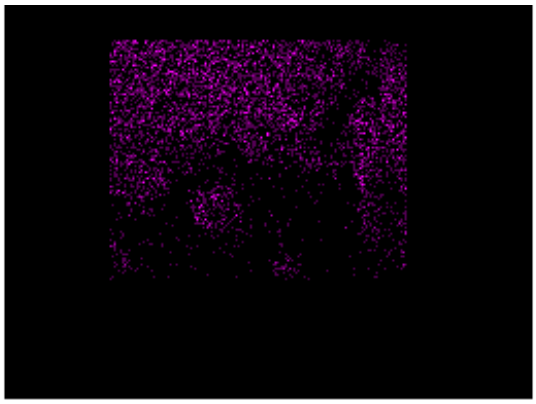

S Ka1

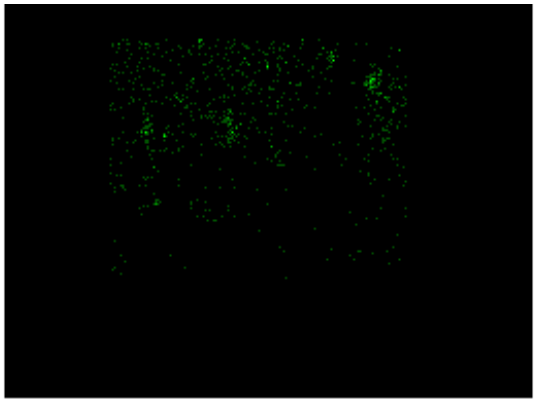

Si Ka1

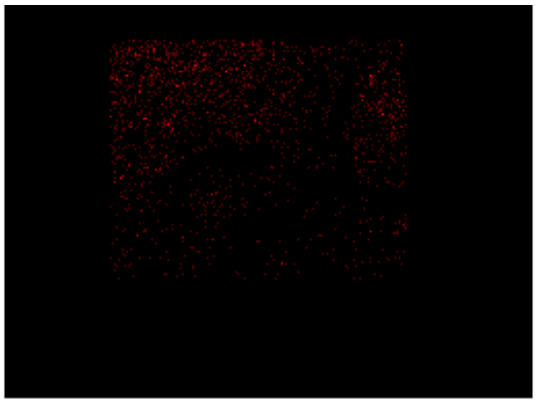

O Ka1

D.5 212-250 μm + HCl + H2O2 + HF Knolls Paleodune A3ex (KNP-A3ex)

Sediment was dry-sieved, the 212-250 μm fraction extracted, treated with a 30 minute 10 wt % hydrochloric acid wash, followed by a 35% hydrogen peroxide wash until reaction completed (typically ~2-3 days), and finally set in a 48-51% hydrofluoric acid wash for 40 minutes. This is in following with traditionally accepted methods of quartz preparation and would typically be finished with a 30 minute HCl treatment to remove fluorisilicate precipitates. However, this investigation probed whether or not gypsum was strong enough to survive HF treatment so a follow up HCl treatment was not pursued. SEM and EDS data provided here investigate effects the hydrofluoric acid has on primarily gypsum samples being prepared for OSL dating.

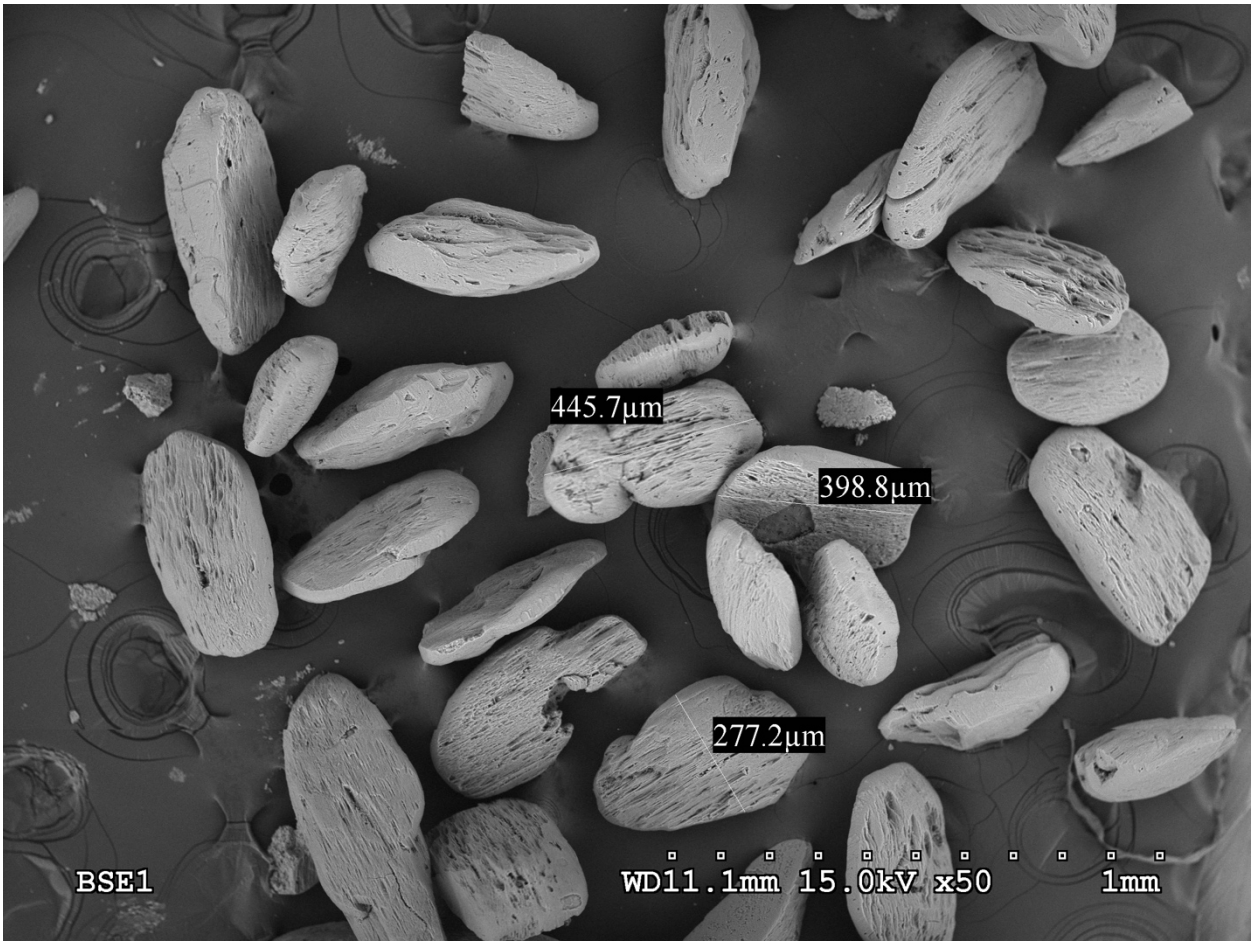

Peaks possibly omitted : 2.843, 5.280 keV

Processing option : All elements analyzed

Number of iterations = 3

Standard :

F MgF2 1-Jun-1999 12:00 AM

Ca Wollastonite 1-Jun-1999 12:00 AM

Element	Weight%	Atomic%
F K	4.06	57.72
Ca K	6.27	42.28
Totals	10.33	

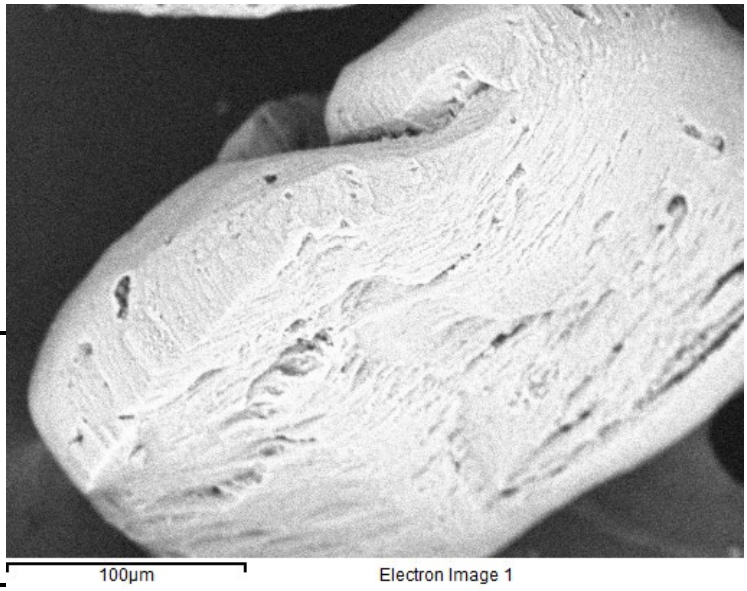

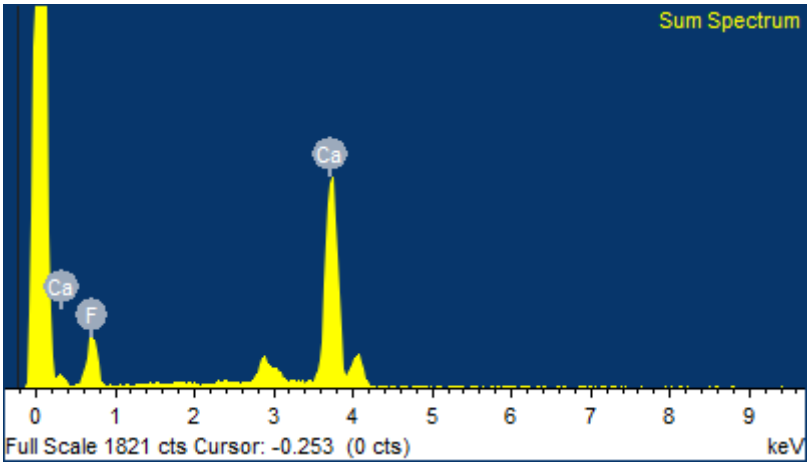

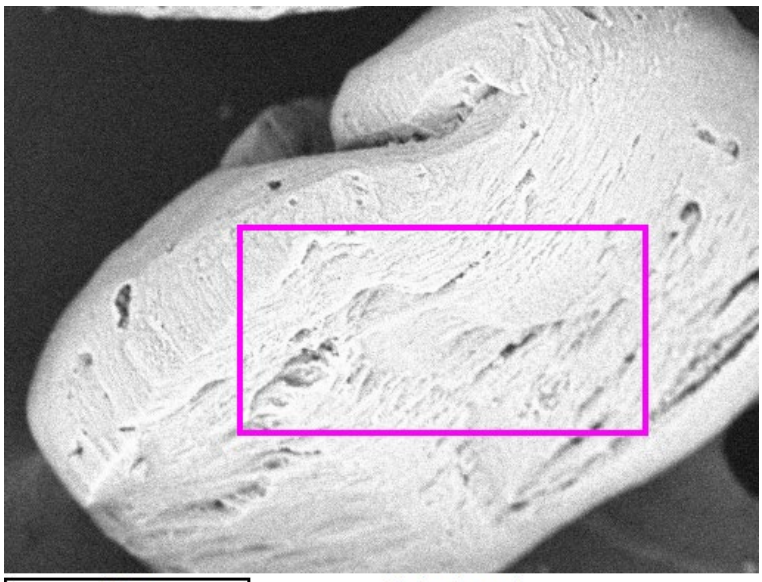

Electron Image 1

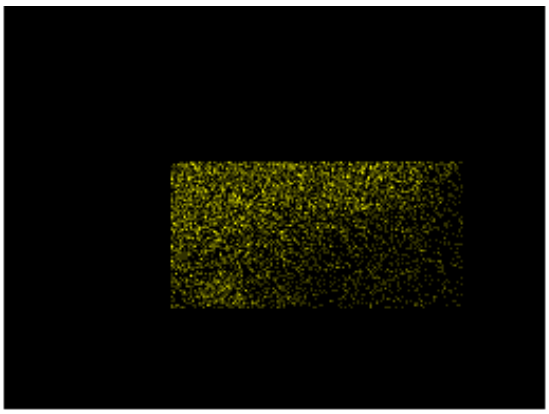

Ca Ka1

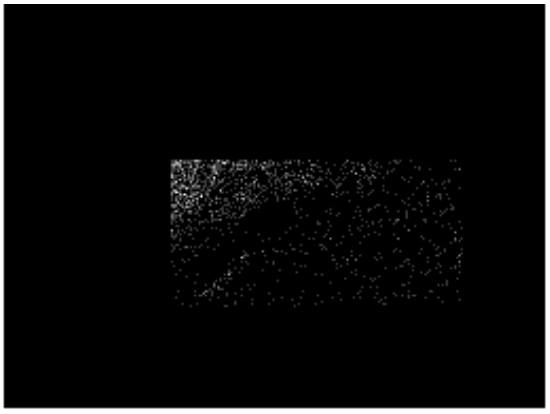

F Ka1_2

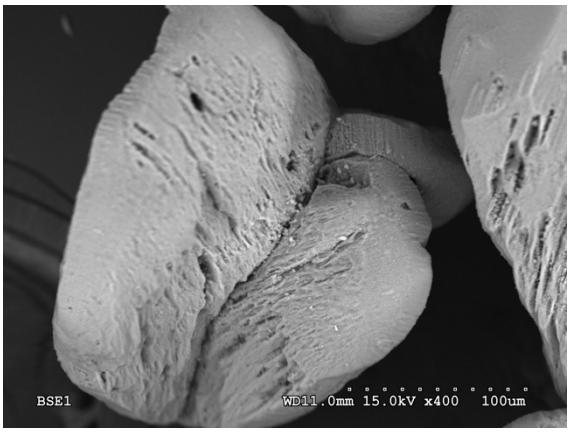

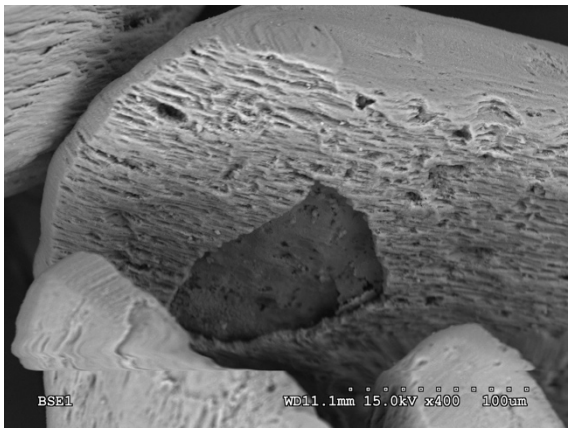

D.6 90-125 μm Quartz Knolls Paleodune A3ex (KNP-A3ex)

SEM and EDS data provided here investigate mineralogy and etching effects on primarily quartz samples prepared for OSL dating.

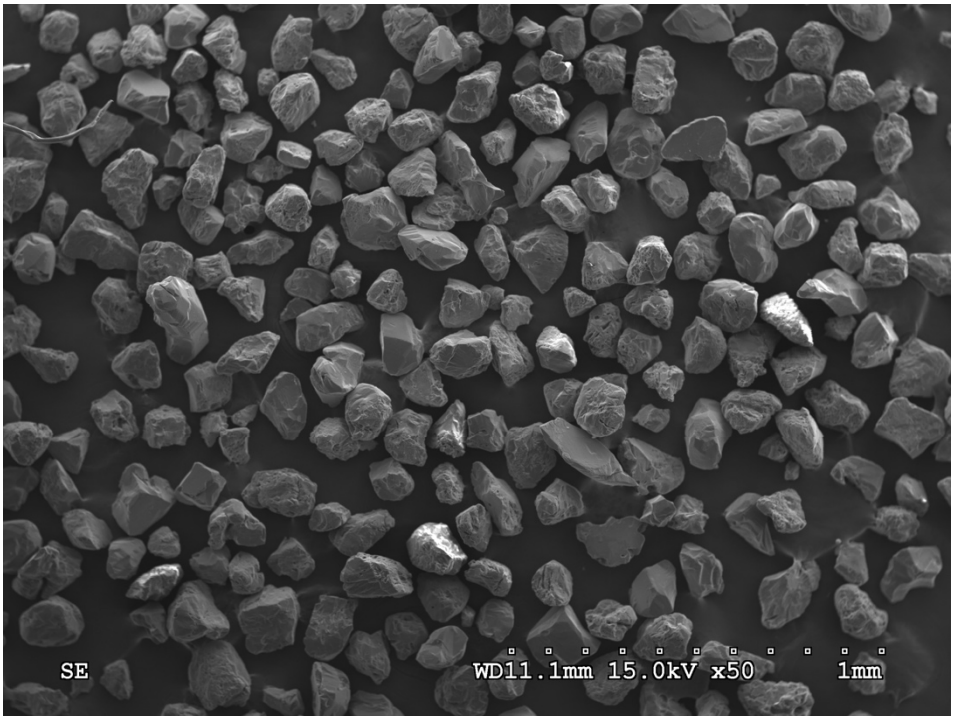

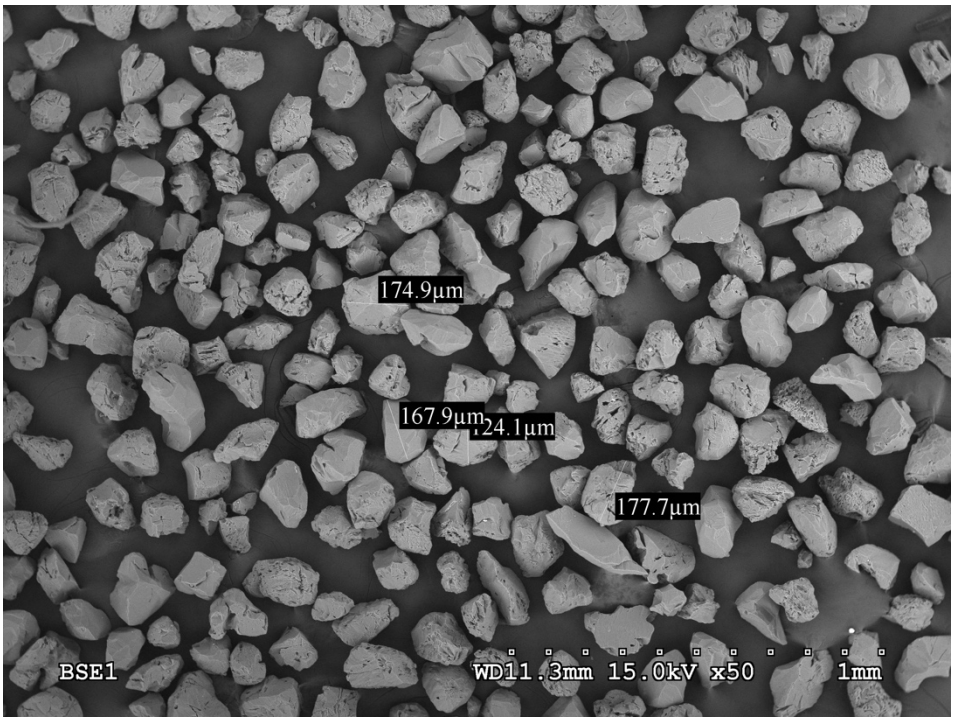

Peak possibly omitted : 2.859 keV

Processing option : All elements analyzed

Number of iterations = 3

Standard :

O SiO2 1-Jun-1999 12:00 AM

Si SiO2 1-Jun-1999 12:00 AM

Sr SrF2 1-Jun-1999 12:00 AM

Element	Weight%	Atomic%
O K	13.80	67.03
Si K	11.46	31.71
Sr L	1.42	1.26
Totals	26.68	

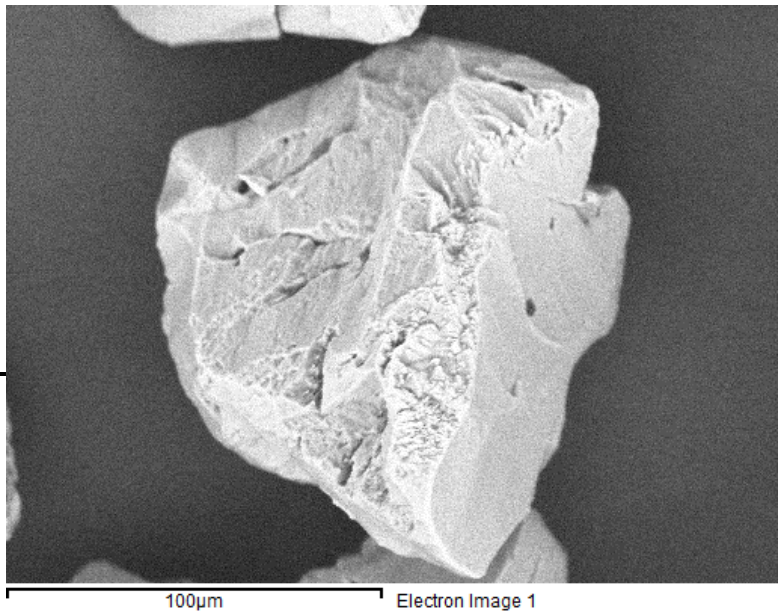

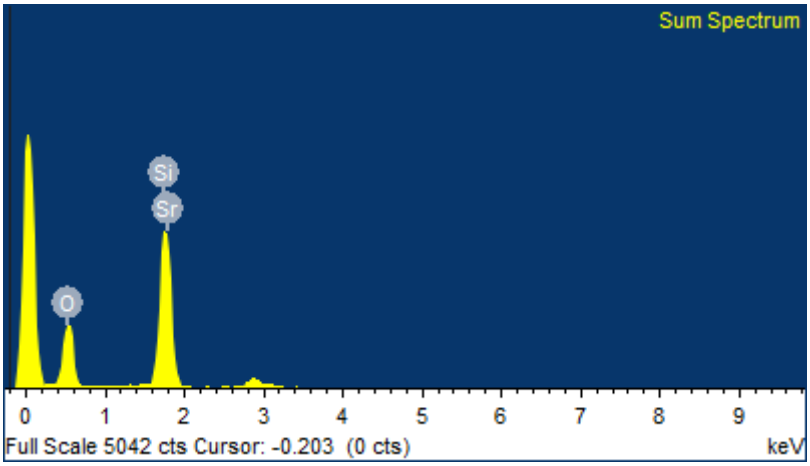

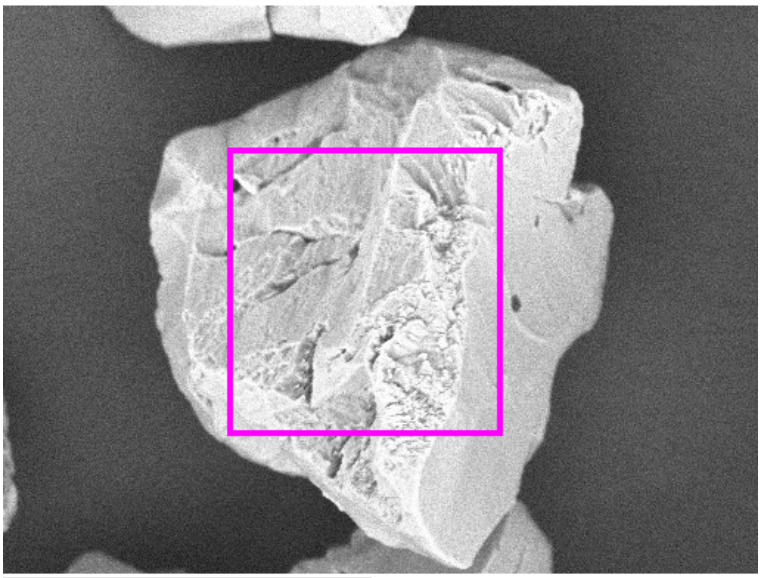

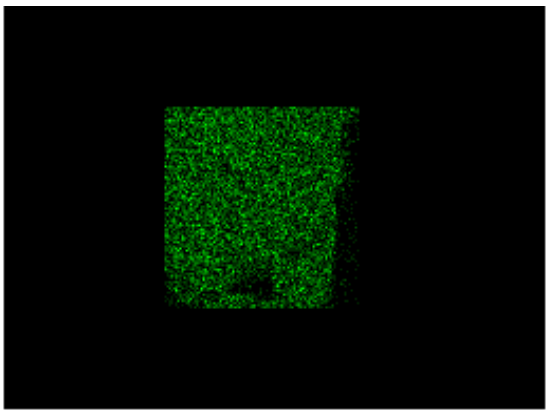

Si Ka1

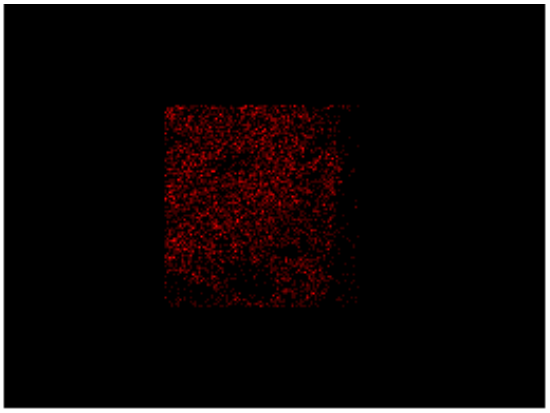

O Ka1

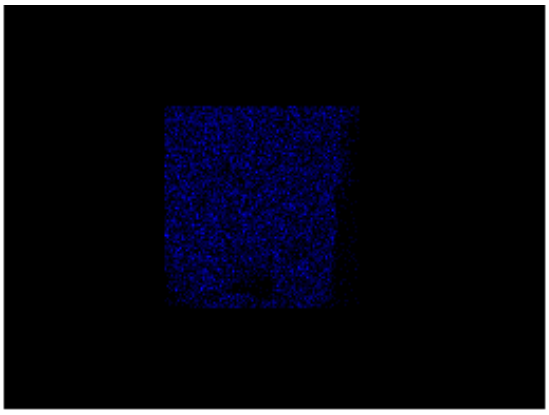

Sr La1

D.7 Lithium metatungstate (LMT) Residue

During the investigation of best gypsum preparation methods for OSL, the heavy liquid lithium metatungstate was used at varying specific gravities to separate and isolate minerals of interest. After the 2.37g/cm^{-3} separations intended to isolate gypsum, stringy to cloudy residue formed in the dirty lithium metatungstate. After cleaning, reconsolidation was very difficult. It was suggested that the free calcium ions had reacted with the tungsten producing calcium tungstate and reducing the heavy liquid's ability to condense. We initially attempted to investigate if this was true using XRD, but could not identify a reference peak to associate the liquid's peak with. Instead we kept the filter after cleaning the lithium metatungstate and used the dried residue remaining on it to produce a sample for SEM analysis. SEM and EDS data presented here proves that the gypsum in fact did react with the lithium metatungstate to produce calcium tungstate. It is highly recommended that this method is not pursued as a standard due to prohibitive costs incurred to purchase new lithium metatungstate after each experiment. Further investigation is necessary to understand how and why copper is also a part of the residue.

No peaks omitted

Processing option : All elements analyzed

Number of iterations = 4

Standard :

O SiO2 1-Jun-1999 12:00 AM

Ca Wollastonite 1-Jun-1999 12:00 AM

Cu Cu 1-Jun-1999 12:00 AM

Sr SrF2 1-Jun-1999 12:00 AM

Pd Pd 1-Jun-1999 12:00 AM

W W 1-Jun-1999 12:00 AM

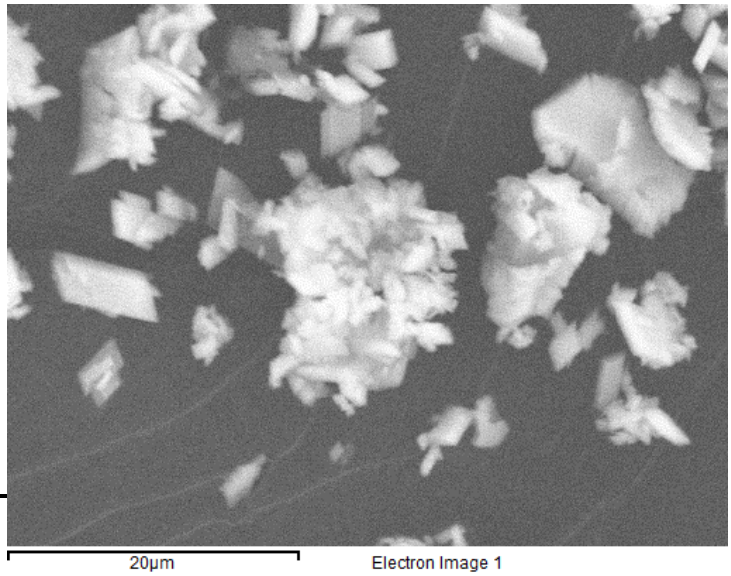

Element	Weight%	Atomic%
O K	69.61	69.01
Ca K	13.34	5.28
Cu K	4.00	1.00
Sr L	10.19	1.85
Pd L	30.51	4.55
W M	212.30	18.32
Totals	339.95	

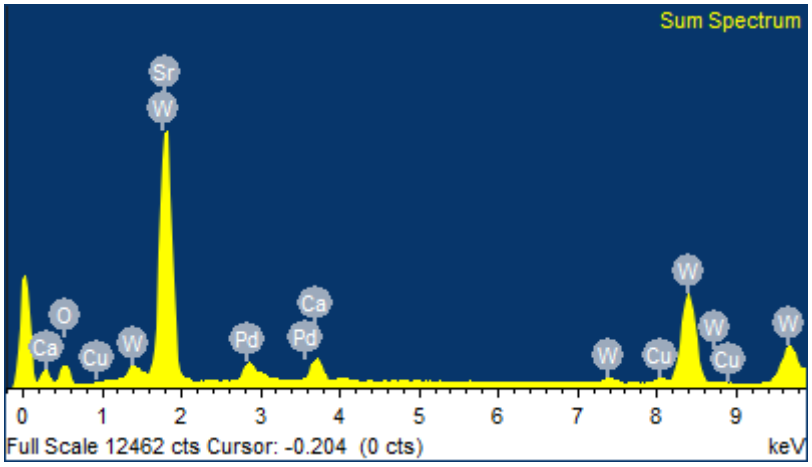

Appendix E - OSL Data

E.1 Bleaching Data

	Preparation technique	Lx/Tx	err			Preparation technique	Lx/Tx	err			Preparation technique	Lx/Tx	err
1	sieved (212-250nm)				**9**	sieved (212-250nm), HCl				**17**	sieved (212-250nm), HCl, density sep		
Natural		0.869	0.024		Natural		0.871	0.082		Natural		1.017	0.169
25		0.374	0.011		25		0.385	0.045		25		0.322	0.093
50		0.898	0.023		50		0.816	0.083		50		1.17	0.193
75		1.684	0.043		75		2.123	0.239		75		1.762	0.28
0		0.001	0.001		0		0.004	0.017		0		-0.036	0.036
25		0.395	0.01		25		0.323	0.036		25		0.406	0.066
Post red light		0.379	0.009		Post red light		0.294	0.035		Post red light		0.393	0.071
% signal change	4.050632911	0.016			% signal change	8.978328173	0.029			% signal change	3.201970443	0.013	
3	sieved (212-250nm)				**11**	sieved (212-250nm), HCl				**19**	sieved (212-250nm), HCl, density sep		
Natural		0.867	0.122		Natural		0.996	0.13		Natural		1.114	0.193
25		0.272	0.053		25		0.447	0.071		25		0.287	0.074
50		0.946	0.121		50		0.83	0.126		50		1.318	0.18
75		4.266	1.055		75		2.564	0.397		75		2.445	0.413
0		-0.053	0.022		0		0.038	0.024		0		0.016	0.037
25		0.381	0.054		25		0.41	0.061		25		0.337	0.085
Post amber light		0.136	0.037		Post amber light		0.187	0.041		Post amber light		0.298	0.061
% signal change	64.30446194	0.245			% signal change	54.3902439	0.223			% signal change	11.5727003	0.039	
5	sieved (212-250nm)				**13**	sieved (212-250nm), HCl				**21**	sieved (212-250nm), HCl, density sep		
Natural		0.696	0.119		Natural		0.695	0.106		Natural		1.097	0.248
25		0.282	0.065		25		0.312	0.067		25		0.335	0.101
50		1.114	0.177		50		0.88	0.122		50		0.837	0.171
75		1.768	0.307		75		2.062	0.347		75		3.14	0.83
0		0.033	0.034		0		-0.029	0.029		0		-0.024	0.041
25		0.362	0.065		25		0.351	0.057		25		0.344	0.09
Post white light		-0.041	0.035		Post white light		-0.003	0.027		Post white light		0.024	0.042
% signal change	111.3259669	0.403			% signal change	100.8547009	0.354			% signal change	93.02325581	0.32	
7	sieved (212-250nm)				**15**	sieved (212-250nm), HCl				**23**	sieved (212-250nm), HCl, density sep		
Natural		1.029	0.182		Natural		0.966	0.13		Natural		0.857	0.157
25		0.306	0.084		25		0.44	0.064		25		0.358	0.086
50		0.957	0.16		50		0.857	0.104		50		1.046	0.179
75		2.231	0.438		75		2.022	0.282		75		2.016	0.386
0		-0.051	0.031		0		-0.014	0.02		0		0.093	0.039
25		0.358	0.071		25		0.307	0.048		25		0.439	0.088
Post control		0.268	0.047		Post control		0.371	0.052		Post control		0.284	0.082
% signal change	25.1396648	0.09			% signal change	-20.84690554	-0.064			% signal change	35.30751708	0.155	

Bleaching Experiment Data; gypsum 212-250 µm (various follow on treatments) with 6 hour exposure time

	Preparation technique	Lx/Tx	err			Preparation technique	Lx/Tx	err			Preparation technique	Lx/Tx	err
1	sieved (63-90nm)				**9**	sieved (63-90nm), HCl				**17**	sieved (63-90nm), HCl, density sep		
Natural		0.942	0.052		Natural		0.806	0.08		Natural		0.875	0.093
25		0.431	0.026		25		0.395	0.043		25		0.348	0.052
50		0.757	0.037		50		0.912	0.075		50		0.882	0.083
75		1.853	0.093		75		1.686	0.15		75		1.96	0.206
0		0.006	0.005		0		-0.011	0.014		0		0.022	0.016
25		0.379	0.019		25		0.407	0.037		25		0.391	0.043
Post red light		0.39	0.02		Post red light		0.348	0.088		Post red light		0.315	0.037
% signal change	-2.90237467	-0.011			% signal change	14.4963145	0.059			% signal change	19.43734015	0.076	
3	sieved (63-90nm)				**11**	sieved (63-90nm), HCl				**19**	sieved (63-90nm), HCl, density sep		
Natural		0.849	0.091		Natural		0.845	0.063		Natural		0.73	0.106
25		0.38	0.045		25		0.406	0.033		25		0.34	0.063
50		0.801	0.073		50		0.855	0.054		50		0.918	0.124
75		1.621	0.148		75		1.661	0.106		75		1.593	0.215
0		0.004	0.016		0		0.001	0.008		0		0.012	0.029
25		0.433	0.04		25		0.349	0.026		25		0.359	0.052
Post amber light		0.147	0.047		Post amber light		0.17	0.019		Post amber light		0.189	0.038
% signal change	66.05080831	0.286			% signal change	51.28939828	0.179			% signal change	47.35376045	0.17	
5	sieved (63-90nm)				**13**	sieved (63-90nm), HCl				**21**	sieved (63-90nm), HCl, density sep		
Natural		1.093	0.315		Natural		0.935	0.058		Natural		0.832	0.147
25		0.818	0.552		25		0.378	0.026		25		0.472	0.081
50		0.565	0.244		50		0.94	0.053		50		0.703	0.107
75		2.445	1.062		75		1.831	0.116		75		1.805	0.309
0		-0.02	0.125		0		0.002	0.007		0		-0.031	0.03
25		0.4	0.194		25		0.365	0.023		25		0.354	0.077
Post white light		0.336	0.224		Post white light		-0.018	0.012		Post white light		0.023	0.032
% signal change	16	0.064			% signal change	104.9315068	0.383			% signal change	93.50282486	0.331	
7	sieved (63-90nm)				**15**	sieved (63-90nm), HCl				**23**	sieved (63-90nm), HCl, density sep		
Natural		0.843	0.091		Natural		0.882	0.059		Natural		0.999	0.048
25		0.41	0.053		25		0.416	0.031		25		0.393	0.022
50		0.852	0.086		50		0.936	0.059		50		0.884	0.041
75		2.195	0.269		75		1.711	0.106		75		1.882	0.094
0		-0.002	0.015		0		-0.006	0.009		0		-0.001	0.005
25		0.346	0.037		25		0.394	0.027		25		0.387	0.02
Post control		0.359	0.038		Post control		0.322	0.021		Post control		0.455	0.071
% signal change	-3.757225434	-0.013			% signal change	18.27411168	0.072			% signal change	-17.57105943	-0.068	

Bleaching Experiment Data; gypsum 63-90nm (various follow on treatments) with 6 hour exposure time

aliquot 3	all from file: kgyp034		Control				212-250nm, HCl, H2O2					
R4(0s ß) Lx/Tx -0.02 ± 0.04	0	-0.01891	0	-0.01891	0.036142				25	25	25	
R6(0s ß) Lx/Tx 0.62 ± 0.09	0	0.621137	0	0.621137	0.093126		Dose	0	0	1	2	
R7(0s ß) Lx/Tx 0.46 ± 0.08	0	0.457487	0	0.457487	0.079783		Subdued I	0.022377	0.502361	0.56931	0.468566	
R8(0s ß) Lx/Tx 0.47 ± 0.08	0	0.470972	0	0.470972	0.079544		Subdued A	0.022377	0.502361	0.590382		
R9(0s ß) Lx/Tx 0.44 ± 0.07	0	0.444156	0	0.444156	0.074014		Sun Light	0.022377	0.502361	0.079712		
R1(25s ß) Lx/Tx 0.57 ± 0.09	25	0.56972	25	0.56972	0.094686		Control (D	-0.01891	0.713466	0.470972	0.621137	
R5(25s ß) Lx/Tx 0.71 ± 0.11	25	0.713466	25	0.713466	0.10964		Subdued A	-0.01891	0.713466	0.444156		
R2(50s ß) Lx/Tx 1.27 ± 0.19	50	1.271429	50	1.271429	0.185529		Sun Light	-0.01891	0.713466	0.457487		
R3(75s ß) Lx/Tx 1.45 ± 0.18	75	1.445283	75	1.445283	0.18146							
aliquot 13			experimental light set up									
R4(0s ß) Lx/Tx 0.02 ± 0.03	0	0.022377	0	0.022377	0.033136							
R6(0s ß) Lx/Tx 0.47 ± 0.07	0	0.468566	0	0.468566	0.067701							
R7(0s ß) Lx/Tx 0.08 ± 0.04	0	0.079712	0	0.079712	0.038771							
R8(0s ß) Lx/Tx 0.57 ± 0.07	0	0.56931	0	0.56931	0.073399							
R9(0s ß) Lx/Tx 0.59 ± 0.07	0	0.590382	0	0.590382	0.071598							
R1(25s ß) Lx/Tx 0.49 ± 0.07	25	0.493774	25	0.493774	0.06788							
R5(25s ß) Lx/Tx 0.50 ± 0.06	25	0.502361	25	0.502361	0.058424							
R2(50s ß) Lx/Tx 0.97 ± 0.10	50	0.974253	50	0.974253	0.09613							
R3(75s ß) Lx/Tx 1.42 ± 0.12	75	1.418253	75	1.418253	0.123793							
aliquot 35			control				212-250nm, HCl					
R4(0s ß) Lx/Tx 0.00 ± 0.02	0	0.00118	0	0.00118	0.015568				25	25	25	
R6(0s ß) Lx/Tx 0.50 ± 0.04	0	0.500522	0	0.500522	0.035354		Dose	0	0	1	2	
R7(0s ß) Lx/Tx 1.49 ± 0.08	0	1.489884	0	1.489884	0.07785		Subdued I	0.00118	0.52814	0.536065	0.500522	
R8(0s ß) Lx/Tx 0.61 ± 0.04	0	0.610879	0	0.610879	0.041395		Subdued A	0.00118	0.52814	0.499834		
R9(0s ß) Lx/Tx 0.51 ± 0.03	0	0.510805	0	0.510805	0.034033		Sun Light	0.00118	0.52814	-0.00439		
R1(25s ß) Lx/Tx 0.48 ± 0.04	25	0.476517	25	0.476517	0.036431		Control (D	-0.00178	0.496073	0.610879	0.500522	
R5(25s ß) Lx/Tx 0.50 ± 0.03	25	0.496073	25	0.496073	0.034106		Subdued A	-0.00178	0.496073	0.510805		
R2(50s ß) Lx/Tx 1.00 ± 0.06	50	0.995216	50	0.995216	0.061162		Sun Light	-0.00178	0.496073	1.489884		
R3(75s ß) Lx/Tx 1.47 ± 0.08	75	1.472265	75	1.472265	0.080948							
aliquot 43			experimental light set up									
R4(0s ß) Lx/Tx 0.00 ± 0.01	0	-0.00178	0	-0.00178	0.009699							
R6(0s ß) Lx/Tx 0.56 ± 0.04	0	0.563421	0	0.563421	0.035386							
R7(0s ß) Lx/Tx 0.00 ± 0.01	0	-0.00439	0	-0.00439	0.010735							
R8(0s ß) Lx/Tx 0.54 ± 0.03	0	0.536065	0	0.536065	0.03489							
R9(0s ß) Lx/Tx 0.50 ± 0.04	0	0.499834	0	0.499834	0.03641							
R1(25s ß) Lx/Tx 0.52 ± 0.04	25	0.519339	25	0.519339	0.03546							
R5(25s ß) Lx/Tx 0.53 ± 0.03	25	0.52814	25	0.52814	0.034557							
R2(50s ß) Lx/Tx 0.93 ± 0.05	50	0.933506	50	0.933506	0.052475							
R3(75s ß) Lx/Tx 1.42 ± 0.07	75	1.41533	75	1.41533	0.072368							

Bleaching Experiment Data; gypsum 212-250nm, HCl treatment, followed by H_2O_2 treatment until reaction completed (n=2); gypsum 212-250nm, HCl treatment (n=2); 1st red-light Lx/Tx data was a 2hour exposure time, other exposure times are 1 hour

E.2 Age Data

Age calculation input for OSL ages using data in the following 3 panes.

													Qtz beta attenuation factors										
Site	Sample	ActLabs Report No.	OSL grain	HF etch	U conc^n	Error	Th conc^n	Error	K conc^n	Error	Rb conc^n	Error	from R.Grun's age program				H2O	Error	H2O	Error	Depth of	Density	Mass pe
			size (µm)	(min)	(ppm)	(ppm)	(ppm)	(ppm)	(%)	(%)	(ppm)	(ppm)	U	Th	K	Rb	content		content		deposit	(g cm^{-3})	unit area
																	(%)	(%)			(cm)		(g cm^{-2})
Knolls Paleodune A	KNP-A1	A18-01676	90-125	N/A	2.1	0.21	3.5	0.35	0.2905	0.01	25	2.50	0.817	0.747	0.907	0.75	2.5	5	0.02	0.05	705	2	1410
	KNP-A1	A18-01676	125-175	49%40	2.1	0.21	3.5	0.35	0.2905	0.01	25	2.50	0.817	0.747	0.907	0.75	2.5	5	0.02	0.05	705	2	1409.22
	KNP-A2	A18-01676	90-125	N/A	1.1	0.11	1.2	0.12	0.0996	0.00	8	0.80	0.817	0.747	0.907	0.75	2.5	5	0.02	0.05	438	2	876.86
	KNP-A3	A18-01676	90-125	N/A	1.1	0.11	1.3	0.13	0.1079	0.01	8	0.80	0.817	0.747	0.907	0.75	2.2	5	0.02	0.05	321	2	642
	KNP-A4	A18-01676	90-125	N/A	2.2	0.22	3.1	0.31	0.2573	0.01	17	1.70	0.817	0.747	0.907	0.75	5.2	5	0.05	0.05	72	2	144
	KNP-A5	A18-01676	90-125	N/A	1.60	0.16	2.2	0.22	0.1826	0.01	12	1.20	0.817	0.747	0.907	0.75	3.1	5	0.03	0.05	28	2	56
Knolls Paleodune B	KNP-B1	A18-01676	90-125	N/A	1.1	0.11	0.9	0.09	0.0747	0.00	4	0.40	0.817	0.747	0.907	0.75	2.0	5	0.02	0.05	415	2	830
	KNP-B2	A18-01676	90-125	N/A	1.5	0.15	1	0.10	0.083	0.00	6	0.60	0.817	0.747	0.907	0.75	1.8	5	0.02	0.05	405	2	810
	KNP-B3	A18-01676	90-125	N/A	1.8	0.18	2.7	0.27	0.2241	0.01	23	2.30	0.817	0.747	0.907	0.75	4.2	5	0.04	0.05	315	2	630
	KNP-B4	A18-01676	90-125	N/A	2	0.20	2.9	0.29	0.2407	0.01	21	2.10	0.817	0.747	0.907	0.75	3.4	5	0.03	0.05	60	2	120
Coppas Dune	CD-5	A18-01676	90-125	N/A	1.3	0.13	1.5	0.15	0.1245	0.01	12	1.20	0.817	0.747	0.907	0.75	2.1	5	0.02	0.05	7	2	14

Cosmic a	Latitude	Longitu	Altitude	Geomag-	F	J	H	**Cosmic**	**Error**	Dry alp	Error	Dry b	Error	Dry gamn	Error	Alpha	Error	**Beta**	**Error**	**Gamma**	**Error**	**Internal alpha**		12.5%	Error
depth	(°N)	(°E)	(m)	lat. (°N)				**(mGya^{-1})**	**(10%)**	(mGya	(mGy	(mGy	(mGya	(mGya^{-1})	(mGya^{-1})	wet		**wet**		**wet**		(Vandenberghe et al., 2		K$_{int}$	(0.5%)
(mGya^{-1})																(mGya^{-1})	(mGya	(mGya^{-1})	(mGya^{-1})	(mGya^{-1})	(mGya^{-1})	(mGya^{-1})	(mGya^{-1})		
0.08645	40.725	-112.7	1284.61	48.583	0.24	0.76	4100	0.11062	0.0111	8.451	0.64	0.54	0.03	0.47438	0.02904	1.0186	0.62	0.5234	0.0459	0.4613	0.0381	0.0100	0.0020	0.34213	0.01369
0.08648	40.725	-112.7	1284.6	48.583	0.24	0.76	4100	0.11067	0.0111	8.451	0.64	0.54	0.03	0.47438	0.02904	1.0186	0.62	0.5234	0.0459	0.4613	0.0381	0.0100	0.0020	0.34213	0.01369
0.11813	40.725	-112.7	1287.27	48.583	0.24	0.76	4100	0.15124	0.0151	3.96	0.32	0.23	0.02	0.20505	0.01361	0.4772	0.291	0.2232	0.0212	0.1994	0.0172	0.0100	0.0020	0.34213	0.01369
0.13677	40.725	-112.7	1288.45	48.583	0.24	0.76	4100	0.17515	0.0175	4.033	0.32	0.24	0.02	0.21191	0.01383	0.4883	0.298	0.2319	0.0217	0.2068	0.0177	0.0100	0.0020	0.34213	0.01369
0.19006	40.725	-112.7	1290.93	48.583	0.24	0.76	4100	0.24352	0.0244	8.435	0.66	0.52	0.03	0.45811	0.02887	0.979	0.596	0.4857	0.0433	0.4326	0.0359	0.0100	0.0020	0.34213	0.01369
0.20196	40.725	-112.7	1291.38	48.583	0.24	0.76	4100	0.25878	0.0259	6.095	0.48	0.37	0.03	0.32943	0.02086	0.7284	0.444	0.3578	0.0324	0.3183	0.0267	0.0100	0.0020	0.34213	0.01369
0.12158	40.725	-112.7	1292	48.583	0.24	0.76	4100	0.1558	0.0156	3.738	0.31	0.2	0.02	0.18448	0.01304	0.454	0.277	0.1998	0.0202	0.1804	0.0162	0.0100	0.0020	0.34213	0.01369
0.12309	40.725	-112.7	1292.1	48.583	0.24	0.76	4100	0.15775	0.0158	4.93	0.43	0.26	0.02	0.23598	0.01744	0.6004	0.367	0.2554	0.0268	0.2313	0.0214	0.0100	0.0020	0.34213	0.01369
0.13782	40.725	-112.7	1293	48.583	0.24	0.76	4100	0.17666	0.0177	7.022	0.54	0.44	0.03	0.38604	0.02405	0.8262	0.503	0.4169	0.0368	0.3684	0.0305	0.0100	0.0020	0.34213	0.01369
0.19322	40.725	-112.7	1295.55	48.583	0.24	0.76	4100	0.24779	0.0248	7.729	0.6	0.48	0.03	0.42208	0.02646	0.92	0.56	0.4589	0.0410	0.4065	0.0339	0.0100	0.0020	0.34213	0.01369
0.20795	40.725	-112.7	1295.55	48.583	0.24	0.76	4100	0.26669	0.0267	4.74	0.38	0.28	0.02	0.24795	0.01626	0.5742	0.35	0.2720	0.0256	0.242	0.0208	0.0100	0.0020	0.34213	0.01369

0.035%	Error	**total**	**Error**		De	Error	Age	Error
Rb_{int}	(0.015%)	**qtz**						
		($mGya^{-1}$)	($mGya^{-1}$)					
0.02899	0.01243	1.1053	0.061		1.6	0	1.45	0.08
0.02899	0.01243	1.1053	0.061		2.5	0.2	2.26	0.22
0.02899	0.01243	0.5838	0.031		0.7	0	1.20	0.06
0.02899	0.01243	0.9849	0.038		0.9	0	0.91	0.04
0.02899	0.01243	1.5329	0.064		0.8	0	0.52	0.02
0.02899	0.01243	1.3059	0.053		0.5	0	0.38	0.02
0.02899	0.01243	0.9072	0.035		0.8	0	0.88	0.03
0.02899	0.01243	1.0155	0.042		0.5	0	0.49	0.02
0.02899	0.01243	1.3332	0.054		0.6	0	0.45	0.02
0.02899	0.01243	1.4843	0.062		0.5	0	0.34	0.01
0.02899	0.01243	1.1518	0.046		0.1	0	0.09	0.00